PROCESSING AND CHARACTERIZATION OF

HIGH PERFORMANCE POLYIMIDE NANOCOMPOSITES

A Dissertation
Presented to
The Academic Faculty

by

Michelle R. Schlea

In Partial Fulfillment
of the Requirements for the Degree
Doctor of Philosophy in the
School of Materials Science and Engineering

Georgia Institute of Technology

May 2011

PROCESSING AND CHARACTERIZATION OF

HIGH PERFORMANCE POLYIMIDE NANOCOMPOSITES

Approved by:

Dr. Meisha L. Shofner, Advisor
School of Materials Science and Engineering
Georgia Institute of Technology

Dr. Yonathan S. Thio
School of Materials Science and Engineering
Georgia Institute of Technology

Dr. Rosario Gerhardt
School of Materials Science and Engineering
Georgia Institute of Technology

Dr. Eric A. Mintz
Department of Chemistry
Clark Atlanta University

Dr. Sundaresan Jayaraman
School of Materials Science and Engineering
Georgia Institute of Technology

Date Approved: March 15, 2011

This work is dedicated to my parents and my sister, who have always supported me.
Life is a winding road, but we always end up where we're supposed to be.

Without your support, I would not be who and where I am today.

ACKNOWLEDGEMENTS

I would like to thank my advisor, Dr. Meisha L. Shofner, for all of her guidance, advice, and, in particular, her flexibility in allowing me to pursue multiple research and academic opportunities at Georgia Tech.

I would like to thank Dr. Shofner in addition to my committee members Dr. Rosario Gerhardt, Dr. Sundaresan Jayaraman, Dr. Eric A. Mintz, and Dr. Yonathan S. Thio for their feedback on my work over the past few years, and for taking the time to participate on my committee. I appreciate the great deal of time and effort that they have donated toward my cause.

I thank my graduate group members, both past and present, including Tracy Brown, Dr. Jasmeet Kaur, R. Bradley Johnson, Ji Hoon Lee, and Jae Ik Choi for their support both in and out of the laboratory, and for their feedback. I especially thank Jordan Bush, Cait Meree, and Emily Goss for their invaluable hard work as undergraduate researchers on my project. This work would not be what it is without the time and effort they put into it.

I would like to thank Dr. Eric Mintz for access to lab equipment at HiPPAC as well as advice and direction throughout all of my work. I would also like to recognize Tracy Brown and Dr. Jim Criss at HiPPAC and M&P Technologies for their guidance over the past few years.

I also thank Yolande Berta for training and support on the scanning electron microscope, and Dr. Rosario Gerhardt for access and training on the electrical characterization equipment in her laboratory. I would like to recognize and thank Dr.

David Bucknall for access to the polymer characterization lab that allowed me to perform thermal analyses on my samples.

I thank Dr. Sandi G. Miller, Dr. Mike Meador, and Dr. Dale Coy for providing valuable experience through my internship work, which directly led to problem solutions in my own work.

I would like to thank various funding sources that provided the resources for my education and my research: through HiPPAC at Clark Atlanta University, NASA cooperative agreements NCC3-1044 and NNX07AT73A; the Technological Innovation: Generating Economic Results (TI:GER) program; and the Science, Mathematics and Research for Transformation (SMART) program. I thank Margi Berbari, Dr. Marie Thursby, and Anne M. Rector for providing me the opportunity to participate in TI:GER, and to Michelle Louis, Andres Velarde, and Melissa Johnson for their knowledge and expertise that allowed us to form a well-working team that took our project seriously. Dr. Davis Lee also provided to be an invaluable asset for discussion and advice throughout the TI:GER program.

Lastly, but certainly not least, I thank my family and friends. My family has always been supportive of any choice I have made, and I am lucky to have such a loving group of people to call my own. My friends, especially Asha, Katie, and Jackie, have not only provided me an outlet from my work, but they have also been patient with me even after I disappeared to work for days and weeks at a time. Without my closest friends, I might not have had the confidence to pursue a graduate degree. I am very grateful to Ryan, who has helped me to remain persistent in my efforts, but who has also taught me stop and enjoy life before it passes me by.

TABLE OF CONTENTS

LIST OF TABLES

LIST OF FIGURES

LIST OF SYMBOLS

A	Cross sectional area
α	Degree of conversion
β	Heating rate
β_G	Critical exponent for rheological percolation
β_σ	Critical exponent for electrical percolation
$d\alpha/dt$	Rate of conversion
E'	Storage modulus by DMA in bending
E''	Loss modulus by DMA in bending
E_a	Activation energy
$E_{a,\alpha}$	Activation energy for a specific degree of conversion
E_c	Composite elastic property
E_{CNF}	Bending modulus for CNFs
E_f	Fiber elastic property
E_m	Matrix elastic property
E_{MWNT}	Bending modulus for MWNTs
f	Filler aspect ratio
$f(\alpha)$	Function of the degree of conversion
η_c^*	Composite complex viscosity
η_m^*	Neat matrix viscosity
G'	Storage modulus by rheometer
G''	Loss modulus by rheometer

ΔH	Heat of reaction
ΔH_T	Ultimate heat of reaction
$(\Delta H)_t$	Heat of reaction up to time t
$k(T)$	Rate constant at temperature T
L	Path length
l	Length of one filler particle
m	Reaction order
m_{cG}	Filler mass loading at rheological percolation threshold
$m_{c\sigma}$	Filler mass loading at electrical percolation threshold
n	Reaction order
R	Universal gas constant
R_g	Radius of gyration
s	Motor speed
$<sin\ \gamma>$	Average of angles between particles
σ_0	Fitting parameter
σ_{AC}	AC conductivity
σ_{DC}	DC conductivity
T	Temperature
t	Time
T_g	Glass transition temperature
T_p	Temperature at exothermic peak
T_q	Torque

V	Volume of one filler particle
v	Filler volume
$<V_e>$	Averaged excluded volume of an object over the characterizing orientation distribution
φ_c	Filler volume concentration at the percolation threshold
w	Diameter of one filler particle
ω	Angular frequency
Z	Pre-exponential factor
Z'	Real component of impedance
Z''	Imaginary component of impedance

LIST OF ABBREVIATIONS

ABS	Acrylonitrile butadiene styrene
AFM	Atomic force microscope
ATR	Attenuated total reflectance
$C_{12}EO_8$	Polyoxyethylene 8 lauryl
CAPRI	Controlled atmospheric resin infusion
CNF	Carbon nanofiber
CNT	Carbon nanotube
CVD	Chemical vapor deposition
DFT	Density functional theory
DMA	Dynamic mechanical analysis
DMAC	Dimethylacetamide
DMF	Dimethylformamide
DSC	Differential scanning calorimetry
DWNTs	Double wall carbon nanotubes
FTIR	Fourier transform infrared spectroscopy
GPC	Gel permeation chromatography
HDPE	High density polyethylene
HIPS	High impact polystyrene
HSCT	High Speed Civil Transport
HT-VARTM	High temperature vacuum assisted resin transfer molding
KBr	Potassium bromide

MDA	Methylenedianiline
MWNT	Multiwall carbon nanotube
NMP	N-Methyl-2-pyrrolidone
PC	Polycarbonate
PEPA	(Phenylethynyl) phthalic anhydride
PETI	Phenylethnyl-terminated imide
PI	Polyimide
PmPV	poly(*m*-phenylenevinylene-*co*-2,5-dioctyloxy-p-phenylenevinylene)
PMR	Polymerization of monomer reactions
PMMA	Polymethylmethacrylate
PP	Polypropylene
PS	Polystyrene
PVA	Polyvinyl alcohol
PVDF	Poly(vinylidene fluoride)
PVK	Poly(9-vinyl carbazole)
RTM	Resin transfer molding
SDBS	Sodium dodecylbenzene sulfonate
SEM	Scanning electron microscope
SWNT	Single wall carbon nanotube
TEM	Transmission electron microscope
VARTM	Vacuum assisted resin transfer molding

SUMMARY

The goal of this work was to achieve a homogeneous morphology of carbon nanotubes in a polyimide matrix, characterize the resulting nanocomposite properties, and understand structure-property relationships. Melt-mixing was used as an effective method for dispersing multiwall nanotubes and carbon nanofibers in a phenylethynyl terminated imide resin where aggregation occurred only in particle-saturated systems. Particle network formation within the nanocomposites was studied using rheology and impedance spectroscopy; results showed that the electrical percolation threshold occurred at a lower particle loading than the rheological percolation threshold, consistent with the oligomer size in comparison to the distance for electrical conductivity (~5 nm). Thermomechanical analysis showed that the addition of nanoparticles enhanced the polyimide storage modulus and thermal behavior indicated that the nanoparticles restricted polymer motion to higher temperatures. A study of the cure mechanism of the oligomer with and without nanoparticles showed that the nanoparticles reduced the activation energy required for cure initiation while increasing the obtainable extent of cure at various isothermal temperatures. The work presented in this dissertation shows that an easy, time effective processing method can be used to homogeneously disperse nanoparticles in an imide oligomer, and the resulting nanocomposites exhibit enhanced properties. A business plan is also presented that reflects the market potential of this technology.

CHAPTER 1
INTRODUCTION

Thermosetting polyimides are a class of polymers that generally exhibit high strength, thermal stability, and robust performance in extreme environments when compared to other polymer systems. Reinforcing polyimides with advanced fillers offers a way to further improve those properties. Nanofillers offer a unique opportunity for reinforcement in that a small quantity has significantly more specific surface area than micro- or larger fillers. When added to a polymer matrix, nanofillers reinforce matrix properties by polymer-particle interactions through the available surface area. Nanoparticle size and dispersion can be critical in these interactions, so a thorough understanding of these mechanisms will aid in achieving optimal properties. This research was geared toward achieving a homogeneous dispersion of nanofillers in an imide oligomer using a relatively low impact processing method, and characterizing the subsequent cured and uncured composites. The resulting material had improved properties that could be beneficial for aerospace performance, so potential commercial opportunities were also explored. The studies in this work could be grouped into four main objectives:

- The use of melt-mixing as a method for achieving homogeneous dispersion and distribution of nanoparticles in an imide oligomer.
- Investigation of mechanisms for nanotube and polyimide network formations and the resulting effects on composite properties.

- Characterization of nanocomposites to determine structure-property relationships.
- Determination of the potential for commercializing the studied technology through market and industry analyses as well as business plan formation.

In Chapter 2, a background on polyimides and carbon nanotubes is given. Nanocomposite properties and processing methods are also covered through literature surveys. In Chapter 3, melt-mixing as a nanocomposite processing method is explored. Multiwalled carbon nanotubes and carbon nanofibers were each dispersed in an imide oligomer while monitoring melt-mixing parameters. Homogeneous morphologies of evenly distributed individual nanotubes were achieved for various loadings of each filler, and additional studies examined the effects of different processing parameters on the resulting morphologies. The glass transition behavior of the nanocomposites was studied, as well as high frequency rheological properties. The glass transition temperature increased to 341°C from 323°C with the addition of 0.5 wt.% multiwalled carbon nanotubes to the neat polyimide. Viscosity increased with filler content but also decreased with increasing processing time.

Chapter 4 concerns nanotube network formation in the melt-mixed and cured samples. Rheological studies determined the rheological percolation threshold in uncured samples using percolation behavior. Electrical percolation was characterized using cured samples. Comparison of the two percolation thresholds gave some knowledge of networks. Modeling was also used to estimate the effective nanotube aspect ratio. In Chapter 5, cured samples were characterized for thermomechanical properties and the

effects of aggregation were studied using thermal analysis. The nanoparticles were shown to enhance the thermomechanical properties of the neat resin, although not to the extent predicted by micromechanical models. Thermal analysis showed that lower loadings were more sensitive to aggregation during curing than higher loadings. The curing mechanism of the imide oligomer was studied using several techniques in Chapter 6. Nanoparticles were shown to reduce the activation energy required to initiate cure and all multiwall nanotube composites achieved a higher degree of conversion due to the nanoparticle inclusions.

In Chapter 7, a commercialization plan for the nanocomposite technology is presented. This was done as part of a program with the Georgia Tech MBA and Emory Law programs. In this plan, intellectual property was explored and market and industry analyses were performed to determine potential customers and applications. Once a position was established, financial and valuation calculations were computed to project potential profits from the technology. Additional experiments were included that would address potential customer questions regarding product usage.

The conclusion in Chapter 8 summarizes the results from the different studies and presents a plan for future work. Appendix A includes a review of structural health monitoring and the applicability of the studied nanocomposites for such applications. Appendix B concerns an overview of electromagnetic interference and electrical properties necessary for shielding applications. Appendices C and D are supplements to the commercialization plan in Chapter 7 and include detailed financial and valuation assumptions and calculations.

CHAPTER 2
BACKGROUND

2.1 Introduction

Polyimides are a class of polymers noted for their high thermal stability, strength, and resistance to chemical corrosion, while carbon nanotubes are noted for their small size and large aspect ratio with one of the highest measured tensile strengths measured to date. Combining polyimides with nanotubes presents an opportunity for a material reflecting the best properties of both components. However, an effective method for processing the nanocomposites has proven to be a difficult task. This chapter covers issues relevant to this challenge with an overview of polyimides, carbon nanotubes, nanotube composites, and nanocomposite processing methods.

2.2 Polyimides

While the first aromatic polyimide was reported in 1908 by Bogart and Renshaw [1], it took until the 1950's for Dupont to establish the first commercial method for producing large quantities of these polyimides. It was another decade until the first commercial polyimide was available from DuPont. By the end of the 1960's DuPont had three major polyimide products: Kapton (film), Vespel (molding), and Pyre-ML (wire insulation). Polyimides are known for their high strength and resistance to high temperatures and chemicals. An imide has the general form shown in Figure 2.1:

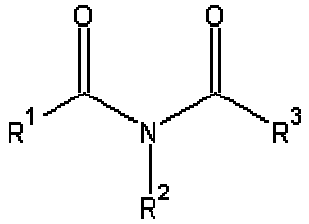

Figure 2.1. Basic imide form.

Polyimides are generally formed from dianhydrides and diamines, and most commercial polyimides are aromatic heterocyclic polyimides. These aromatic polyimides are high strength due to the degree of aromaticity and charge transfer complex within and between the polyimide chains [2-3]. Endcapping the reactive chain ends also helps in enhancing thermal stability by reducing the number of potential reaction points [2].

Polyimides are used in many forms, particularly films, varnish, foam, composite prepregs, and molded and extruded components in electronics, aircraft engines, and automobiles. Aromatic polyimides have a unique and valuable property in that they are self extinguishing; as a polyimide begins to burn, it forms a surface char which then smothers the flame [3]. NASA has also been a driver in polyimide research; it has been the leader in developing bis-maleimide composites, the LaRC polyimide series, the phenylethynyl-terminated imide (PETI) series, colorless imides, and poly(imide/etherketone) copolymers [4].

Polyimides are generally synthesized in either a two- or one- step approach. In the two-step method, a dianhydride is added to a diamine in a polar aprotic solvent, such as dimethylformamide (DMF), dimethylacetamide (DMAC), or n-methyl-2-pyrrolidone (NMP), at an ambient temperature and poly(amic acid) is rapidly formed [5-6]. The poly(amic acid) is formed by a nucleophilic substitution reaction between the diamine

and one of the carbonyl carbon atoms on the dianhydride [5]. The poly(amic acid) is cyclohydrated to the corresponding polyimide, then, by additional heating at higher temperatures or through dehydrating agents.

Insoluble polyimides, usually in the form of coatings or films, are mostly made by poly(amic acid). Polyimides that are soluble to organic solvents, however, are usually made by a one step method [7]. Poly(amic acid) formation is not required in this method; the dianhydride and diamine are stirred at 180-220°C in a high boiling solvent to promote chain growth and imidization, which occur spontaneously [6]. While the two-step and high temperature one-step methods are the most prevalent methods for synthesizing polyimides, other processes can also be used: low temperature solution polymerization, diamine and tetracarboxylic acid reactions, exchange reaction polymerization, or cycloaddition reaction polymerization.

A major area of interest for polyimides includes aerospace applications. It is beneficial in weight and fuel savings for aerospace components to move from traditional metals to lighter and easier to process polymer composites. While properties such as high strength and temperature resistance make polyimides a candidate for these composites, there is an obstacle in creating a polyimide with these properties as well as maintaining processability characteristics. In 1972, polymerization of monomer reactions (PMR) polyimides were first introduced as a solution to this problem by Serafini *et al.* [8]. PMR polyimides use an alcohol solution of monomers to make a prepreg, which negates the issue of removing any high boiling solvents. PMR-15 was the first commercialized PMR resin and is still available today; it is noted for its processability, thermo-oxidative stability, and mechanical properties. However, it also has poor oxidative stability above

316°C, solvent must also be removed during composite manufacturing, and it also utilizes a carcinogenic monomer (MDA) that could lead to unwanted health effects.

NASA's High Speed Civil Transport (HSCT) program ran from 1989-1998 and concentrated on advancing the technology in reusable launch vehicles. Even though the program was terminated after only nine years, it did initiate the development of processable polyimides. One of the most successful classes of these include imide oligomers end-capped with reactive functional groups. For high temperature applications, phenylethynyl groups are preferred because they have a high curing temperature, which leads to a broader processing window, and they also have a low melt viscosity without any by-products [9]. These phenylethynyl terminated imides, or PETIs, generally use (phenylethynyl) pthalic anhydride (PEPA) as the endcapping agent due to its low toxicity.

A series of PETI resins have been developed to meet the needs of the industry. Table 2.1 summarizes the properties of several PETI resins [10-15]. PETI-1 was the first synthesized in the series, while PETI-5 was formulated to improve thermal properties and reduce viscosity by an overall reduction in molecular weight [10-12]. PETI-298 and PETI-330 formulations also improved on previous thermal and viscoelastic properties, with PETI-330 exhibiting the highest post-cured T_g and the lowest viscosity, which makes it an excellent candidate for conventional composite manufacturing methods such as resin transfer molding (RTM) or vacuum assisted resin transfer molding (VARTM) [14-15].

Table 2.1: Select PETI resins and their properties.

	Molecular Weight	Post-cured T_g	Minimum viscosity
	(g/mol)	(°C)	(Pa·s)
PETI-1[10]	9000	249	N/A
PETI-5[11-12]	5000	270	N/A
PETI-298[13]	750	298	0.1-10
PETI-330[14-15]	750	330	0.06-0.1

PETI-330 is of particular interest for this work because of its thermal and rheological properties. The synthesis method for PETI-330 has been previously reported [16-19]. Briefly, aromatic diamines are dissolved in NMP at room temperature in a nitrogen environment [18]. Dianhydride, s-BPDA, and end-capping agent, PEPA, are mixed with NMP and added as a slurry to the diamine solution. The reaction is stirred for ~24 hours at ambient temperatures under a nitrogen environment and results in an amid acid solution. Imide oligomers are prepared from these solutions by distillation with toluene. The imide oligomers are then isolated by adding to a water bath and rinsing with warm water; the oligomer is then dried at ~120°C to form yellow powder [18].

Many studies have concentrated on characterizing PETI resins for high temperature VARTM (HT-VARTM) applications, which is an extension of Boeing's controlled atmospheric resin infusion (CAPRI) process [20]. Potential applications for PETI components include many aircraft components due to their ability to withstand high temperatures for long periods of time; it has also been suggested that PETI-330 would serve well in or around jet engines because of its increased thermal stability over other PETIs [21]. PETI-330 is also commercially available in several forms from UBE

Industries, Ltd. UBE sells it as a powdered imide form for composite molders and manufacturers, but also provides PETIs as carbon fiber reinforced plates, prepregs, and foam panels.

2.3 Carbon nanotubes

Nanofillers possess a high amount of surface area, so a smaller quantity is needed to achieve the same surface area of similar but larger fillers. In particular, carbon nanotubes exhibit advanced properties that can be used to enhance composite behavior through surface area interactions. These nanotubes can be classified by their structures, synthesis methods, and properties. In most cases, the structure or synthesis method dictates the resulting nanotube properties. An overview of these mechanisms can relate these different factors.

2.3.1 Structure

Single wall nanotubes (SWNTs) are graphite sheets rolled into seamless tubes, sometimes capped at the ends. The graphite sheets can be rolled in many ways, each imposing different hexagonal lattice directions with respect to the tube length axis. These different directions can be described by chirality, all of which greatly affects the carbon nanotube (CNT) transport properties. There are three primary types of orientation: arm chair, zig zag, and chiral [22]. Electronic properties are most significantly affected by the lattice orientation, with arm chairs being metallic while zig zag and chiral are semi-

conducting [23]. The density is also orientation specific with values of 1.33 g/cm^3 for armchair CNTs, 1.34 g/cm^3 for zig zag CNTs, and 1.40 g/cm^3 for chiral CNTs [24].

Multiwall nanotubes (MWNTs) are nested individual tubes, each spaced apart by approximately 0.34 nm, which is the same as the basal plane in graphite [25-26]. While SWNTs have diameters measuring only 0.4-1.4 nm [27], MWNT diameters can range from 1.4 nm to 100 nm [28]. Structurally, each individual tube within a MWNT has its own chiralty, so predicting physical properties is difficult. Carbon nanofibers (CNFs) are similar to MWNTs but have a stacked cup and cone structure instead of concentric tubes. CNFs are also large with diameters ranging from 50 to 200 nm [29].

2.3.2 Synthesis

There are a growing number of methods for CNT production, but three primary methods currently exist: arc discharge, laser ablation, and chemical vapor deposition. The arc discharge method was originally used for producing fullerenes, but then adjusted for manufacturing CNTs as well. A high current electric arc, in the presence of metal catalyst particles, is passed through graphite electrodes and CNTs are formed from the resulting condensation of hot, gaseous carbon [29-30]. Arc discharge CNTs are used commercially, but large-scale production is currently not possible. Laser ablation is used based on the same principles as the arc discharge method, but, instead, a laser is shot at a carbon target with metal catalysts present [29-30]. Metal catalyst particles are also produced from this reaction, which are then used again to form CNFs [29]. Chemical vapor deposition (CVD) is the most common method used today. Nanotubes are deposited or grown on a substrate while a gaseous carbon source is decomposed

catalytically. CVD CNTs generally have more structural flaws and defects than tubes produced using other methods, but the resulting properties can be improved by heat treating at high temperatures [31]. CVD production of CNTs is more scalable to industrial quantities and can be produced in much larger batches.

2.3.3 Physical properties

Physically measuring the elastic properties of individual carbon nanotubes has proven to be a difficult task. The in-plane modulus of graphite is approximately 1.06 TPa and, due to their similar structure, carbon nanotubes are expected to reflect similar behavior [32]. The first mechanical measurements were done by Treacy *et al.* [33] on MWNTs by using *in situ* measurements of intrinsic thermal vibrations in transmission electron microscope (TEM). The study calculated the moduli for several individual MWNTs and found an average of 1.8 TPa from samples ranging 0.41 TPa to 4.15 TPa. Wong *et al.* directly measured an average modulus of 1.28 TPa for arc-discharge MWNTs using atomic force microscopy (AFM) with a cantilever beam model [34]. The group also calculated an average bending strength of 14 GPa. A nanostressing stage inside a scanning electron microscope (SEM) was used by Yu *et al.* to obtain a range of 11-63 GPa for tensile strength and 270-950 GPa for the Young's modulus of the outermost shell of several individual MWNTs [35]. This range is much smaller than that of previous studies, removing some of the variability in the obtained values.

Debundling SWNT ropes is difficult, making it difficult to measure individual SWNT elastic properties. Salvetat *et al.* measured small diameter SWNT bundles using

Table 2.2. Experimental data for various forms of carbon nanotubes.

	Diameter	Cost per gram	Young's modulus	Tensile strength
SWNTs	1.2-1.4 nm[25]	$95+[35]	~1 Tpa[33,34,40]	~30 GPa[33]
MWNTs	1.4-100 nm[26]	$5-15+[35]	~ 1 TPa[29-31]	11-150 GPa[41]
CNFs	50-200 nm[27]	$0.50+	100-300 GPa[37]	2-3 GPa[37]

AFM and determined the bundle modulus to be on the order of 1 TPa [36]. However, tube slippage and displacement within the bundle during testing can cause inaccuracies in calculating individual tube properties. Yu *et al.* used the nanostressing stage method with SWNT bundles to measure the bundle tensile strength as 13-52 GPa with an average of 30 GPa [37]. The study also included measuring individual SWNTs in the same way, obtaining an average value of 1.00 TPa from samples ranging 0.32 -1.47 TPa. Similar values were measured by Krishnan *et al.* [38] using a TEM method similar to Treacy *et al.*'s [33], resulting in a value of 1.3 TPa.

CNFs are structurally similar to MWNTs, but with larger diameters. CNFs are also less expensive [39-40], so they are more favorable for use in commercial products. However, the elastic properties of CNFs are not as good as those of MWNTs or SWNTs. The Young's modulus of CNFs has been measured at 100-300 GPa [41], less than 1/3 of CNTs. CNF tensile strength is also nearly a magnitude less at 2-3 GPa [41].

Experimental measured values are summarized in Table 2.2.

2.4 Nanocomposites

Carbon nanotubes are added to polymer matrices to produce nanocomposites with improved properties. In particular, the mechanical properties of nanotubes can aid in increasing the tensile strength and modulus of a polymer through interfacial interactions. Many of the resulting properties depend on the morphology of the nanoparticles with the polymer matrix. Morphology is the property that is reflected by how the filler particles are spread throughout the system. Dispersion is the morphological property that relates the total surface area with the available surface area. This can be described by particle clumping, where particles in the center of clumps or aggregates are not able to interact with the surrounding matrix. Distribution is the morphological property that details how well the filler particles are spread throughout the entire matrix. Good dispersion would include individual nanoparticles fully surrounded by polymer chains while good distribution would include a homogeneous spread of individual particles or clumps of particles throughout the polymer matrix.

Many studies have found enhanced composite properties due to the addition of nanotubes. Cadek *et al.* reinforced polyvinyl alcohol (PVA) and poly(9-vinyl carbazole) (PVK) films with arc-discharged MWNTs and achieved the first significant increase in stiffness due to nanotubes [42]. Moduli values increased from 7 GPa to 12.6 GPa with 0.6 vol.% MWNTs in PVA and from 2 GPa to 5.6 GPa with 4.8 vol.% MWNTs in PVK. A study of only 1 wt.% MWNTs in polystyrene (PS) by Qian *et al.* resulted in an increase of 25% in tensile strength and 42% in the modulus. [43]. Some of the nanotubes in the composite were shown to act as bridges during crack propagation; like carbon fibers in

traditional composites, the nanotube bridging behavior showed good adhesion and aided in enhanced strength. Melt processing by Liu *et al.* led to a good dispersion of 2 wt.% MWNTs in nylon-6 and resulted in an increase in modulus from 0.4 GPa to 1.24 GPa and an increase in tensile strength from 18 GPa to 47 GPa [44]. Unlike other studies [45], only a small loss in nanocomposite ductility occurred (from 150% to 110%), which was attributed to the good morphological properties.

Significant property enhancement can be achieved with even small particle loadings; for example, Putz *et al.* used only 0.008 vol.% SWNTs in polymethylmethacrylate (PMMA) and observed an increase in modulus from 0.3 to 0.38 GPa, a nearly 27% improvement [46]. Thermoset systems have also experienced significant enhancement through nanoparticle reinforcement. Ogasawara *et al.* measured the storage modulus of a cured phenylethynyl terminated imide by dynamic mechanical analysis (DMA) to be 2.84 GPa, which then increased by 15% with the addition of 7.7 wt.% MWNTs and by 37% with 14.3 wt.% MWNTs [47]. Models such as the rule of mixtures or the Halpin-Tsai equations can be used to predict property enhancement from nanofillers. For example, for a polymer with a modulus of 3 GPa reinforced with a nanofiller with modulus of 200 GPa and aspect ratio of 100, expected property enhancement is displayed in Figure 2.2. At a loading of 1 wt.%, the rule of mixtures predicts an enhancement of 66% and the Halpin-Tsai equations predict 20%. However, experimental values may be less than those predicted because of poor particle dispersion or poor load transfer between polymer and matrix. Also, the models both assume dispersed and non-interacting particles, which is not true for higher loadings.

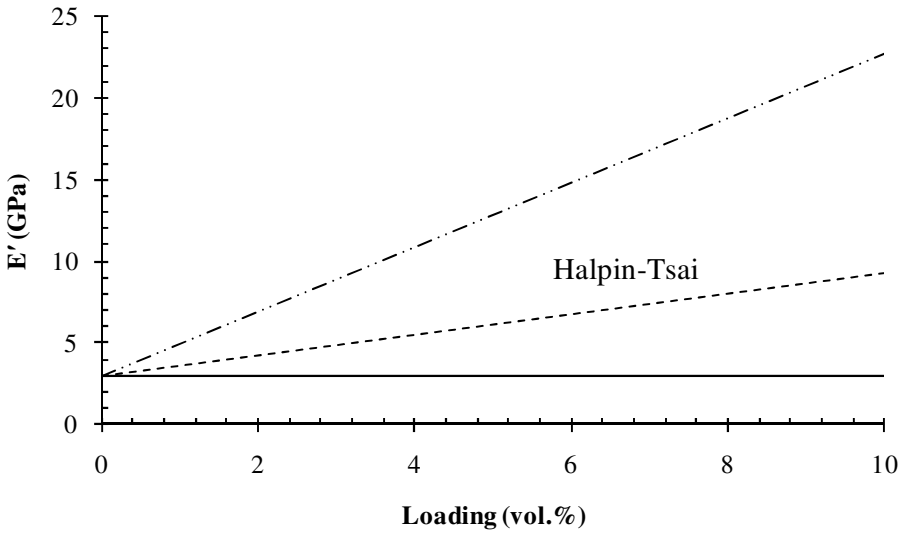

Figure 2.2: Theoretical storage modulus enhancement using the rule of mixtures and the Halpin-Tsai equations. The solid line represents the matrix modulus. Predictions were based on a polymer with modulus of 3 GPa and a nanofiller with modulus of 200 GPa and aspect ratio of 100.

Nanocomposite properties are also dependent on CNT properties; the method of nanotube synthesis, quantity, size, and location of impurities within the nanotubes, whether or not the CNTs were purified and the purification process, physical dimensions (diameter, length aspect ratio), and alignment of nanotube particles all affect property enhancement of the final composite [30]. These properties affect morphological properties which, in turn, affect composite properties as well. During nanocomposite fabrication, CNTs can be purchased with many of the listed properties already known, such as the synthesis method, fraction of impurities present in the batch, and physical dimensions. The fabricator may also choose to purify the nanotubes, or use as-is. Alignment, however, is not as easily controlled and may occur both intentionally and unintentionally due to the high aspect ratios of the CNTs [30]. Understanding the nanotube processing method may aid in achieving desired degrees of alignment. For

example, a study by Haggenmueller *et al.* found greater CNT alignment in fibers when the fiber diameter decreased and also a lesser degree of alignment as the nanotube content increased [48].

Stress transfer between the polymer matrix and filler particles dictates mechanical properties, so interfacial interactions and bonding are key mechanisms in nanotube composites [22]. Nanotube and polymer functionalization is a popular choice for increasing polymer-particle interactions, as well as enhancing dispersion; this is covered more in-depth in Section 2.5.4. Molecular mechanics modeling by Lordi and Yao found that strong interfacial bonding occurs when a polymer has a helical conformation around the nanotubes [49]. The modeling showed that this entanglement forces long range ordering within the composite and enhances interfacial strength. Interfacial interactions can also be promoted in crosslinked systems; modeling by Frankland *et al.* showed that even low density crosslinking influenced polymer-particle interfacial properties [50].

There are a growing number of applications for polymer nanocomposites. The improvement in mechanical properties due to CNTs allows for polymer nanocomposites to be used in structural reinforcement applications where high strength and stiffness are necessary. CNTs, which are either metallic or semi-metallic depending on the structure, can also impart a degree of electrical conductivity to a polymer matrix that is typically insulating. These nanocomposites can then be used in applications such as electrostatic dissipation, electrostatic painting, electromagnetic interference shielding, or printable circuit wiring [51]. On a more commercial basis, CNTs are slowly making their way into items such as bicycle frames, tennis rackets, and golf clubs; additionally, the completely

carbon structure of CNTs make them compatible with organic materials and good candidates for the biotechnology field [51].

2.5 Processing nanocomposites

Due to the characteristic large aspect ratios of CNTs, attractive forces can cause problems with dispersing the particles within polymer matrices, particularly for SWNTs. Many techniques have been developed to overcome CNT's inherent tendency to form aggregates, and several review papers have been published which explore these methods in depth [30, 52-54]. Each of these reviews covers polymer nanocomposites and processing from different angles and present valuable information. Coleman *et al.*'s paper covers a review of processing methods and effects of the processing on mechanical properties [52]. Xie, Mai, and Zhu give an overview of methods for dispersing as well as ways of aligning CNTs [53]. Moniruzzaman and Winey present an overall review of CNT nanocomposites, covering types of nanocomposites, properties, and processing methods [30]. Most optimal morphologies are obtained by using several of these methods, such as Liao *et al.*'s study of SWNT/epoxy nanocomposites [55]. The group tried different combinations of processing by tip sonication, bath sonication, surfactant suspension, and solution processing and determined that the best dispersion could only be achieved if both solution processing and tip sonication were used. Below is a brief overview of some of these dispersion methods and more examples from literature.

2.5.1 Comparison of methods

While many of the processing methods presented here are used in conjunction with each other, each one presents a different approach. Solution based processing methods require solvents and a source of agitation, and may also include surfactants or chemical functionalization of nanoparticles or polymer. The resulting composites can have good morphological properties but, potentially, at the expense of costly chemicals and long processing times. Optimal morphologies may also only be achieved in small quantities, making large batch sizes difficult to achieve. Melt mixing offers an alternative method that results in fewer chemical changes to composite components, but may not achieve as good morphologies. A processing method can be selected for a particular nanocomposite by examining the different dispersion options.

2.5.2 Solution processing

Solution processing uses a low viscosity solvent to infiltrate filler aggregates and separate through agitation or polar interactions. Solubility and compatibility play an important role in solution processing where pristine nanotubes may have good dispersion with a different solvent than that of functionalized nanotubes. It is a common processing mechanism, but is generally only done on small sample sizes (milligrams to grams) and may take long periods of time to obtain the desired final composite form. It can also be difficult to find a solvent that is compatible with a particular particle/polymer system. Surfactants are also often used to aid in solution processing, and will be covered in a subsequent section due to the breadth of research utilizing that mechanism. Solution processing can be used alone or with other forms of nanocomposite processing such as

melt blending or *in situ* methods [43, 55-65]. Many of these combination methods are outlined under the following process methods; however, some polymers are insoluble so solution processing is not possible.

For CNT composites, nanotubes are first dispersed in the solvent, usually followed by sonication, added to the polymer, and then the solvent is evaporated out. Lau *et al.* [56] dispersed SWNTs into acetone, ethanol, or DMF, separately. Each suspension was sonicated to break apart agglomerates, added to epoxy, and then sonicated again. After the solvent was evaporated the nanocomposites were sonicated again. SEM images showed that ethanol and DMF produced composites with smaller diameter SWNT bundles (20-30 nm) than acetone (40-50 nm). By sonicating the SWNTs in the solvent prior to the addition of epoxy, there were no monomer chains present to interfere with aggregate bundle loosening. Qian *et al.* [43] dispersed MWNTs in toluene and sonicated to disperse the nanotubes from agglomerates. PS matrix was also dissolved in toluene, and then the solution was mixed with the MWNT solution under sonication. After the toluene was evaporated out, the group found homogeneous dispersion in the films. A coagulation method was used by Du, Fischer and Winey [57] to disperse purified SWNTs in PMMA. The SWNTs were suspended in DMF and sonicated for 24 hours before PMMA was dissolved into the solution. As the suspension was slowly dripped into distilled water, the PMMA immediately precipitated out due to its insolubility with DMF/water. The PMMA chains had entrapped the SWNTs, resulting in uniform morphology.

2.5.3 Surfactant-assisted solution processing

As previously noted, surfactants are often used in solution processing as an additional dispersion aid. In particular, surfactant processing has been the most successful at exfoliating SWNTs [66]. Surfactants migrate to surfaces and interfaces to promote dispersions and have been used in many types of processing [67]. Surfactants can also be used in CNT dispersion to aid in debundling of aggregates and also to promote particle-polymer interactions [55, 58, 61, 64, 68-69]. Gong *et al.* [68] added MWNTs to polyoxyethylene 8 lauryl ($C_{12}EO_8$) surfactant and dispersed by stirring at room temperature for 15 minutes. Epoxy monomer and hardener were then added simultaneously, stirred for an additional 15 minutes, and cured in a mold. Composites with surfactant-assisted particle dispersion displayed better morphological and thermomechanical properties than composites without surfactant. Dalmas *et al.* [69] utilized surfactants with latex chemistry by dispersing MWNTs in sodium dodecylbenzene sulfonate (SDBS), sonicating, then adding to an amorphous poly(styrene-co-butyl acrylate) latex suspension. Cured composite films exhibited good dispersion and distribution by TEM. Purified and heat treated MWNTs were dispersed in epoxy by Cui *et al.* by using Tergitol surfactant and acetone solution and cured *in situ* [58]. SEM images comparing the surfactant assisted dispersions with only solution processed dispersion illustrated that surfactants greatly aided morphological properties in this system.

2.5.4 Functional groups

Improved dispersion can also be achieved by promoting polymer-particle interactions, and this can be done by adding functional groups to the polymer chains or particles. The functional groups should be matched to interact with the other composite component, reducing the aggregating attractive forces. This chemical interaction can also result in improved adhesion because the polymer chains and particles are not just mechanically linked but also chemically linked. Many studies have used functionalization to improve nanocomposite morphological properties [44, 59-62, 70-72]. Polymers can be synthesized to have optimal interaction with a filler, which is often accomplished through π-π interactions [54]. McCarthy *et al.* illustrated that the π-π interactions can result in polymer wrapping of the nanotubes, which leads to maximized particle wetting [73].

More often CNTs are functionalized to improve interactions. Seyhan *et al.* [70] functionalized MWNTs and double wall nanotubes (DWNTs) with amine groups ($-NH_2$). After ballmilling the CNTs with unsaturated polyester resin and curing, SEM and TEM analyses showed that the amine groups aided MWNT dispersion, but DWNT dispersion remained poor. Zhu *et al.* [59] used a combination of acid modified MWNTs with solvent dispersion (DMAC), sonication, and *in situ* polymerization to determine, by SEM, that the modified MWNT aggregates were smaller and less frequent than unmodified. The group attributed the improved dispersion to the functional groups as well as the shorter tube length that resulted from the modification process. Purified and then acid treated MWNTs were melt compounded by Liu *et al* [44]. SEM identified MWNTs that were randomly and loosely entangled while tensile testing showed that the acid treated MWNTs failed by breaking, not slipping. This indicated that the acid treatment enhanced

the interaction and covalently bonded with the nylon 6,6 matrix. Other studies, such as Chen *et al.* [60], have explored multiple functional groups to find overall improved morphological properties from the improved interaction.

2.5.5 *In situ* polymerization dispersion

Nanoparticles can also be dispersed by polymerizing the monomer reactants around the nanoparticles. The polymer chains form around the particles, dispersing and distributing them throughout the matrix. Many studies have shown this *in situ* polymerization dispersion method to have favorable results [4, 5, 8, 10, 14, 17-19, 22, 24-26, 32, 61]. Haggenmueller *et al.* [61] developed an "interfacial *in situ* polymerization" method where SWNTs were purified, functionalized with carboxylic acid groups, or suspended in surfactant. The purified and functionalized SWNTs were suspended in toluene, and nylon 6,6 was polymerized in the presence of each of the three types of SWNTs. The group showed that *in situ* polymerization with surfactant assisted dispersions of SWNTs developed the most homogeneous morphology. *In situ* polymerization is most often used with epoxy resin systems [55-56, 58, 62-63, 65, 68, 72, 74-75]. Schadler *et al.* [74] sonicated MWNTs and epoxy resin prior to curing and found that the resulting nanocomposites had a good dispersion of debundled tubes, but a poor distribution of the particles. Martin *et al.* [75] dispersed MWNTs into an epoxy precursor, stirred at various temperatures until a homogeneous dispersion was established, then hardener was added to complete the cured network. Interestingly, MWNT dispersion and distribution was homogeneous in all precursor samples, but optimal morphological properties in cured samples were reached only under certain curing conditions.

Using additional processing methods with *in situ* polymerization helps to optimize morphological properties. Zhu *et al.* [62] compared purified, end functionalized with carboxylic acid, and fluorinated end functionalized SWNTs that were dispersed first into DMF, then into epoxy resin and sonicated in each. Each set of SWNTs were stirred until gelled, then cured and analyzed under SEM. Images identified that both of the sets of functionalized SWNT composites had good homogeneity and primary failure through SWNT breakage and not slippage, indicating bonding between the polymer and particles. The unfunctionalized SWNTs had nonuniform agglomerates. So *et al.* [71] mixed MWNTs modified with carboxyl functionalized with poly(amic) acid and polymerized the polyimide to achieve a homogeneous morphology. Barrau *et al.* [72] used palmitic acid as a process aid to disperse acid treated CNTs homogeneously in epoxy during the curing mechanism.

2.5.6 Melt processing

Previous nanocomposite processing methods concentrated on chemical interactions to disperse nanoparticles in a polymer matrix; melt processing is a different method that relies more on rheological properties. When nanoparticles are added to a polymer melt, the resistance to flow of the polymer chains can aid in dispersion through shear forces. High viscosity results in higher shear forces when mixed, and these shear forces can be used to overcome the attractive forces that cause nanotubes to aggregate. Many groups have used melt-mixing as another processing method that utilizes polymer melt properties to disperse and distribute nanoparticles throughout the matrix [44, 63-65 76-79]. Sandler *et al.* [63] dispersed a CNT suspension in ethanol into epoxy resin and

stirred at 2000 rpm at 80ºC for 1 hour. After curing the samples were studied under SEM and found to have agglomerates, but smaller and less frequent than samples that were not suspended in ethanol and stirred under shear. Haggenmueller *et al.* [64] mixed SWNTs into PMMA using DMF and sonication. Additional samples were hot pressed repeatedly into films; optimal microscopy identified hot pressed samples to have homogeneous distribution while samples that did not undergo the melt mixing had large agglomerates and large voids present.

Extruders and batch mixers are common tools used in nanocomposite melt blending. Chen *et al.* [76] compared conventional extrusion with an ultra high shear extrusion method developed by the group, and found that the ultra high shear method was able to achieve good dispersion and distribution of MWNTs in poly(vinylidene fluoride) (PVDF) by mixing the materials at 200ºC for 4 minutes at 1000 rpm. The conventional extrusion samples exhibited aggregates and voids when mixed under similar conditions at only 100 rpm. Andrews *et al.* [77] studied the dispersion of MWNTs into four different polymer systems (polypropylene (PP), acrylonitrile butadiene styrene (ABS), polystyrene, high impact polystyrene (HIPS)) using a high shear mixer and found that adjusting processing conditions led to both good and poor morphology. Pötschke *et al.* [78] used a twin screw microcompounder to disperse MWNTs in polycarbonate (PC) and high density polyethelyne (HDPE)/PC blends. The study adjusted mixing speed and mixing time to determine that longer mixing times at lower speeds resulted in the best morphology, which exhibited no significant aggregates or clusters.

While MWNT dispersion using melt mixing methods has been achieved more readily, SWNT dispersion has proven to be more difficult. A batch mixer was used to

melt mix PP with purified SWNTs for 30 minutes by Bhattacharyya *et al.* and only a poor dispersion could be achieved [65]. The study did find, however, that even the poorly dispersed aggregates acted as nucleating agents for PP crystals. Moniruzzaman *et al.* [79] found that agglomerates were visible to the naked eye when SWNTs were sonicated in DMF, added to an epoxy resin and then sonicated again. However, the aggregates were dispersed and evenly distributed after the samples were mixed in a twin screw batch mixer for 1 hour at 100 rpm and room temperature.

2.6 Goal of dissertation

The work in this dissertation is concerned with processing and characterizing high performance polymer nanocomposites. Composite materials were selected for component properties, and a processing method was chosen to optimize processing time and efficacy. Homogeneous morphologies were obtained and resulting composites were characterized for polymer and nanotube network behavior with resulting properties. A business plan was also formulated, based primarily on the composite properties and the ability to produce the nanocomposite materials in kilogram and higher batch sizes.

CHAPTER 3

PROCESSING PETI-330 NANOCOMPOSITES

3.1 Introduction

Composites for use in high performance aerospace applications such as space exploratory vehicles, airframes, and propulsion require specialized properties in order to improve current designs. Potential improvements include increased strength and impact resistance, increased thermal stability, and environmental stability. Weight reduction could aid in energy conservation for propulsion performance, and enhanced electrical properties could help to shield vehicles through lightning strike mitigation and electromagnetic interference shielding. One way to achieve these properties is by using high temperature polymer systems with nanofillers creating multifunctional composites that exploit each component's properties. Carbon nanotubes offer inherent properties such as high mechanical strength and stiffness [33-35, 37, 80-81], thermal conductivity [82-84] and electrical conductivity [83, 85-86] that can lead to a lightweight material with enhanced characteristics. In this study, we investigated the processing of nanoparticles with PETI-330, a phenylethynyl-terminated imide [87], using melt mixing. Analysis of processing variables identified energy requirements for obtaining both good dispersion and good distribution of nanofillers in PETI-330. Through the adjustment of filler concentration and processing conditions and measurements of thermal and rheological properties, data were obtained that could be used in identifying a processing performance

relationship and producing a system with appropriate viscosity for resin transfer molding (RTM).

Polyimides (PIs), which account for many high performance polymer systems, are noted for their thermal and mechanical properties; however, they are generally difficult to process [88] due to small windows between the melting and curing or degradation temperatures; PIs are also resistant to many solvents, making solution processing difficult. Polyimide oligomers incorporating phenylethynyl end groups lead upon processing to crosslinked materials with high thermal stability [89]. These phenylethynyl-terminated imides (PETI) have become a focus of aerospace research because of the combined properties resulting in thermo-oxidative stability, high mechanical properties, and large processing windows that are generally not identified with other PIs [88, 90].

By adding nanotubes to a high performance polymer such as PETI, thermal and mechanical properties may be further enhanced. Producing a homogeneous dispersion of nanoparticles in polymer matrices, however, has proven to be more difficult than with larger particles due to strong interparticle forces that cause them to agglomerate. A number of studies have been performed to determine effective ways to achieve such a dispersion with nanotubes in thermoset polymers. Ghose *et al*. had success in preparing composites composed of a PETI resin and multiwalled carbon nanotubes (MWNTs) via dry mixing, *in situ*, and solution dispersion [89, 91-92]. Choi *et al*. dispersed carbon nanofibers in an epoxy resin *in situ* using sonication in a solvent [93]. The composites exhibited a homogeneous dispersion at loadings up to 10 wt.% and increased the glass transition temperature (T_g). Zhu *et al*. achieved good dispersion and particle integration by using a multistep processing protocol with chemical functionalization [62]. The

composite containing functionalized nanotubes exhibited better dispersion and mechanical properties than the corresponding composite containing pristine nanotubes.

The methods described above have been shown to be effective in dispersing nanotubes into thermosetting matrices; however, methods such as solution dispersion or ball milling may take hours or days to complete. In this research, we investigated a conventional thermoplastic polymer processing method, melt mixing, to reduce the processing time needed to produce nanoreinforced resins. Melt mixing is a desirable method for processing thermoplastic systems and has been successfully applied to the fabrication of thermoplastic nanocomposites. Andrews *et al.* [77] showed that melt mixing could be used to disperse MWNTs in a variety of matrices under relatively mild mixing conditions. Kasaliwal *et al.* [94] used a small scale twin screw extruder to prepare polycarbonate composites containing 1 wt.% MWNTs. Using electrical resistivity as a measure of dispersion, higher processing temperatures and motor speeds led to composites with the lowest resistivity and highest particle dispersion. Similarly, Krause *et al.* [95] varied the processing conditions for a small scale twin screw extruder mixing polyamide-MWNT composites and reported that improved dispersion was achieved with increasing energy. Shofner *et al.* [96] have shown that small ropes of single walled carbon nanotubes (SWNTs) may be dispersed by melt mixing to achieve improved mechanical properties. Zhang *et al.* [97] were able to achieve dramatic improvements in MWNT/nylon composites produced by melt mixing, achieving strength and modulus improvements of 120% and 115%, respectively, at 1 wt.% MWNTs. However, melt mixing can be a challenge with thermosets due to the possibility of crosslinking during processing. Once polymerization is initiated, viscosity increases as polymer chains begin

to extend and form networks, thus preventing further use of the system in fabrication methods that require low injection viscosities such as RTM or vacuum assisted resin transfer molding (VARTM). Because of the large processing window between the oligomer melting temperature and the gel temperature in PETI resins, there is an opportunity to use melt mixing with these systems [92].

In this research, we investigated the efficacy of melt mixing as a dispersion method of carbon nanofibers (CNFs) and MWNTs in PETI-330. By studying the torque and energy applied to a system along with the resulting filler and polymer behavior, the minimum torque for homogenous filler dispersion could be established. These values can be used to establish optimal processing conditions to achieve a desired composite morphology and properties. Mixed and unmixed materials were characterized using electron microscopy as well as changes in glass transition temperature and viscosity to assess MWNT dispersion and distribution, differential scanning calorimetry (DSC) before and after curing, and dynamic rheology measurements to simulate RTM processing. The results of this study indicated that melt mixing may be used to disperse and distribute MWNTs in PETI resins, MWNTs increase post-cure T_g when a good dispersion is achieved, and the viscosity of the nanocomposite resin is acceptable for RTM processing with an appropriate choice of MWNT loading.

3.2 Materials and Methods

Polymer nanocomposites containing PETI-330, from Ube Industries, Ltd., PR-24-PS CNFs from Pyrograf Products, Inc., and Elicarb PR0940 MWNTs from Thomas Swan

& Company were used for this study. Neat PETI-330 liquefies at approximately 180°C and has a post-cure T_g of 330°C as well as a low and stable melt viscosity that makes it an excellent candidate for conventional composite manufacturing methods such as RTM or VARTM [14-15]. The uncured resin is an odorless, light-yellow powder with a density of 1.3 g/cm^3 at room temperature. The Elicarb PR0940 MWNTs have diameters in the range of 10 to 12 nm and micron lengths with a bulk density of 1.7 g/cm^3 and a purity of 70-90%. The PETI-330 and MWNTs were used as received and the CNFs were cleaned using a method by Lozano *et al.* [98]. This method involved a five day reflux in methylene chloride followed by washing and a one day reflux in water.

Processing studies were performed to determine the effects of filler concentration and mixing energy on the morphology and properties of the resulting nanocomposites. In the first study, samples were prepared with 0, 0.5, 3, 5, and 10 wt.% CNFs as well as 0.2, 0.5, 0.8, 1, 3, 5 and 7 wt.% MWNTs at 188°C using the same time and motor speed processing conditions. In the second study, three additional batches of 0.5 wt.% MWNT/PETI-330 resin were each processed at 200, 215, and 230°C with the same motor speed, resulting in successively lower torque as the melt viscosity of the underlying resin decreased with increasing temperature. A third set of studies determined the efficacy of loading and steady state torque during mixing.

The processing protocol involved initial mixing of 50.0 g of the dry materials by simple shaking, followed by melt mixing using an internal mixer with roller blades operated by a Brabender Intelli-Torque drive unit. In the first study, the materials were mixed at 188°C for 12 minutes using a rotor speed of 60 rpm. In the second study, the residence time and rotor speed were 12 minutes and 60 rpm, respectively, while the

temperature was adjusted to 200, 215, and 230°C. In these studies, the mixer was charged with material during the first three minutes and after the material was fully liquefied, the mixing torque attained an approximately constant value referred to as the steady state torque. The steady state torque value was dependent on the mixing speed, mixing temperature, and concentration used. The entire mixing torque curve was used to calculate the mixing energy for each batch in order to compare the materials processed in both studies and correlate the processing data with the material morphology and properties. The mixing energy was obtained using the following equation:

$$Mixing\ Energy = \int (T_q * s)\, dt \qquad (3.1)$$

where T_q is torque, s is motor speed, and t is time.

The third study concentrated on determining the efficacy of the loading and steady state portions of the torque mixing curve in dispersing nanoparticles. The importance of the steady state region was determined by mixing a batch of 0.5 wt.% MWNT at 188°C and 60 rpm, but terminating the mixing process once steady state was reached. The significance of specific torque values was examined by mixing an additional 0.5 wt.% MWNT composite at 200°C, but with an increased mixing time that allowed the energy of the steady state region to match the energy of the steady state region of the same composite mixed at 188°C. The loading region was examined by mixing another 0.5 wt.% MWNT composite at 188°C and 60 rpm for 12 minutes but adding the MWNTs to the mixing bowl only after the PETI-330 reached steady state. The

morphology of all of these composites was compared to determine the mixing processes that most significantly affected nanoparticle dispersion and distribution.

The materials were characterized by electron microscopy, differential scanning calorimetry (DSC), and rheology after processing. A LEO 1530 scanning electron microscope (SEM) was used to image fractured surfaces in order to determine the distribution and dispersion of MWNTs in the uncured resin. The neat resin and nanocomposites were sputter coated with gold to facilitate imaging with the exception of MWNT composite loadings of 1 wt.% or higher, which possessed sufficient inherent conductivity to be imaged without coating.

A TA Instruments Q200 DSC was used to measure the thermal behavior of 5 mg samples of each material processed. Two studies were completed to determine pre- and post-cure behavior. In the first study, several specimens from each batch were analyzed for pre-cure T_g with a temperature sweep from 40 to 420°C at a rate of 10°C per minute. In the second study, T_g was measured after fully curing the material at 371°C for 60 minutes, cooling to room temperature, and completing another temperature sweep.

Rheology was used to understand the feasibility of processing select MWNT composites in methods such as RTM. Dynamic experiments were conducted using parallel-plate geometry with a TA Instruments AR-G2 rheometer. Samples were prepared by powdering the material and then pressing the material at 13,000 psi for 2 minutes at room temperature into a 25 mm diameter disk. A temperature sweep was performed on each sample with 20% strain at a constant frequency of 100 radians per second. These conditions were chosen to simulate RTM injection conditions. Laboratory testing has shown that material can be used in RTM if the viscosity is below 2.0 Pa·s [99].

3.3 Results

3.3.1 Torque, energy, and morphology for filler and process temperature studies

As shown in Figures 3.1-3.3, the features of the torque curve generated during melt mixing were dependent on the CNF and MWNT loadings and processing temperatures. The additional spike in the torque for the 1 wt.% MWNT sample shown in Figure 3.2 was caused by material caught in the loading chute. Overall, increasing nanoparticle concentration and decreasing processing temperature increased the values of the steady state torque and the mixing energy. These trends were attributed to an expected increase in resin viscosity with increasing nanoparticle concentration, particularly for MWNT composites, and decreasing processing temperature. By comparing torque and energy measurements with microscopy observations, targeted torque or energy for specific morphologies could be established.

The energy values calculated from the torque curves described the total amount of work done to disperse and distribute the particles. Further analysis allowed the total energy to be divided into two mixing regimes, loading and steady state energy, as shown in Figure 3.4. The loading region is defined as the material loading (torque spikes) and the transient decreasing torque values indicating melting. The starting point for the steady state region of each graph was taken as the point where the torque consistently changed by approximately 2% or less over a 20 second period. The 0.5 wt.% sample mixed at 230°C exhibited a much lower viscosity than the other samples and lead to more variability in the observed torque. Initiation of the steady state region of this sample was

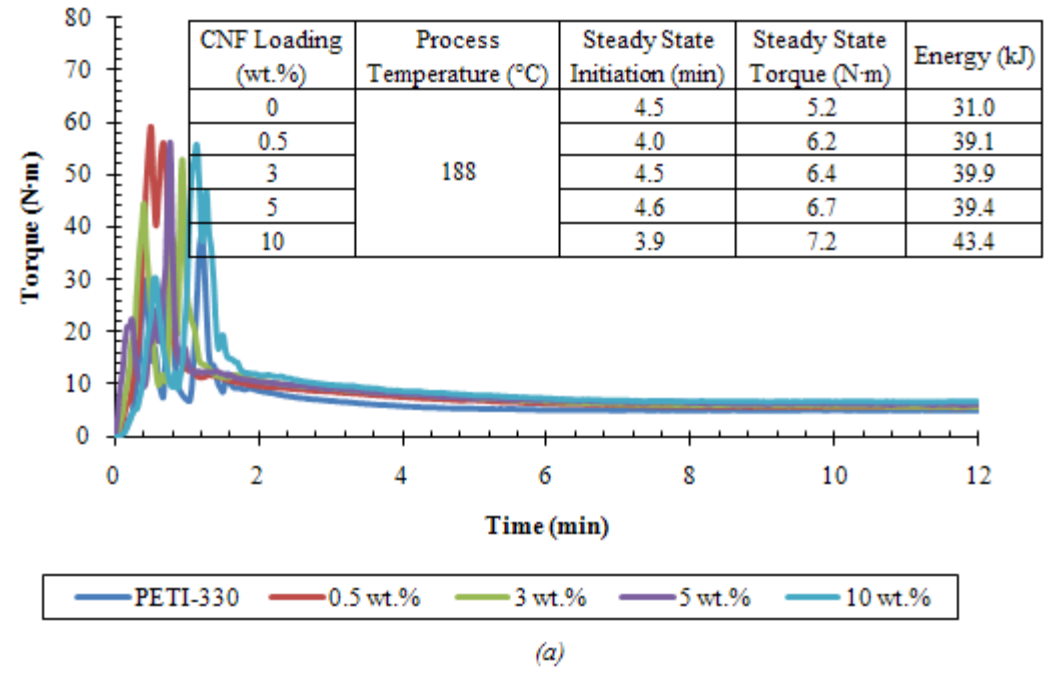

CNF Loading (wt.%)	Process Temperature (°C)	Steady State Initiation (min)	Steady State Torque (N·m)	Energy (kJ)
0	188	4.5	5.2	31.0
0.5		4.0	6.2	39.1
3		4.5	6.4	39.9
5		4.6	6.7	39.4
10		3.9	7.2	43.4

(a)

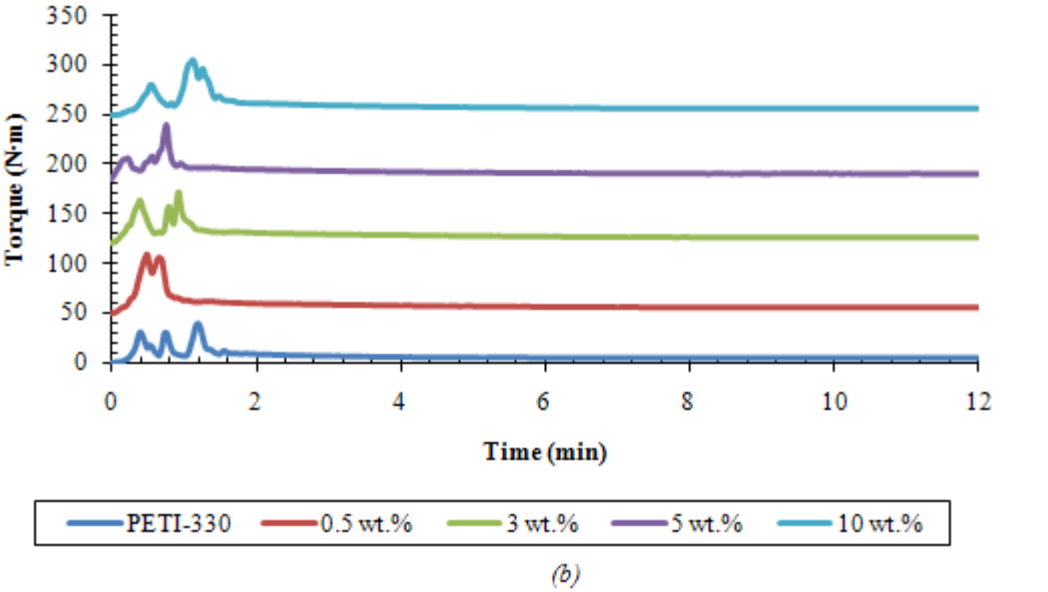

(b)

Figure 3.1: Torque measurements taken during the melt mixing process for varying CNF content (a), offset for easier comparison (b).

MWNT Loading (wt.%)	Process Temperature (°C)	Steady State Initiation (min)	Steady State Torque (N·m)	Energy (kJ)
0	188	4.5	5.2	31.0
0.2		4.5	5.8	37.9
0.5		5.2	5.7	33.0
0.8		5.4	5.4	32.8
1		5.5	7.1	39.6
3		5.5	8.9	49.9
5		4.9	11.0	63.0
7		5.5	13.1	74.9

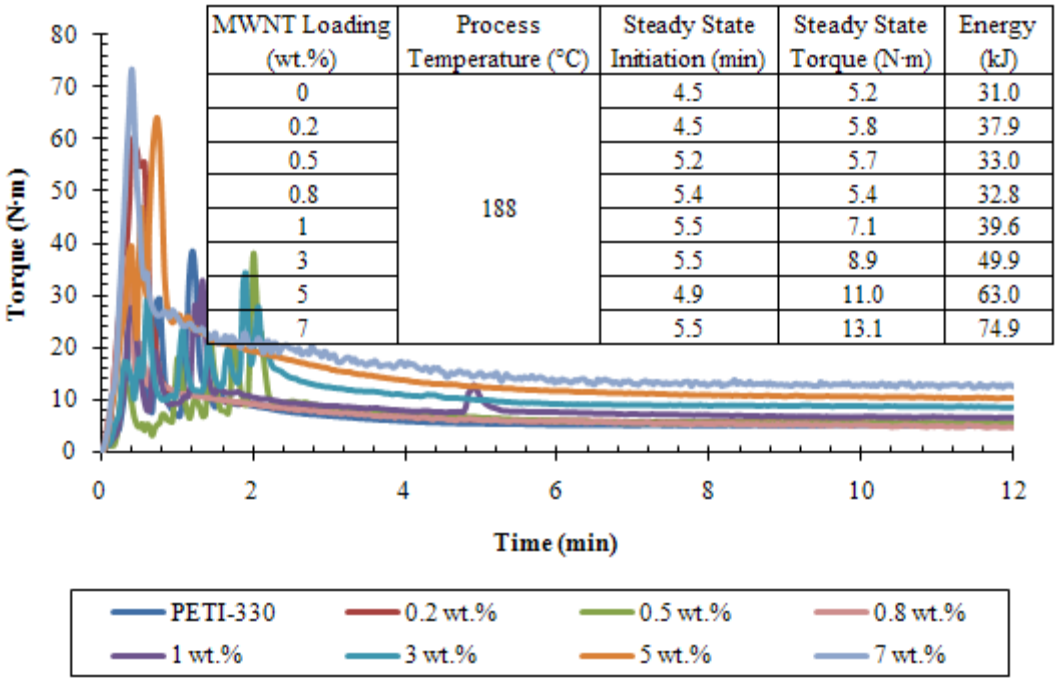

(a)

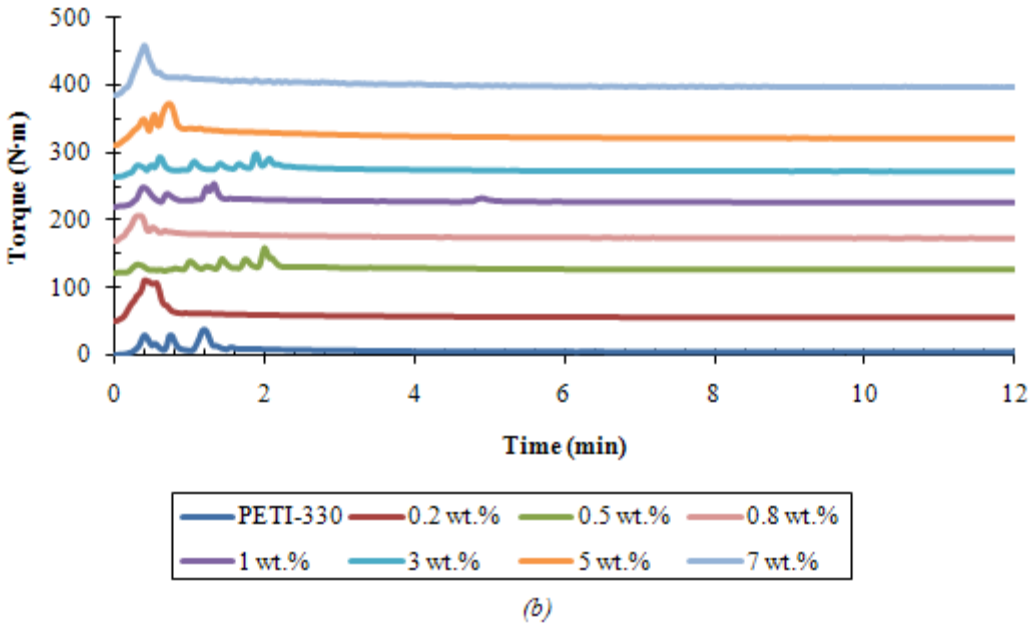

(b)

Figure 3.2: Torque measurements taken during the melt mixing process for varying MWNT content (a), offset for easier comparison (b).

MWNT Loading (wt%)	Process Temperature (°C)	Steady State Initiation (min)	Steady State Torque (N·m)	Energy (kJ)
0.5	188	5	6.6	32.4
	200	5	3.6	20.4
	215	4.5	1	7.0
	230	3	0.3	2.0

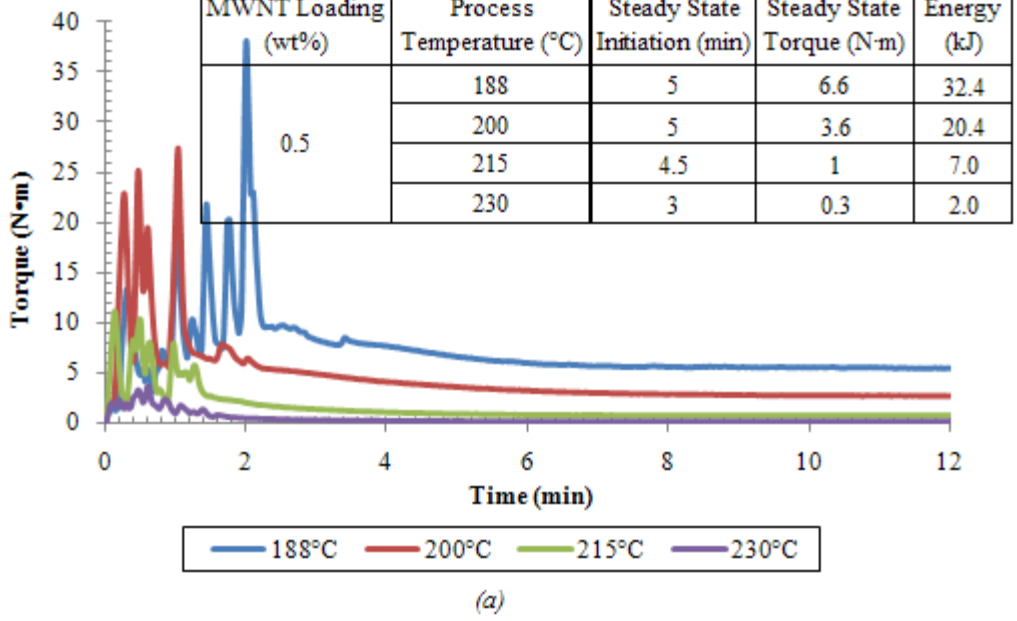

(a)

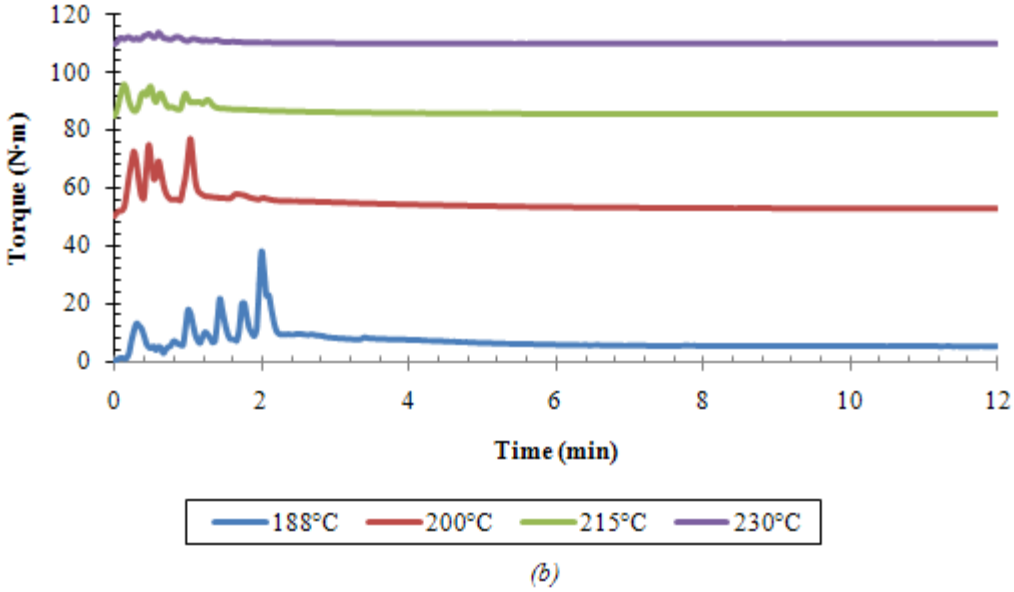

(b)

Figure 3.3: Torque measurements taken during the melt mixing process for various process temperatures of 0.5 wt.% MWNT composites (a), offset for easier comparison (b).

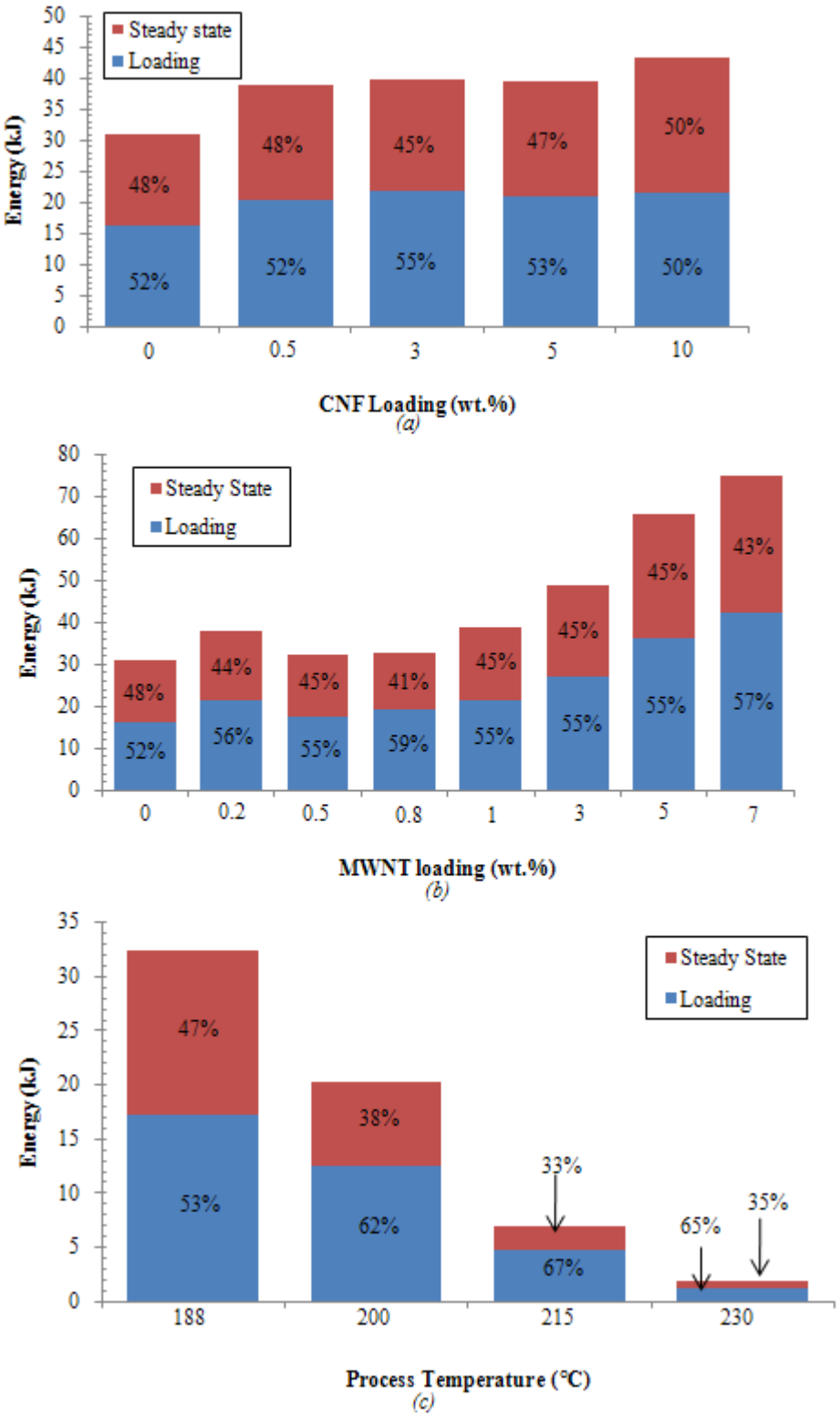

Figure 3.4: Energy contributions to mixing during loading and steady state for varying CNF content (a) MWNT content (b) and processing temperature (c). Process temperatures studies were performed with 0.5 wt.% MWNTs.

taken as the point where torque changed consistently by less than 5% over a 20 second period. Both studies showed that loading was the dominant contribution to total energy for all materials. From the particle loading study it was found that the total mixing energy increased from 3.1 kJ for the neat resin to 43.4 kJ for 10 wt.% CNF and 74.9 kJ for the 7 wt.% MWNT loading. The CNF composites had very little change in energy and energy contributions for lower loadings, although the 10 wt.% loading did show an increase. The MWNT composite energies were more sensitive to increases in filler loading; however, for both fillers, the percentage contribution to the total energy remained similar.

From the mixing temperature study, the total mixing energy decreased as mixing temperature increased, and the loading energy contribution to the total energy increased from 55% at a mixing temperature of 188°C to 64, 69, and 68% for samples processed at 200, 215, and 230°C, respectively. At processing temperatures of 200°C and above, there was a 5% or less change in the ratio of loading and steady state contributions to the total energy. This indicated that, as the melt viscosity of the PETI-330 decreases, total energy contributions can be roughly estimated as 2/3 from loading and 1/3 from steady state for the given mixing conditions. Overall, the data indicated that, like the steady state torque, the total applied energy increased with increasing filler content or decreasing processing temperature.

SEM imaging was used as one method to assess the efficacy of processing by observing nanoparticle dispersion and distribution in the PETI resin. Good dispersion was indicated by the absence of agglomerates or bundles, while good distribution was indicated by homogeneous nanotube concentration over the entire surface. As an example, a sample with agglomerates uniformly spaced throughout the polymer matrix

would be considered to have poor dispersion but good distribution. In this work, we aimed to achieve both good dispersion and good distribution of nanofillers through changing processing parameters.

In addition to the physical mixing provided by melt mixing, interfacial interactions aided in achieving dispersion in this system. Force-field-based molecular mechanics and density functional theory (DFT) calculations have shown that PETI-330 can wrap and form charge transfer complexes with carbon nanotubes providing a driving force for dispersion [100]. This result is qualitatively consistent with the study of other systems conducted by the same authors, such as a helical assembly of flavin interacting

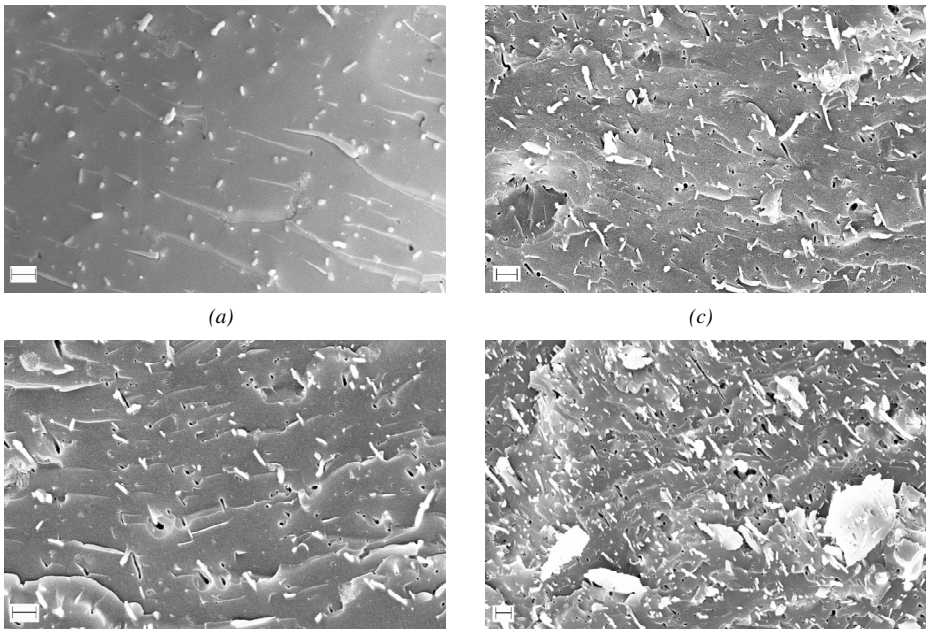

Figure 3.5: SEM images for melt mixed (a) 0.5 wt.% (b) 3 wt.% (c) 5 wt.% and (d) 10 wt.% loadings of CNFs in PETI-330. All samples show good dispersion and good distribution. Scale bars represent 1 μm.

with carbon nanotubes [101] or polymers interacting with carbon nanotubes and graphene nanoribbons [102]. The results presented here indicated that some threshold of energy was required to attain homogeneous dispersion and distribution. Figure 3.5 shows good dispersion and good distribution for all CNF composites. It was assumed that MWNTs would be more difficult to disperse so homogeneously due to their smaller sizes and larger aspect ratios which lend to higher attractive forces. SEM images confirmed that MWNTs were more difficult to disperse for higher loadings. Figures 3.6 (a)-(d) show uniform distribution with increasing MWNT content from 0.2 to 0.8 to 3 to 7 wt.%, respectively. Lower loadings of 0.2-0.8 wt.% exhibited similar behavior with good distributions of dispersed and isolated nanotubes. Higher loadings of 1-7 wt.% also had similar behavior; they showed good distributive properties, however, they also exhibited

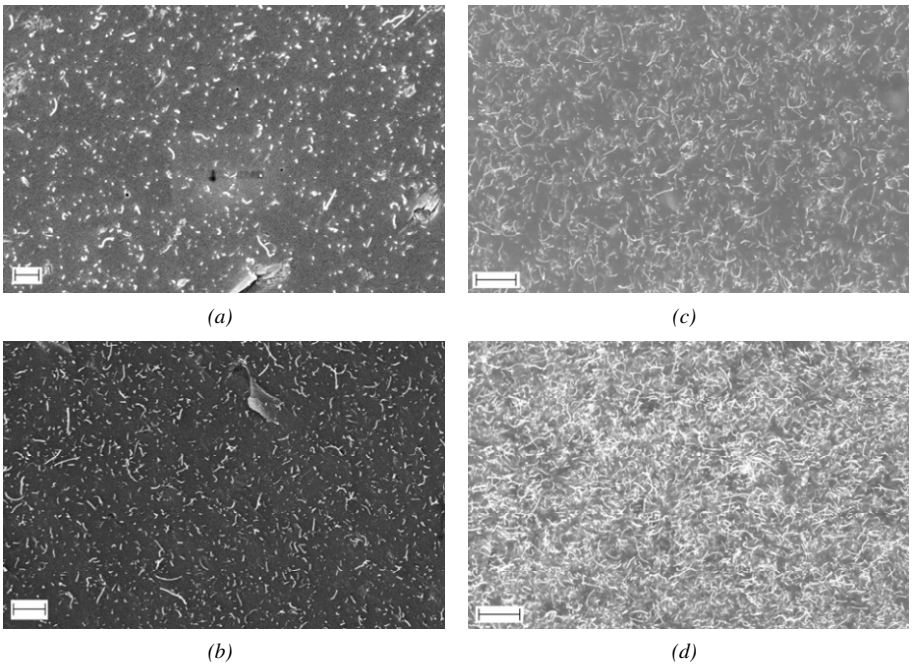

Figure 3.6: SEM images for melt mixed (a) 0.2 wt.% (b) 0.8 wt.% (c) 3 wt.% and (d) 7 wt.% loadings of MWNTs in PETI-330. All samples show good dispersion and good distribution. Scale bars represent 1 μm.

some agglomerates wetted with the PETI resin. These agglomerates suggested that as the MWNT content increased and the polymer content decreased, the processing conditions were not adequate to fully integrate the components. From these observations, the 0.5 wt.% MWNT loading was chosen as the best sample for examining the effects of processing temperature.

As shown in Figure 3.7, a comparison of similar images from 0.5 wt.% MWNT samples processed at increasing temperatures can be made. As the temperature increased from 188 to 230°C, agglomeration also increased. Compared with the data in Figure 3.3, which shows that the torque and energy decreased with increasing temperature, the viscosity of the sample had decreased to a degree that impacted mixing efficiency.

It was apparent that process temperature variation caused changes in both

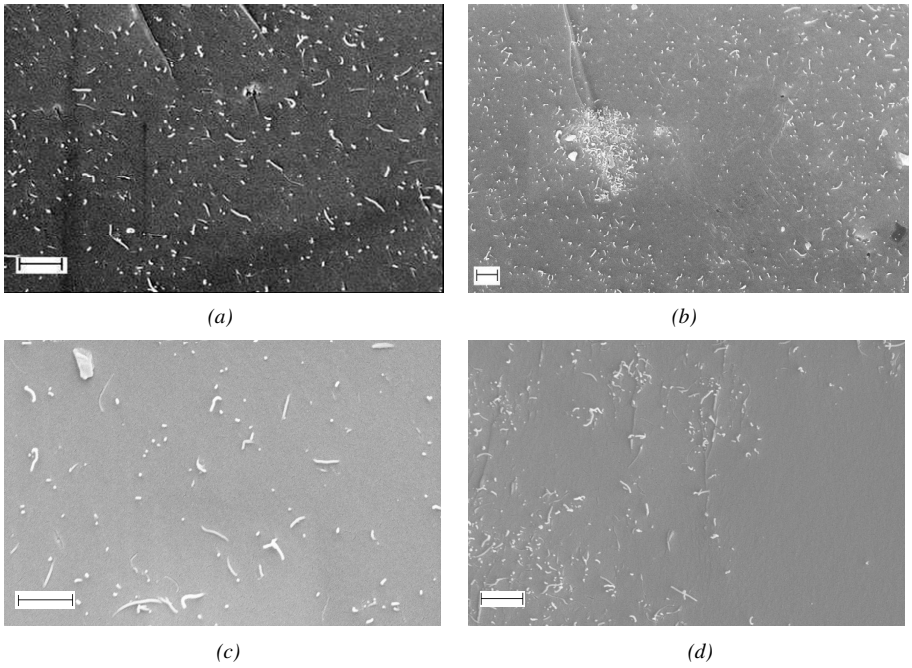

Figure 3.7: SEM images of 0.5 wt.% MWNT morphology when mixed at 188°C (a), 200°C (b), 215°C (c), and 230°C (d). Scale bars represent 1 μm.

dispersion and distribution. Agglomerates were observed once the melt mixing temperature was increased to 200°C. The distribution, however, was not affected until the temperature was raised to 230°C. By comparing with the values in Figure 3.3, it can be observed that a minimum energy of 32 kJ and steady state torque of 6.6 N·m is necessary for good dispersion at similar loadings of PETI-330/MWNT systems. The energy contributions during processing indicated that dispersion, which worsened between 188°C and 200°C, improved when the steady state energy contributions were increased. As previously noted, process temperatures above 188°C yielded a steady state energy that was approximately 1/3 of the total energy; at 188°C, where dispersion was homogeneous, steady state energy contributions were closer to 1/2 of the total energy. This indicated that dispersion can be improved through additional steady state processing after loading. Similarly, a minimum energy of 7 kJ and steady state torque of 1 N·m is suggested for good distribution. The effect of steady state torque values and their combination with energy regime contributors was examined in the following study.

3.3.2 Loading and steady state energy contribution studies

The third study included a set of experiments to determine the efficacy of the loading and steady state energy contributions. The mixing curves of these additional samples are shown in Figure 3.8. In one experiment, a 0.5 wt.% MWNT sample was mixed at 188°C and 60 rpm, but mixing was terminated once the torque readings reached steady state. This occurred after 5.4 minutes of mixing with a torque of 6.5 N·m. An SEM image in Figure 3.10 (a) confirmed that the morphology was not as homogeneous as the

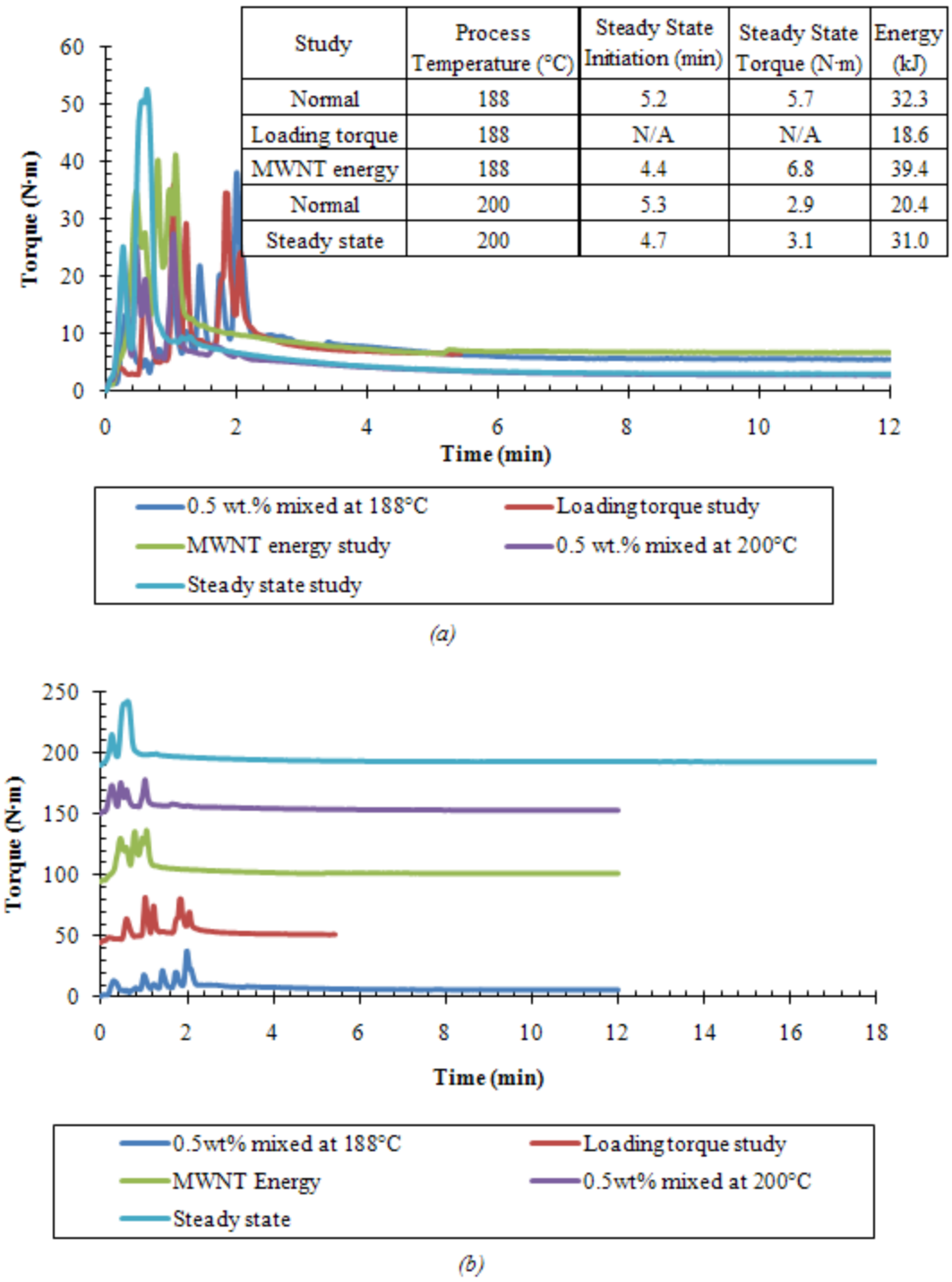

Figure 3.8: Torque measurements taken during melt mixing for mixing studies performed to determine the effects of the loading and steady state regimes on MWNT morphology (a), offset for easier comparison (b).

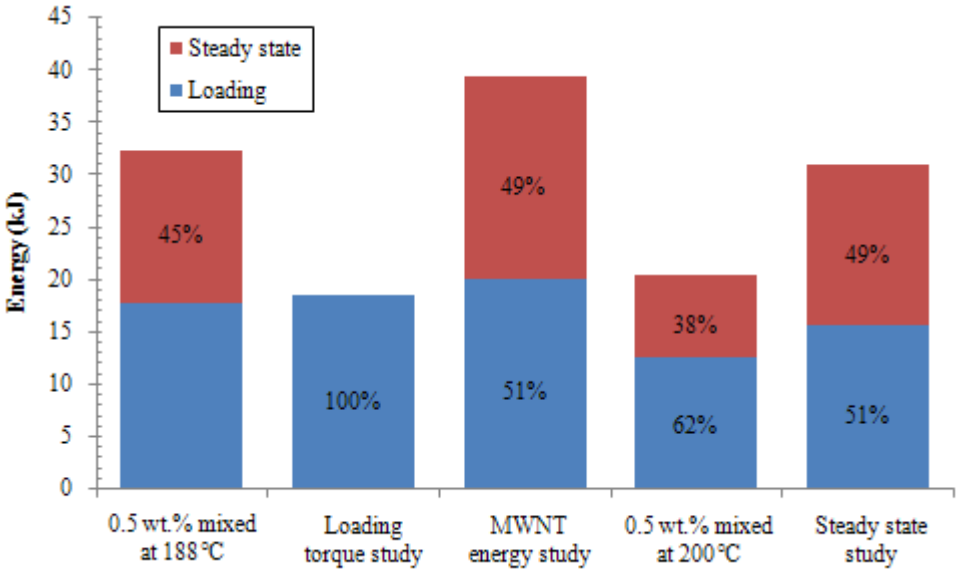

Figure 3.9: Energy calculations for mixing studies performed to determine the effects of the loading and steady state regimes on particle morphology.

same sample mixed for 12 minutes; distributive properties were maintained, but agglomerates were identified throughout the sample. These results reinforced the importance of the steady state mixing step in achieving dispersion in the nanocomposite system.

In order to study the effects of the loading energy, an additional 0.5 wt.% MWNT sample was mixed at 200°C at 60 rpm. Mixing was terminated after the steady state energy equaled to that of the steady state region of the 0.5 wt.% sample mixed at 188°C, or 15.1 kJ, as seen in Figure 3.8. This took 18 minutes. This experiment was based on the observations that the 0.5 wt.% sample mixed at 188°C had good dispersion and distribution while the one mixed at 200°C had only good distribution. By prolonging mixing on another sample mixed at 200°C it could be determined if the steady state

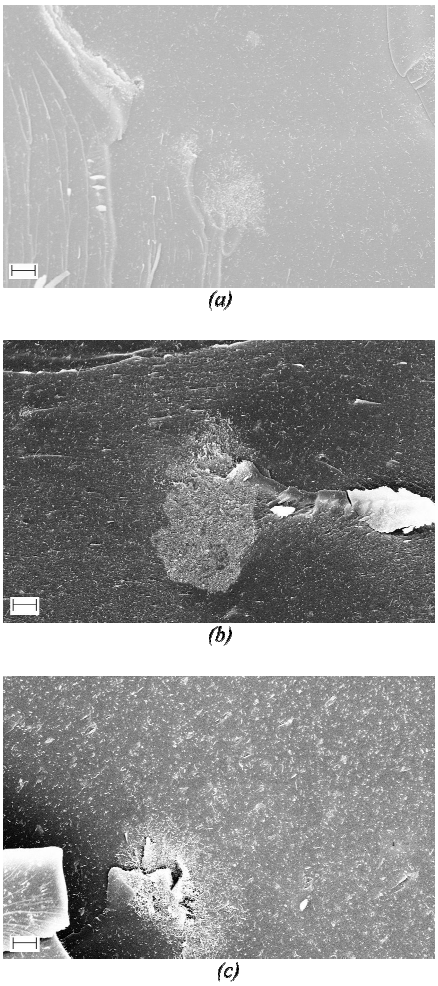

Figure 3.10: SEM images of 0.5 wt.% MWNT morphology in PETI-330 for (a) loading torque contributions study (b) steady state contributions study and (c) MWNT filler contributions study. Scale bars represent 3μm.

region was the main contributor for dispersion or if the magnitude of the loading region torque or energy was more significant. Figure 3.10 (b) shows that the resulting sample had agglomerates, indicating that the energy of the steady state region was not the main force breaking up agglomerates. Instead, the loading region and absolute torque values were the more significant contributors. The sample with good dispersion had 17.2 kJ during loading and steady state torque of 5.7 N·m while the current samples mixed at 200°C had only 16.1 kJ and a steady state torque of 3.1 N·m.

A final experiment was completed to determine the contribution toward energy from the MWNTs, and also the significance of the loading region of the polymer toward the morphology of the nanocomposite. In this study, neat polymer was melt mixed at 188°C at 60 rpm until it reached steady state, which took approximately 5.2 minutes. At that time, MWNTs were added to the system; total mixing time was 12 minutes and the end product had 0.5 wt.% filler content. From the torque curve in Figure 3.8 it could be seen that the addition of MWNTs caused a 0.7 N·m spike in the torque values. The steady state torque increased by only 0.2 N·m after the addition of the MWNTs. SEM images in Figure 3.10 (c) indicated good particle distribution although the presence of agglomerates, indicating that the loading region with the PETI-330 polymer significantly aided in dispersion. The small jump in torque caused by the MWNTs was not significant enough to break up MWNT agglomerates.

The process temperature study showed that loading energy contributions of approximately 67% resulted in good distribution but not good dispersion, while loading contributions closer to 50% resulted in good dispersion and distribution. However, both the MWNT energy and steady state studies exhibited loading energy contributions of

51% as shown in Figure 3.9, but with poor dispersion. This indicated two important factors in mixing: the fillers underwent significant dispersion during the loading stage that did not occur during steady state, and the value of the applied torque was more important than the overall energy. The loading torque study showed that the steady state regime was the third important factor in creating homogeneous morphology and that good dispersion was not possible without it. These studies showed, then, that a good balance of loading and steady state contributions alongside a high enough torque would result in well dispersed composites, and a loss in any of these would be a loss in morphological properties.

3.3.3 Thermal analysis

DSC tests were performed to determine the effects of processing and particle loading on the pre-cure T_g. From the results of the loading study shown in Table 3.1, the effects of processing are shown by comparing the as-received PETI-330 resin with mixed PETI-330 resin. The neat unmixed material had a pre-cure T_g of 145°C while all samples mixed at 188°C were 3-4°C lower regardless of nanotube loading. PETI-330 exhibits a polymodal molecular weight by gel permeation chromatography (GPC) [103] which may be segregated in the as-received material, with melt mixing giving a homogenous sample with a lower energy necessary for the segmental motion leading to the pre-cured T_g.

Isothermal studies were performed to identify curing and post-cure T_g behavior. The values for the cured resin T_g are shown in Table 3.1. The measured T_g of neat unmixed material was 324°C. Processing the neat material resulted in a 2°C increase with a post-

Table 3.1: Glass transition temperatures for various particle loadings and process temperatures.

Filler	Loading (wt.%)	Process temperature (°C)	Pre-cure T_g (°C)			Post-cure T_g (°C)		
			Avg	+	-	Avg	+	-
None	0	N/A	145	1	1	323	2	1
	0	188	142	1	1	327	2	3
CNF	0.5	188	142	0	1	321	2	4
	3		141	1	1	319	3	3
	5		141	1	1	325	1	1
	10		141	0	0	333	1	1
MWNT	0.2	188	141	1	1	333	0	0
	0.5		141	1	0	341	1	2
	0.8		141	1	1	340	3	3
	1		142	1	0	340	3	2
	3		142	1	1	338	3	2
	5		144	0	0	341	0	0
	7		142	3	3	342	2	2
	0.5	188	141	1	0	341	1	2
	0.5	200	144	0	0	336	4	2
	0.5	215	145	1	2	337	1	1
	0.5	230	143	2	1	330	3	2

cure T_g to 326°C. Low loadings of CNFs (0.5-5 wt.%) resulted in a decrease in T_g while the highest loading of 10 wt.% exhibited a T_g of 333°C. As MWNTs were added to the system at a mixing temperature of 188°C, a loading of 0.5 wt.% led to a 16°C increase in T_g relative to the neat mixed material at 341°C. Additional loadings did not exhibit the same drastic increase in T_g with 1 wt.% at 340°C and 3 wt.% at 338°C. The close proximity of T_g for the three loadings suggests a thermal property threshold value. The increase in T_g with nanotube addition indicated that more thermal energy was required for chain segmental motion. The MWNTs acted as rigid reinforcements and, due to the high surface area interactions, resulted in an increase in T_g. CNFs, however, had the opposite effect at lower loadings, most likely another result of their large particle size. The CNFs were too large to effectively reduce chain motion in PETI-330 matrix until a more sufficient loading was added to the system. The threshold behavior seen in the MWNT composite post-cured T_g could be due to a decreased amount of available nanotube surface area occurring during curing or changes in the polymer network structure with respect to the neat resin. Additional studies to determine the evolution of nanotube dispersion/distribution and crosslink density in mixed and cured samples at various particle loadings are further explored in Chapter 6.

The thermal behavior for the process temperature study composites in Table 3.1 showed that, unlike the pre-cure trend, post-cure T_g decreased with increasing process temperature but still remained above the neat PETI-330 T_g. The highest T_g was observed for the 0.5 wt.% sample, 341°C, which was processed at 188°C. As the process temperature was raised to 200, 215, and 230°C, the T_g dropped to 336, 337, and 330°C, respectively. The 42°C temperature span in processing temperature resulted in a 4%

decrease in the T_g. This decreasing T_g with increasing process temperature correlated to the nanotube dispersion state and available surface area, where T_g decreased with decreasing nanotube dispersion.

3.3.4 Rheological behavior

Rheological studies were completed on select MWNT composites to determine if the composites could be used in RTM applications. MWNT composites were selected because torque curves in Figures 3.1 and 3.2 indicated torque sensitivity to particle loading while CNFs did not; torque values at similar process conditions can be indicative of viscosity values, so MWNT composites presented a more thorough study. In rheological studies each nanocomposite exhibited different flow properties due to the presence of varying amounts of MWNTs and possible polymerization during processing. While Ghose *et al*. have reported that no significant crosslinking occurred in neat PETI-330 during rheology measurements performed at 100 radians per second and held at temperatures as high as 280°C for 2 hours [92], it is possible that frictional forces with higher processing temperatures may initiate polymerization in some composites. The minimum viscosities for 0.5, 1, and 3 wt.% MWNT composites are given in Figure 3.11 (a) and (b). The viscosity for the neat material was too low for the rheometer to make accurate measurements at 100 radians per second, so only composite data are reported here. The minimum viscosity increased in a linear fashion with respect to MWNT loading, indicating that the impact of the small numbers of agglomerates observed in 1 and 3 wt.% MWNT/PETI-330 materials was low at this high measurement frequency.

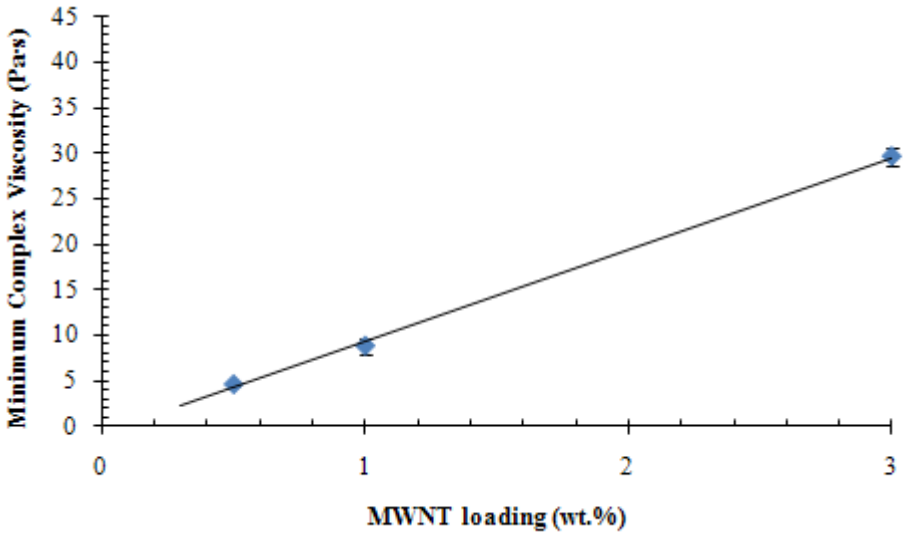

(a)

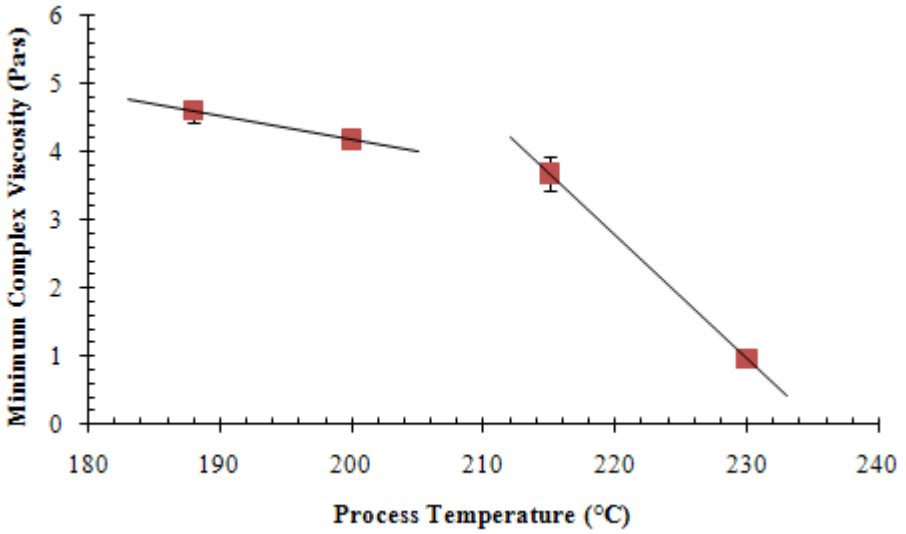

(b)

Figure 3.11: Minimum complex viscosity as a function of (a) MWNT content and (b) processing temperature. Lines are shown as a visual guide on the graphs.

Lower measurement frequencies would be expected to show a different trend that would be more sensitive to the dispersion achieved and network formation. Other results in the literature have seen evidence of rheological network formation through frequency-independent dynamic moduli values at low frequency ranges [104-106]. However, the frequency chosen for this study was chosen to simulate RTM, which is higher and outside the region of frequency-independent behavior, so conclusions concerning MWNT network formation in these materials could not be made from these data. Chapter 4 examines network formation in the MWNT composites.

The processing temperature study showed that the value of the minimum viscosity measured during the rheology experiments decreased as the sample processing temperature increased, correlating to the dispersion and distribution behavior observed with SEM and T_g values. Unlike the MWNT loading study where more subtle changes in dispersion were seen, the larger scale agglomerates and decreasing distribution impacted the viscosity value at this measurement frequency. When distribution was largely maintained (188, 200, and 215°C), the drop in viscosity was roughly linear, but when distribution suffered at the highest processing temperature, the minimum viscosity decreased by 89% with respect to the sample melt mixed at 188°C.

For all composites, a viscosity of 2 Pa·s or less is required for RTM processing. In the case of the studied sample, the only composite to meet this requirement was the 0.5 wt.% loading mixed at 230°C with poor morphology. Even poor morphological properties may result in increased neat properties, as seen in T_g behavior, so this composite could still be a good candidate. Additionally, lower particle loadings may lead to a minimum viscosity at or below the 2 Pa·s threshold.

3.4 Conclusion

Melt mixing was used to make polymer nanocomposites with controlled morphology by using CNFs and MWNTs and PETI-330. Process energy was used as a tool for understanding particle morphology and determining the energy and steady state torque needed for obtaining homogeneous dispersion. The morphology affected nanocomposite properties, and the dispersion and distribution could be changed by adjusting processing conditions. Thermal analysis showed that CNFs impeded network formation while MWNTs acted as physical crosslink points due to possible strong interactions with resin molecules, increasing the post-cure T_g from that of the neat material subjected to melt mixing in all composite samples. The maximum T_g increase was found at the 0.5 wt.% MWNT loadings. The increase in processing temperature showed a decrease in T_g when compared to samples with the same nanotube loading, attributed to the presence of agglomerates. Rheological analysis showed that viscosity increased with MWNT loading and decreased with increasing mixing temperature. It was also shown that the processing caused no significant curing using the specified temperature windows. Results from this study showed that it is possible to use melt mixing with thermosets and nanoparticles to create a homogeneous nanocomposite for use in composite fabrication.

CHAPTER 4

NETWORK BEHAVIOR OF PETI-330/MULTIWALL NANOTUBE COMPOSITES

4.1 Introduction

Recent advances in polymer composite technology have been through the use of nanofillers, which possess similar surface areas at low loadings as higher loadings of larger filler particles. It is through these large surface areas that polymers interact with the filler particles and experience polymer enhancement. Carbon nanotubes (CNTs) are a noted type of nanofillers for their high mechanical strength and stiffness [33, 35, 37, 80-81, 107], thermal conductivity [82-84], and electrical conductivity [83, 85-86]. CNTs have diameters ranging from 1.2-1.4 nm for singlewall nanotubes (SWNTs) [27] or 1.4-100 nm for multiwall nanotubes (MWNTs) [28] with micron lengths, resulting in large aspect ratios. The high surface areas are available through these large aspect ratios, and only small quantities of CNTs are required to enhance composite properties.

However, the large aspect ratio also results in strong attractive forces that cause the CNTs to aggregate together, potentially reducing the area available for polymer-particle interactions. Several methods for reducing aggregation in nanotube composites have been used, including the use of surfactants [55, 68-69], particle functionalization [44, 59, 70], *in situ* polymerization [63-64, 72], or melt processing [64, 77-78, 108]. All of these methods have shown success, but changes to system chemistry can also result in restricted property enhancement. To better understand the interaction mechanisms of

CNTs and polymer chains, an effective dispersion method that makes minimal changes to the actual materials is needed.

CNTs can enhance a polymer matrix with their strong mechanical properties through stiffening effects that aid in increasing elasticity, with their thermal properties by reducing long-range polymer motion at raised temperatures, or with their electrical properties by adding a conducting element to an insulating matrix. These enhancements require minimum nanotube concentrations, however, to have a significant effect. In some cases, nanotubes sparsely spread through a polymer matrix grants an improvement in properties. Other cases require a high concentration of nanotubes that interact with each other. In this way, nanoparticle network formation is an important characteristic to understand when designing polymer nanocomposites. The key aspect to network formation is the percolation threshold, which is the lowest filler concentration where a complete network of interactions exists. The type of interactions can be between a range of composite components such as polymer-particle or particle-particle. Nearly all percolation thresholds are dependent on particle morphology; some are specific to certain particle-polymer systems while others are more universal. When determining universalities, one should consider dimensions and other general properties of the studied systems.

Many studies have concentrated on reducing the percolation threshold for nanofilled resins. Epoxy systems have achieved thresholds on the order of 10^{-3} wt.% [75, 109-110] while thermoplastic systems have had minimum thresholds on the order of 10^{-2} wt.% [77, 108, 111-112]. Sandler *et al.* dispersed CVD MWNTs into an epoxy precursor using shear intensive stirring; electrical conductivity experiments estimated the electrical

percolation threshold to be 0.0025 wt.% [109]. A similar method was used by Martin *et al.* with CVD MWNTs of two lengths [75]. The group estimated a lower percolation threshold of 0.0021 wt.% for shorter nanotubes (10 μm) and a threshold of 0.0039 wt.% for longer tubes (43 μm) [75]. Bryning *et al.* calculated a similar percolation threshold for aggregated SWNTs in epoxy as 0.0052 vol.% or 0.01 vol.% for dispersed SWNTs in the same system [110]. Modeling by Garboczi *et al.* predicted percolation thresholds in the range of 0.12-0.7 vol.% for randomly dispersed needles with aspect ratios ranging from 100 to 500 [113]. Overall these studies show that percolation thresholds depend on the filler particles as well as their morphology within the system.

In this work, the network formation of MWNTs in uncured and cured imide resin was studied. The MWNT network was characterized rheologically and electrically as well as through a modeling technique to understand polymer-particle and particle-particle interactions within a thermosetting system.

4.2. Materials and methods

The nanocomposites processed and characterized in this research were comprised of PETI-330, a phenylethynyl-terminated imide oligomer manufactured by Ube Industries, Ltd., and Elicarb PR0940 MWNTs from Thomas Swan & Co., Ltd. PETI-330 has a reported melting temperature of approximately 185°C and a post-cured glass transition temperature (T_g) of 330°C. The MWNTs had diameters of 10-12 nm. Both composite precursors were used as-received.

Nanocomposites were made using the melt-mixing method from Chapter 3. Nominal 50 gram batches of material were melt-mixed in an internal mixer with roller blades operated by a Brabender Intelli Torque drive unit. The melt mixing parameters used were a mixing temperature of 188°C, a mixing speed of 60 rpm, and a residence time of 12 minutes. The residence time included sample loading. Composite samples containing 0.0, 0.2, 0.5, 1.0, 3.0, 5.0, and 7.0 wt.% MWNTs were mixed and then cured using a custom-built three piece mold. The curing was accomplished in three steps. The material was initially heated in a press to 288°C with only the bottom two mold pieces assembled. After the material was completely liquefied, the press temperature was increased to 343°C, and the material was allowed to gel before adding the top plate with 9 MPa pressure. The samples were cured at this temperature and pressure for 4 hours before allowing to air-cool for testing. All conductivity samples were then cut using a Buehler Isomet diamond saw. The MWNT dispersion attained was observed after mixing and after curing using a LEO 1530 scanning electron microscope (SEM) to image fracture surfaces. Samples were brittle enough to create a fracture surface using hand strength. Cured samples and lower loadings (0.2 wt.% and 0.5 wt.%) of uncured samples were sputter coated with gold to prevent sample charging. As observed previously in Chapter 3, higher MWNT loadings in the uncured PETI had sufficient inherent conductivity to be imaged without coating.

The MWNT network structure in the composites was characterized after mixing and after curing using dynamic rheological measurements and impedance spectroscopy, respectively. The data obtained from both methods were fit to a percolation model to understand the changes in network behavior as a result of curing. For the rheological

measurements, a TA AR2000EX parallel plate rheometer was used to measure the storage modulus (G') and the loss modulus (G'') of the composite samples. Energy stored is reflected in G' while energy lost due to dissipation is reflected in G''. Uncured sample materials were powdered and pressed into pellets. Frequency scans were performed on 25 mm diameter plates with a 1 mm gap at 188°C and 1% strain from 0.01 to 100 rad/sec. All samples equilibrated at the testing temperature 10-20 minutes prior to beginning the experiments to ensure the pellets were fully liquefied.

For the impedance spectroscopy measurements, real (Z') and imaginary (Z'') components of impedance were measured using a Solartron SI 1260 impedance-gain analyzer with a Solartron 1296 dielectric interface. Cured pellets were first coated with silver paint and placed in a parallel plate set up. Impedance data were collected from 10^7 to 10^{-2} Hz at room temperature under an AC voltage of 0.1 V. AC conductivity (σ_{AC}) was calculated using the collected impedance data and Equation 4.1 below:

$$Z = Z' + iZ'' \tag{4.1}$$

$$\sigma_{AC} = \frac{Z'}{Z'^2 + Z''^2} \cdot \frac{L}{A} \tag{4.2}$$

Where σ_{AC} in this case is the real component of AC conductivity, L is the path length of the electrons (the sample thickness), and A is the cross sectional area of the electrode [114].

4.3 Results

4.3.1 Characterization

SEM imaging was used to observe the nanotube dispersion and distribution in the composites. Dispersion and distribution levels were qualitatively assessed by the presence of nanotube aggregates in individual SEM images and changes in nanotube concentration across the fracture surface based on many SEM images, respectively. Since two processing operations, melt-mixing and curing, were involved in this research, imaging was performed after each step in order to understand the nanotube dispersion and distribution resulting from each process. Representative images are shown in Figure 4.1. Figures 4.1 (a) and (c) show the dispersion and distribution of 0.5 wt.% and 5 wt.% samples, respectively, before curing. As previously reported in Chapter 3, melt-mixing resulted in largely homogenous MWNT dispersion and distribution in PETI-330. Melt mixing at a temperature just above the melting point of PETI-330 maximized the applied torque, resulting in shear forces strong enough to separate the MWNTs from agglomerates and distribute them through the resin. However, after curing, some changes in the dispersion and distribution were observed, and these changes were related to the MWNT loading as shown in Figure 4.1 (b) and (d), for the 0.5 wt.% and 5 wt.% MWNT samples, respectively. At loadings less than 1 wt.%, the images after curing showed aggregates of MWNTs that were not observed prior to curing though overall distribution appeared unaffected by curing. The aggregates also contained the PETI resin, not just entangled MWNTs. Conversely, similar dispersion and distribution levels were observed

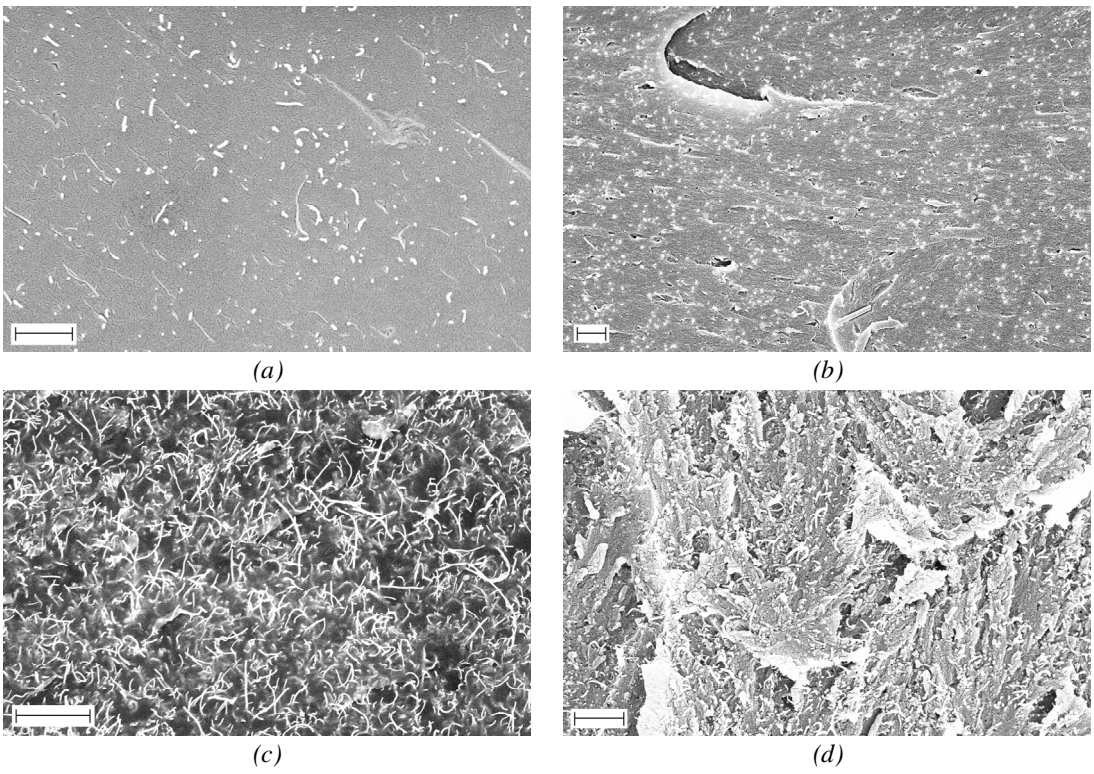

Figure 4.1: SEM images of (a) uncured 0.5 wt.%, (b) cured 0.5 wt.%, (c) uncured 5 wt.%, and (d) cured 5 wt.% MWNT composites. Scale bars represent 1 μm. At MWNT loadings less than 1 wt.%, a change in MWNT dispersion was observed after curing with respect to the uncured MWNT/oligomer mixture. MWNT images (a) and (c) show that good dispersion and distribution was achieved in the uncured samples.

in samples containing 1, 3, 5, and 7 wt.% MWNTs before and after curing. Previous research has reported similar aggregation of CNTs during curing of thermosetting matrices, some attributing the behavior to a combination of reduced resin viscosity and increased thermal energy [75, 115-116], others to the increased ionic concentration with the addition of hardener in epoxy systems [75, 109], or differences in nanoparticle concentrations and aspect ratios [75, 117-119]. In this case, no hardener was added to the system and all composites utilized the same MWNTs. For nanofillers of varying size, larger aspect ratios generally lead to more aggregation due to stronger physical entanglements [117]. However, once dispersed, nanoparticles with smaller aspect ratios reaggregate more quickly because the reduced ratio leads to an increase in the translational diffusion coefficient [75]. It is likely, then, that the aggregation could be attributed to the reduced polymer viscosity that allowed for increased nanotube mobility, effectively reducing the diffusion coefficient because it is inversely related to viscosity [75]. Also, the increased temperatures result in increased particle kinetic energy that could have been large enough to overcome the potential barrier [75]. As seen here, this effect would be less at higher MWNT loadings due to a larger number of physical CNT-CNT network interactions hindering the mobility of individual MWNTs.

The results of dynamic rheological testing also indicated that samples with a MWNT loading of 1 wt.% or higher contained a physical CNT network. Figures 4.2 (a) and (b) shows the storage modulus and loss modulus behavior of the nanocomposites as a function of frequency. Modulus trends were similar for the neat PETI-330, 0.2 wt.%, and 0.5 wt.% MWNT composites. G'' was larger than G' across all studied frequencies for

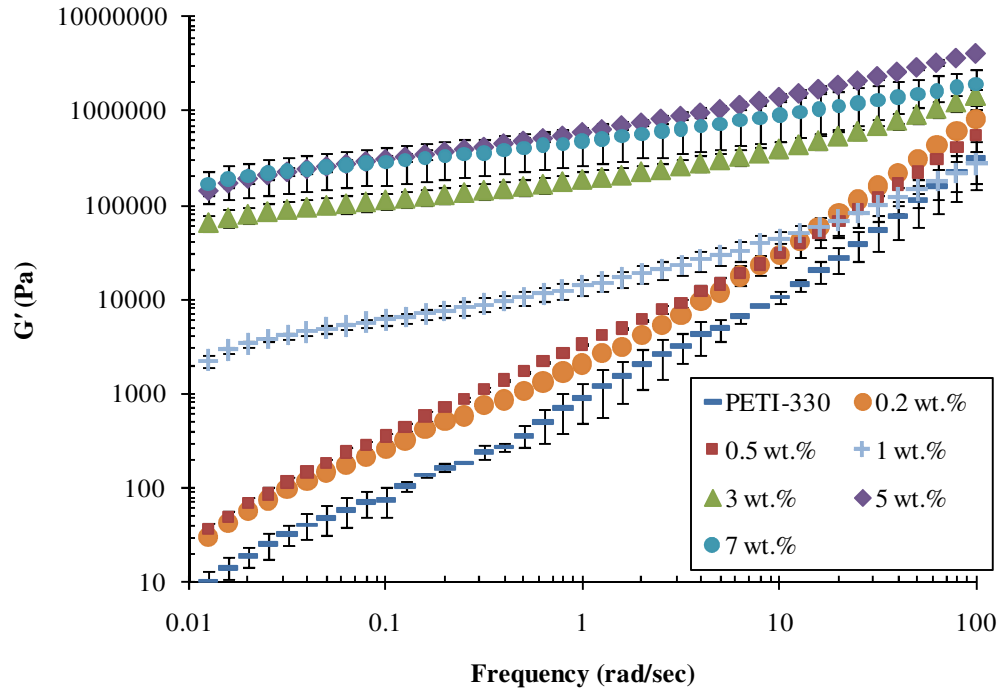

(a)

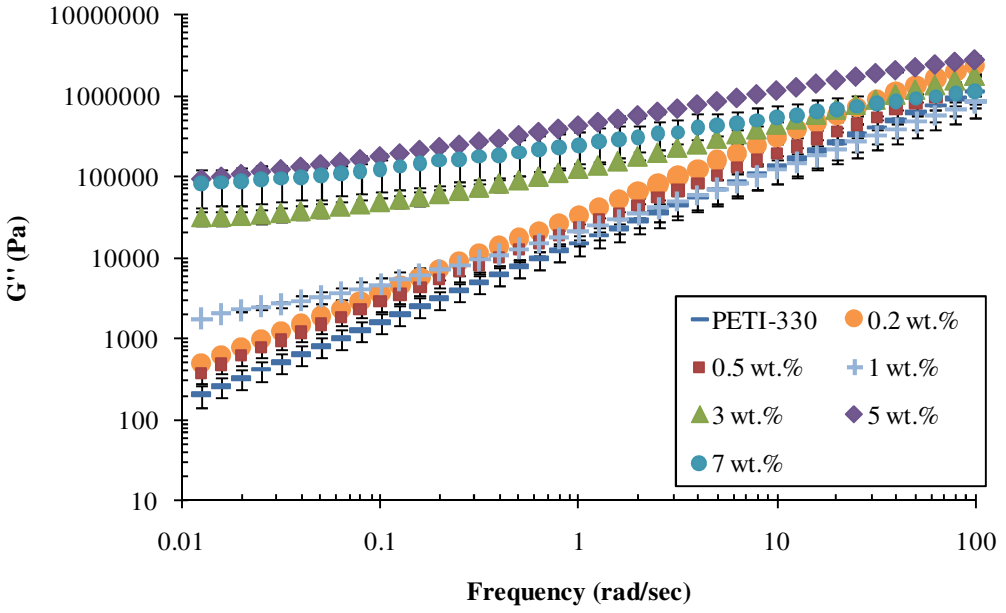

(b)

Figure 4.2: (a) Storage modulus (G') and (b) loss modulus (G'') as a function of frequency for PETI/MWNT composites. Both moduli increased as more MWNTs were added to the system. Modulus trends indicated the formation of a nanotube network above 0.5 wt.% MWNTs. Error bars are shown for all data sets; some sets have a small error range that is overlapped by the markers.

these composites, indicating liquid-like behavior. As the filler content was increased to 1 wt.%, G' and G'' increased at low frequencies, which again increased for the 3 wt.% nanocomposite. Both 1 wt.% and 3 wt.% composites exhibited pseudo solid-like behavior with crossovers from G' to G'' at 0.3 and 10 rad/sec, respectively. At higher MWNT loadings, G' was larger than G'' for all studied frequencies for the composites, indicating solid-like behavior [120-121]. Additionally, the values of G' and G'' at CNT loadings of 5 and 7 wt.% were similar in magnitude suggesting that the nanotube network was the dominant feature of the material. These results indicate that as the MWNT loading increased from 0.2 to 7 wt.%, the PETI composites transitioned from a rheological response characteristic of the matrix (liquid-like), to a response influenced by both components (pseudo-solid-like), and finally to a response dominated by a network of CNTs (solid-like).

Impedance spectroscopy measurement further supported the results of SEM imaging and rheological testing. Electrical conductivity of the nanocomposites was calculated from impedance data using Equation 4.2. As shown in Figure 4.3, the neat, 0.2, and 0.5 wt.% samples had similar AC conductivity values that increased with frequency, which is typical behavior for an insulating matrix [122]. Higher loadings of 1, 3, 5, and 7 wt.% exhibited a plateau behavior where conductivity values remained constant until a critical frequency, above which conductivity either increased or decreased with frequency. This frequency independent region below the critical frequency indicates a switch from AC to DC dominated conduction behavior, where the nanoparticles are interconnected or close enough for rapid electron hopping [122-123].

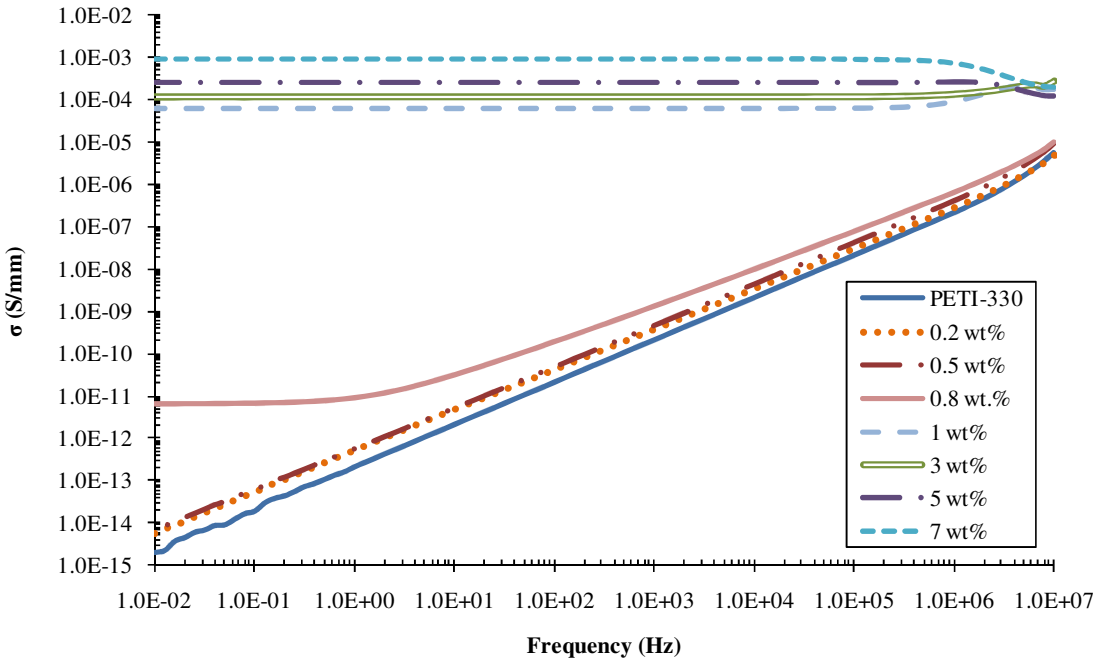

Figure 4.3: Frequency behavior of electrical conductivity properties of MWNT composites. Lower composite loadings (0.2-0.5 wt.%) showed frequency dependence across the entire studied frequency range. Higher loadings (1-7 wt.%) exhibit frequency independence across almost the entire studied range. Frequency independency indicates DC conductivity. Values shown are averages from two or more samples; error bars are not shown here due to the size of the data set, but are included in Figure 4.5.

To better estimate the electrical percolation threshold, a sample with both a frequency dependent and independent region was needed, so an additional sample was prepared and tested with a loading of 0.8 wt.% MWNTs. This composite exhibited distinctly different behavior with respect to the other samples in that it acted as an insulator with frequency dependence above 1 Hz but also had frequency independence below 1 Hz. The frequency plateaus were indicative of direct current pathways, so the samples could be assumed to be electrically conductive. The change in σ_{AC} and frequency behavior between 0.5 wt.% and 1 wt.% indicated the percolation threshold existed between the two values; the split

frequency dependence and independence of 0.8 wt.% indicated the threshold was near that particle loading.

The rheological testing results and electrical conductivity results were used to estimate the rheological and geometrical percolation thresholds for the nanocomposites, respectively. Classic percolation theory states a power law relation in elastic and conductive properties near the percolation threshold [124-126]:

$$G' \propto (m - m_{cG})^{\beta_G} \qquad m > m_{cG} \qquad (4.3)$$

$$\sigma_{DC} = \sigma_0 (m - m_{c\sigma})^{\beta_\sigma} \qquad m > m_{c\sigma} \qquad (4.4)$$

where m_{cG} is the filler mass loading at the percolation threshold and β_G is the critical exponent for $m>m_{cG}$ for rheological percolation threshold calculations in Equation 4.3. For electrical percolation threshold calculations in Equation 4.4, σ_{DC} is DC conductivity, σ_0 is the fitting parameter, $m_{c\sigma}$ is the critical mass fraction at electrical percolation, and β_σ is the critical exponent for $m>m_{c\sigma}$. To estimate both types of percolation thresholds, data at a single frequency were plotted as a function of MWNT concentration and fit to the appropriate expression (Equation 4.3 or 4.4) by adjusting the critical mass fraction and exponent.

4.3.2 Rheological percolation

Figure 4.4 shows G' for the different MWNT loadings at 0.1 rad/sec. While the 0.2 wt.% and 0.5 wt.% samples had only a small increase in G', the 1 wt.% sample

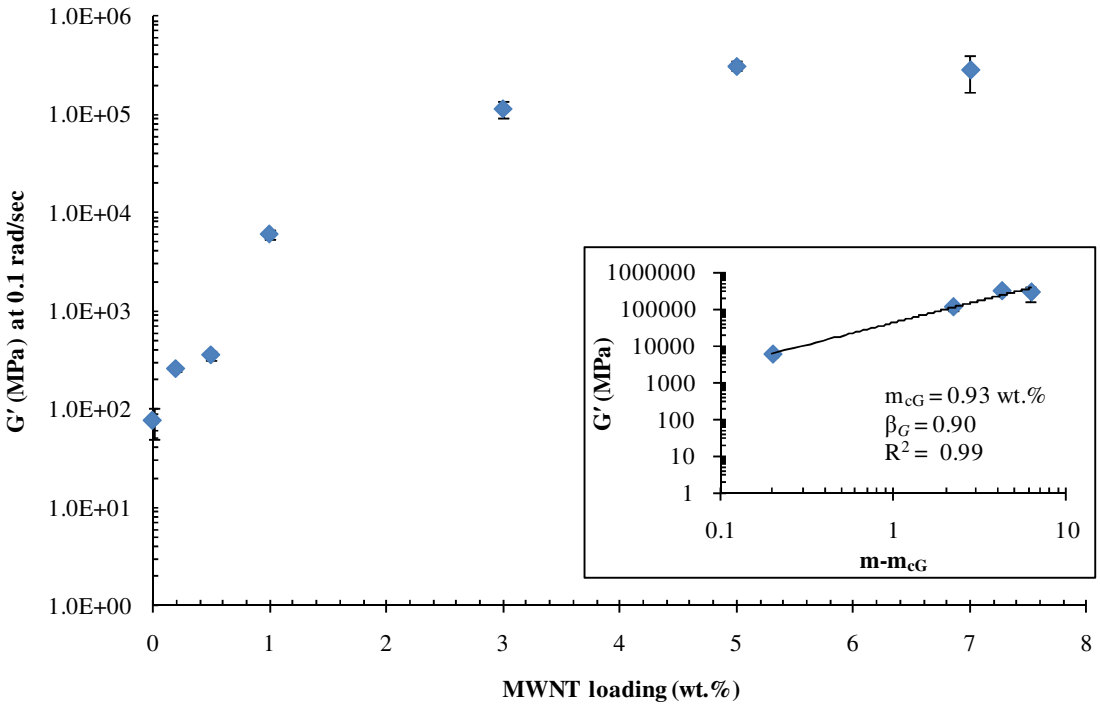

Figure 4.4: Storage modulus as a function of MWNT loading at 0.1 rad/sec. A large increase in G' was seen between 0.5 wt.% and 3 wt.%, indicating the rheological percolation threshold. Inset: Power law fit for determining the rheological percolation threshold. Error bars are included in the main figure and inset.

exhibited a sharp jump of two orders of magnitude in G' with respect to the neat polymer. Further increases in MWNT loading caused lesser modulus increases. The discontinuous increase in G' indicated the rheological percolation threshold was between 0.5 wt.% and 1 wt.% MWNT. Using Equation 4.3, m_{cG} for rheological percolation could be determined by fitting the data using the least squares method. As shown in the inset in Figure 4.4, the critical mass fraction for this frequency was 0.93 wt.% with a critical exponent of 0.90. As expected, this concentration was higher than rheological percolation thresholds traditionally reported for SWNTs; Du *et al.* found m_{cG} to be just 0.12 wt.% for SWNT/PMMA composites prepared by a coagulation method [124] and Kayatin and

Davis calculated m_{cG} as 0.13 wt.% for unsaturated polyester/SWNT composites [127]. However, MWNT composite studies have yielded a wider range of critical thresholds, from 0.5 wt.% for polyester terephthalate/MWNT composites [111] to 7.1 wt.% for HDPE/MWNT composites [128]. This range is mostly due to differences in CNT dispersion and polymer chain dimensions.

4.3.3 Electrical percolation

For electrical percolation, data for σ_{DC} were taken at 0.1 Hz for the cured materials because all conducting samples showed frequency independent behavior at this frequency, and these data are shown in Figure 4.5 with the power law fit in the inset. The fit produced $m_{c\sigma}$ = 0.80 wt.% and β_{σ} = 1.33 which agrees with the frequency behavior in Figure 4.3. This value was in the range of electrical percolation thresholds found in other studies [111, 129-131]. A review by Bauhofer and Kovacs [129] used the power law relation with data from a study by Allaoui *et al.* [131] to calculate a threshold of 0.7 wt.% of an epoxy/MWNT composite. Optical micrographs of the epoxy composites showed very high local MWNT concentrations [131], which are visually more concentrated than the MWNTs in the SEM images from this study. Polyimide/MWNT films made using *in situ* polymerization by Jiang *et al.* with filler contents ranging from 0.77-3.71 vol.% [132]. Using a two-terminal conductivity method, electrical resistance was measured and the percolation threshold was calculated as 0.15 vol.%. Another study using a similar fabrication method for polyimide/MWNT films by Zhu *et al*. calculated a percolation threshold of approximately 7 vol.% [61]. However, Jiang's study exhibited homogeneous

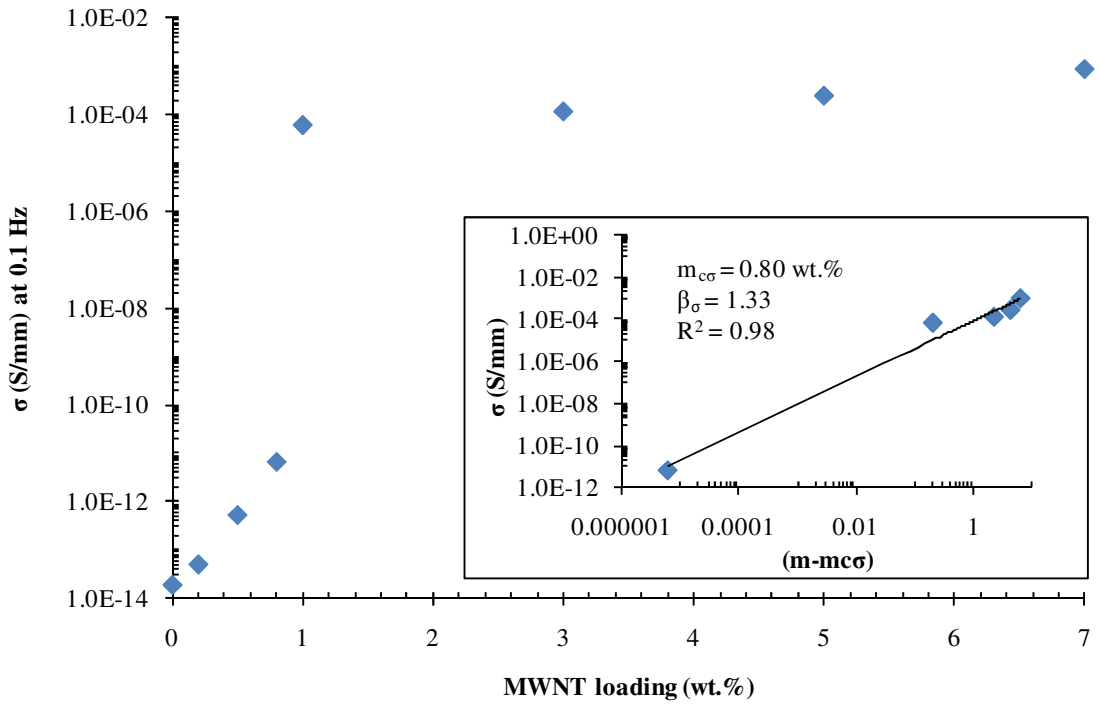

Figure 4.5: Conductivity at 0.1 Hz as a function of MWNT content. The 10^7-10^8 magnitude increase from lower loadings to higher loadings indicates the electrical percolation threshold. Inset: Power law fit for determining the percolation threshold. Error bars are included in the main figure and the inset, but are overlapped by the markers due to their small range.

distribution of aggregates while the SEM images in Zhu's study did not show good distributive properties. Both studies included SEM images that showed aggregation in the studied composites; the order of magnitude difference between the two sets of samples could be caused by the different morphologies.

The fitting parameter, σ_0, could be used to estimate the conductivity of the conducting phase [125]. The estimated value of 8.16×10^{-5} S/mm is much smaller than previously measured value of individual MWNTs, 10^4 S/mm [133]. The individual nanotubes were separated by insulating polymer phase, which resulted in contact resistance and decreased the efficiency of the overall electrical conduction [134-136].

Previous modeling work has shown that PETI-330 has an affinity for wrapping around carbon nanotubes, which adds to the insulating phase between conducting particles [101]. As a result, σ_0 had a reduced value due to inefficiencies of the conducting network.

4.3.4 Rheological versus electrical percolation

The critical exponent for both rheological and electrical percolation is a measure of the dimensionality of the system. While Sahimi reports an ideal value of 2.1 for the critical exponent of a three dimensional system when $m>m_c$, more generalized studies have set a guideline of $\beta \approx 2$ for three dimensional and $\beta \approx 1.3$ for two dimensional [125, 137]. The values of 0.90 and 1.33 are both much less than the predicted values for three dimensional systems, indicating that the rheological and electrical transport mechanisms occurred in a two dimensional manner. Many studies relate dimensionality only to the electrical conductivity critical exponents, but several other studies have also reported rheological critical exponents less than the electrical critical exponents for the same composite systems [111, 124, 128]. Du *et al.* reported β_G as 0.70 and β_σ as 2.3 for SWNT/PMMA composites [124]. In this case, β_G indicated a two dimensional system while the electrical system indicated a three dimensional mechanism. Hu *et al.* reported similar behavior for PET/MWNT composites with $\beta_G = 1.3$ and $\beta_\sigma = 2.2$ [111]. An HDPE/MWNT system studied by Kim *et al.* yielded more similar values with $\beta_G = 1.6$ and $\beta_\sigma = 1.97$ [128], but the β_G value remained less than β_σ. The first two studies yielded percolation thresholds ranging from 0.1-0.9 wt.% while the threshold from Kim's study had thresholds around 7.1-7.3 wt.%. The more saturated system may have resulted in more similar rheological and electrical transport systems. The different β values from

rheological and electrical percolation thresholds may be an indication that the two networks are different. Current available literature does not address this issue, but future experiments will be designed to elucidate these differences.

Several other studies have calculated similar β_σ values for dispersed MWNT/polymer systems [104, 136]. For example, Kilbride *et al.* sonicated poly(*m*-phenylenevinylene-*co*-2,5-dioctyloxy-p-phenylenevinylene) (PmPV) with arc grown MWNTs and calculated a critical exponent (β_σ) of 1.4 [136]. Simlarly, Jiang *et al.* measured β_σ to be 1.6 for a polyimide/CVD-MWNT composite system [104], which is comparable to the PETI/MWNT system in the present study. Bauhofer and Kovacs argue that the variability of CNTs make them incomparable to the "ideal" systems these generalizations are based on [129]. Several studies attribute low β_σ values to electron hopping mechanisms across loosely formed conductive networks [104, 136-138] while others attribute it to particle dimensions and interacting forces [109, 139], the existence of conducting particles that do not contribute to the overall conductivity of the system [140], or the fact that the conductive network may be a fractal object with a dimension of two without accounting for the polymeric system [136]. The low critical values in this study were likely due to a combination of these effects; while electron hopping and tunneling may have been one cause, it would not affect the rheological critical exponent. Particle aggregation was identified in cured samples, and it is likely that shearing during rheology experiments caused some alignment or aggregation as well; this may also have led to the reduced exponent values.

Although the threshold for rheological percolation and electrical percolation may be similar, they represent different types of networks. Rheological percolation is based on

particle-polymer-particle interactions while electrical percolation is achieved when conducting particles are close enough for electron hopping or tunneling. Rheological percolation, then, is dependent on the size of the polymer chain while electrical percolation is dependent on the distance electrons can hop or tunnel. A recent study has shown that the electron donor, acceptor, and bridge combination affects the tunneling regime, indicating that electron transfer rates have a loose dependence on distance [141]. For this study, the generally accepted tunneling distance of 5 nm [57, 142-143] is used as a rough estimate for the spacing between nanoparticles at the electrical percolation threshold. Previously, it has been shown that the onset of rheological percolation coincided with a nanoparticle spacing approximately equal to the matrix polymer's radius of gyration (R_g) [124, 144]. When the particle spacing was smaller than the polymer chain's radius of gyration, polymer chain dimensions were perturbed, leading to altered matrix dynamics. Most polymers have an R_g of 5-50 nm, which would result in a rheological percolation threshold less than electrical percolation. A similar imide, PETI-5, has a molecular weight of 5000 g/mol with an R_g of 3.6-5.7 nm [145] and PETI-330 has an approximate molecular weight of 2000 g/mol; the R_g of PETI-330 can be estimated as less than that of PETI-5 and other polymers examined previously. These PETI-330 composites should have become electrically conductive before they shifted from pseudo-solid- to solid-like behavior as more particles were added to the system. The experimental data followed this trend with $m_{c\sigma}$ (0.80 wt.%) < m_{cG} (0.93 wt.%).

It is important to acknowledge that there were some changes to particle and polymer morphology in the uncured rheological studies and the cured electrical studies. This could raise the question asking if the two threshold values are indeed different, or if

the changes in morphology make them roughly equal. Unfortunately, these morphological changes are difficult to quantify that would allow a more direct comparison. For the purposes of this study, the values are taken as a rough estimate that the electrical percolation threshold occurs at a lower filler concentration than the rheological percolation threshold.

4.3.5 Aspect ratio estimation

To further understand the network morphology in these materials, the complex viscosity values of the uncured samples were used to estimate the effective CNT aspect ratio and volume fraction using Guth's model [146]:

$$\eta_c^* = \eta_m^*(1 + 0.67fv + 1.62f^2v^2) \qquad (4.5)$$

where η_c* is the composite complex viscosity, η_m* is the neat matrix complex modulus, f is the filler aspect ratio, and v is the filler volume. By using the known viscosity values, the theoretical filler volume could be computed for the corresponding composite flow properties. The as-received MWNTs used in this study had aspect ratios of 1000. However, studies have reported that high shear forces such as those used in melt-mixing cause tube shortening that leads to a reduction in the filler aspect ratio. In particular, Andrews *et al.* used TEM to identify degradation to MWNT aspect ratio with increasing mixing energy during melt-mixing [77]. For this work, rheology data were fit with Equation 4.5 by adjusting f. This led to an average effective aspect ratio of 250 for the

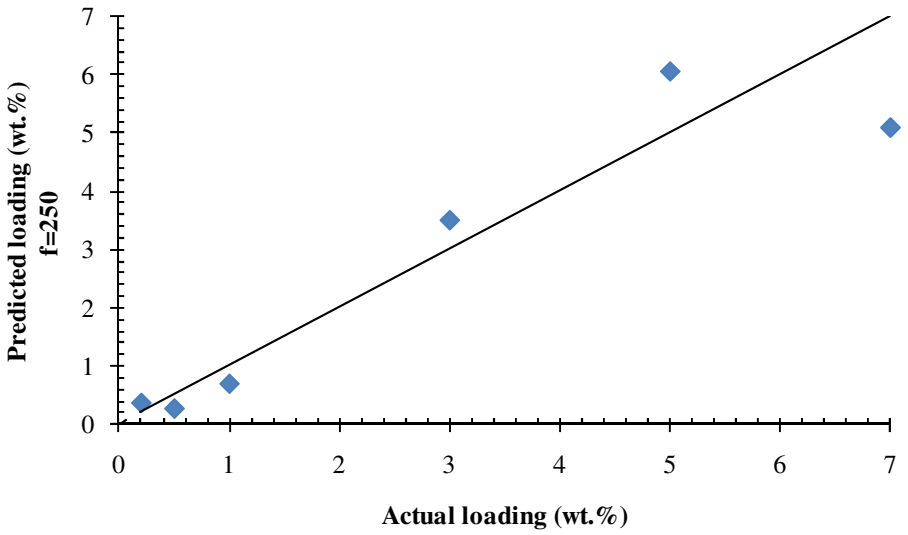

Figure 4.6: Actual filler loading compared with predicted filler loading using Guth's model. The line represents actual equals predicted loading. The data show that the MWNTs used in this study likely have a reduced aspect ratio of 250.

MWNTs.

Figure 4.6 shows the results from Equation 4.5 at 0.1 rad/sec for MWNT composites. The line represents the point where predicted filler concentration equals actual filler concentration; the predicted values and actual values were similar with most variability in actual loading being less than predicted. Andrews *et al.* [77] also showed that filler aspect ratio decreased when more energy was used during melt-mixing. The processing study in Chapter 3 showed that higher filler loadings resulted in higher mixing energies when mixed under the same conditions, such as this study. It is likely, therefore, that lower filler loadings had larger aspect ratios than composites with higher filler loadings, resulting in prediction errors. Also, Guth's method is for rod-shaped, non-interacting particles, so predictions for composites above the percolation threshold become less accurate as more particles are added to the system.

4.3.6 Model comparison for percolation

Experimental results for percolation characteristics were also compared with theory through micromechanical models. Celzard *et al.* identified a range of concentrations where the threshold may occur when the lower limit is based on a system of infinitely long rods and the upper limit is based on spherical particles [147]. For the MWNT composites studied here, the high aspect ratio particles behaved more like infinitely long rods than spheres, so percolation threshold estimates were based on the infinitely long rod system. The Celzard model assumes spherocylinder particle shape for the calculations:

$$\varphi_c = 1 - exp\left(\frac{-1.4V}{<V_e>}\right) \tag{4.6}$$

$$< V_e > = \frac{4}{3}\pi w^3 + 2\pi w^2 l + 2wl^2 < sin\gamma > \tag{4.7}$$

where φ_c is the filler volume concentration at the percolation threshold, V is the volume of one filler particle, $<V_e>$ is the averaged excluded volume of an object over the characterizing orientation distribution, w is the diameter of one filler particle, l is the length of one filler particle, and $<sin\ \gamma>$ is an average of angles between particles and can be estimated as 0.6 when the particles are randomly oriented [148].

The MWNT diameters were 10 nm and, from the aspect ratio calculations, lengths were estimated to be 2500 nm. Using these dimensions, the critical percolation threshold was calculated to be approximately 0.47 wt.%. This value represents the estimated concentration of particles needed before a network of interacting particles is formed; this differs from rheological and electrical percolation because it requires the particles to

physically touch regardless of polymer interactions or electron hopping. The calculated value of 0.47 wt.% is comparable to another modeling study [113] where Garboczi *et al.* estimated a percolation threshold of 0.12-0.7 vol.% for needles with an aspect ratio of 100-500. This geometric threshold should be the greatest filler concentration because there is no additional spacing of polymer chain lengths or electron hopping distances for this network. However, the data for these composites yielded a geometrical percolation threshold that was smaller than both rheological and electrical percolation. This could be due to the morphological properties of the studied systems; while the Celzard model assumes an isotropic system with randomly dispersed particles, SEM imaging already illustrated aggregation in the cured system of lower MWNT loadings. Aggregation or inhomogeneity across the polymer matrix would result in a higher network formation in all the percolation models.

The effect of aggregation during the cure process could be compared with the percolation thresholds. The electrical percolation threshold may be prematurely lower than if the system had homogenous morphology. Several studies have reported a decrease in $m_{c\sigma}$ as the nanoparticles become more aggregated [75, 149-150]. For this study, however, the rheological percolation threshold occurred at only 16% higher MWNT loading than electrical percolation. The network theory presented here showed that $m_{c\sigma} < m_{cG}$ assuming homogeneous morphology, so if morphology was improved in the cured composites it is likely that $m_{c\sigma}$ would increase. This leaves only a 16% increase from the current particle loading before reaching m_{cG}; with a small PETI-330 R_g, it is unlikely that $m_{c\sigma}$ will increase much with improved dispersion.

4.4 Conclusion

Network formation in polyimide/MWNT nanocomposites was studied through rheological and electrical property characterization. The elastic modulus was used to model percolation behavior and a critical filler concentration of 0.93 wt.% was determined for achieving a network of polymer-particle interactions throughout the composites. Alternatively, DC conductivity values of cured samples were used to estimate a critical filler concentration of 0.80 wt.% to establish a network with particles close enough for electron hopping and tunneling. For an oligomer system, m_{cG} is expected to be larger than $m_{c\sigma}$ because the electron hopping distance is larger than the oligomer size. Using a theoretical model, the geometric percolation threshold was estimated as 0.47 wt.%; because geometric percolation requires a network of direct physical interactions between the nanoparticles, it is expected to have a higher critical filler concentration than both rheological and electrical percolation. The composites in this study exhibited a theoretical geometric percolation below the experimental filler concentrations for other networks, indicating that some aggregation existed within these systems and affected rheological and electrical behavior. However, the percolation thresholds were comparable and, in many cases, low when compared with other studies. The study showed that nanocomposite behavior could dramatically change through percolation by adding only small quantities of MWNTs, and that network formation in nanocomposites is driven by the particle dispersion as well as the polymer system.

CHAPTER 5

THERMOMECHANICAL PROPERTIES AND MORPHOLOGICAL EFFECTS ON CURED NANOCOMPOSITES

5.1 Introduction

Networks of carbon nanotubes enhance polymer properties through their advanced thermal [82-84], mechanical [32-36], and electrical [85-86] properties. Interactions between polymer chains and particles occur at the surface area of the particles, so the small size and large aspect ratio of nanotubes maximizes the available surface area for interactions when compared to the same amount of larger fillers. However, the characteristic large aspect ratio of CNTs that imparts many of the favorable properties also causes strong attractive forces between the particles that lead to aggregation. Overcoming these attractive forces can be difficult in many cases. A mechanical reinforcement network is established when filler particles are well dispersed and distributed, interacting with as many of the polymer chains as possible. For a homogeneous system, polymer conformations are restricted by the nanotubes as the temperature of the system is raised. Similarly, the nanotubes also help to reinforce the strength and modulus of a polymer when under a tensile load. Aggregates in tight bundles with nanotubes that are not directly interacting with polymer chains or aggregates in loose bundles with mostly polymer-interacting particles may be present for composites that could not overcome the inter-tube attractive forces during processing. The potential for obtaining maximum reinforcement with these less-than-ideal morphologies is

unknown as well as the degree of dispersion and wetting out required to obtain maximized or nearly maximized reinforcement efficacy.

Nanotube aggregates can exist as small clumps of a few of particles measuring nanometers in diameter or as larger clumps measuring micrometers and even centimeters in size [62, 75, 151-153]. The size of the agglomerates can dictate final composite properties, where certain sizes may be more effective in some property enhancement than others. A modeling study by Shi *et al.* predicted a relationship between the size and frequency of nanotube agglomerates and the overall composite modulus based on nanotube stiffness [154]. The model showed that losses in morphological homogeneity as well as increases in aggregate size resulted in decreased elastic moduli, where homogeneity was the more sensitive factor. The study used an agglomeration factor to rate the degree of aggregation; it also identified a threshold below which additional CNTs no longer had a stiffening effect. In an experimental study, Song *et al.* created good and poor dispersions of 0.5-1.5 wt.% MWNTs in epoxy using solvent to control the morphologies [155]. Composites with poor dispersions had higher complex viscosities than samples with good dispersions of the same loading and they also exhibited higher storage moduli. Microscope images identified agglomerates for the poor dispersions, but also showed wetted-out particles. Another study by Gojny *et al.* incorporated singlewall nanotubes (SWNTs), purified and amino functionalized doublewall nanotubes (DWNTs) and MWNTs into epoxy resin using a calendering technique [156]. Both MWNT composites and both DWNT composites exhibited good morphology with small agglomerates. SWNT composites had mostly small agglomerates but with a few large ones measuring 2 μm in diameter. The study found that the best toughening mechanism

was not a homogeneous distribution of individual nanotubes but well wetted-out small agglomerates less than 1 μm in size.

Previous studies have shown that homogeneous CNT morphology can be achieved in uncured polymer systems but aggregation then occurs during the cure reaction [75, 109, 115, 117-118]. This was discussed in more detail in Chapter 4, Section 4.3.1. Briefly, this reaggregation is usually reportedly due to attraction between system constituents or a combination of reduced system viscosity and increased kinetic energy. Sandler *et al.* reported that the ionic concentration of an amine hardener decreased the repulsive barriers between particles in an epoxy precursor and resulted in nanotube aggregation [109]. The nanocomposites in this study did not have an epoxy matrix, so it is more likely that diffusion was reduced as viscosity decreased and that the increased temperature resulted in increased particle energy that could overcome the barrier potential [75].

Morphology plays an important role in the reinforcement efficacy of nanoparticles in a polymer matrix. However, it is not known if there is a threshold in the degree of dispersion or distribution above which mechanical and thermal properties are maximized or nearly maximized. Problems in processing completely homogeneous morphologies would be greatly reduced if it could be determined that aggregation that sometimes occurs during the final steps of processing has minimal effects on end composite properties. In this study, multiwall carbon nanotubes (MWNTs) and carbon nanofibers (CNFs) were homogeneously dispersed in a polyimide matrix. The nanocomposites were then cured and MWNT loadings of 0.5 wt.% or less as well as CNF composites experienced some aggregation, which was correlated qualitatively with imaging and

quantitatively with modeling. The effect of this aggregation on the different reinforcement mechanisms of the composite was studied mechanically and thermally for each of the filler types. Results showed that MWNT reinforcement networks were more sensitive to aggregation and that sensitivity of both systems depended on overall filler concentration.

5.2 Materials and methods

PETI-330, a phenylethynyl-terminated imide resin manufactured by Ube Industries, Ltd., was used as the polymer matrix for this work. PETI-330 has a post-cured T_g of 330°C. Elicarb PR0940 MWNTs with diameters averaging between 10-12 nm from Thomas Swan & Co., Ltd. were used as well as PR-24-PS carbon nanofibers (CNFs) with diameters averaging between 60-150 nm from Pyrograf Products, Inc. MWNT and CNF dimensions were reported by the respective manufacturers. The PETI-330 and MWNTs were used as received and the CNFs were cleaned using a method by Lozano *et al.* [98]. This method involved a five day reflux in methylene chloride followed by washing and a one day reflux in water.

Composite samples were made using the methods outlined in Chapters 3 and 4. Briefly, PETI-330 was melt-mixed with MWNTs or CNFs using an internal mixer with roller blades operated by a Brabender Intelli Torque drive unit. Fifty grams of dry materials were initially mixed by simple shaking, then mixed at 188°C and 60 rpm for 12 minutes in the melt-mixer. Samples containing 0, 0.2, 0.5, 1, 3, 5, and 7 wt.% MWNTs and 0.5, 3, 5, and 10 wt.% CNFs were prepared. Nanocomposites were then cured into

round plaques measuring approximately 5 cm in diameter and 1 mm in thickness. Curing was performed in a three piece mold; the material was initially heated without the top mold piece to 288°C and held until the material was completely liquefied. The sample was then heated to the curing temperature and held for 15-30 minutes to allow the material to gel. The top piece was added to the mold under approximately 9 MPa and cured at 343°C for 4 hours. Fourier transform infrared spectroscopy (FTIR) was performed using a Bruker Vector 22 to show that each sample was fully cured. Uncured PETI-330 was mixed with KBr and pressed into a pellet which contained 1 wt.% oligomer. Cured PETI-330 composites were tested in their final form without KBr with an attenuated total reflectance (ATR) attachment. FTIR spectra were collected at room temperature with 32 scans between 4000-400 cm^{-1} at a resolution of 4 cm^{-1}.

A LEO 1530 scanning electron microscope (SEM) was used to image morphological properties of fractured surfaces from each composite. All cured samples, uncured CNF composites, and lower uncured MWNT loading composites (0.2-0.8 wt.%) were sputter coated with gold to facilitate imaging. Higher uncured MWNT loadings possessed sufficient inherent conductivity to be imaged without coating. Dynamic mechanical analysis (DMA) was performed with a Mettler Toledo DMA861 in three-point bending mode to measure thermomechanical properties for the nanocomposites. Cured samples were cut into rectangular geometries using a Buehler diamond saw. Specimens measured 6 mm or less in width and approximately 1 mm in thickness; the DMA bending clamp was attached at a specimen length of 30 μm. Samples were tested from -50°C to 200°C at a rate of 2°C/min and at a frequency of 1 Hz with a maximum displacement amplitude of 20 μm. All nanocomposite loadings were tested at least twice.

Thermal analysis was performed using a TA Instruments Q200 differential scanning calorimeter (DSC) on uncured and cured material to determine the effects of nanoparticles and mold processing on composite properties. Uncured samples were heated at 50°C/min to 371°C, held isothermally for 60 minutes, cooled at 50°C/min to 100°C, heated at 50°C/min to 400°C, then cooled at 10°C/min. Cured samples were heated at 50°C/min to 400°C and cooled at 10°C/min. The T_g was taken as the inflection point on cooling; T_g for some DSC-cured MWNT composites were reported in Chapter 3.

5.3 Results

5.3.1 Morphology and FTIR

Images of uncured samples in Figure 5.1 (a) and (c) show that melt-mixing produced homogeneous distributions of individual MWNT and CNF particles. Higher MWNT loadings did exhibit some aggregation due to high saturation, which was discussed in more detail in Chapter 3. Images of cured samples in Figure 5.1 (b) and (d) showed that dispersion was affected by the formation of agglomerates during the cure process. Lower loadings, which had no agglomerates in uncured samples, experienced aggregation during curing. Higher loadings that had aggregation in the uncured form still exhibited aggregation in the cured form. This reagglomeration behavior in the PETI-330 composite system during cure was thought to be due to nanotube saturation and the reduced viscosity that occurred in the melt phase prior to curing.

FTIR scans of uncured PETI-330 and all cured samples were compared to

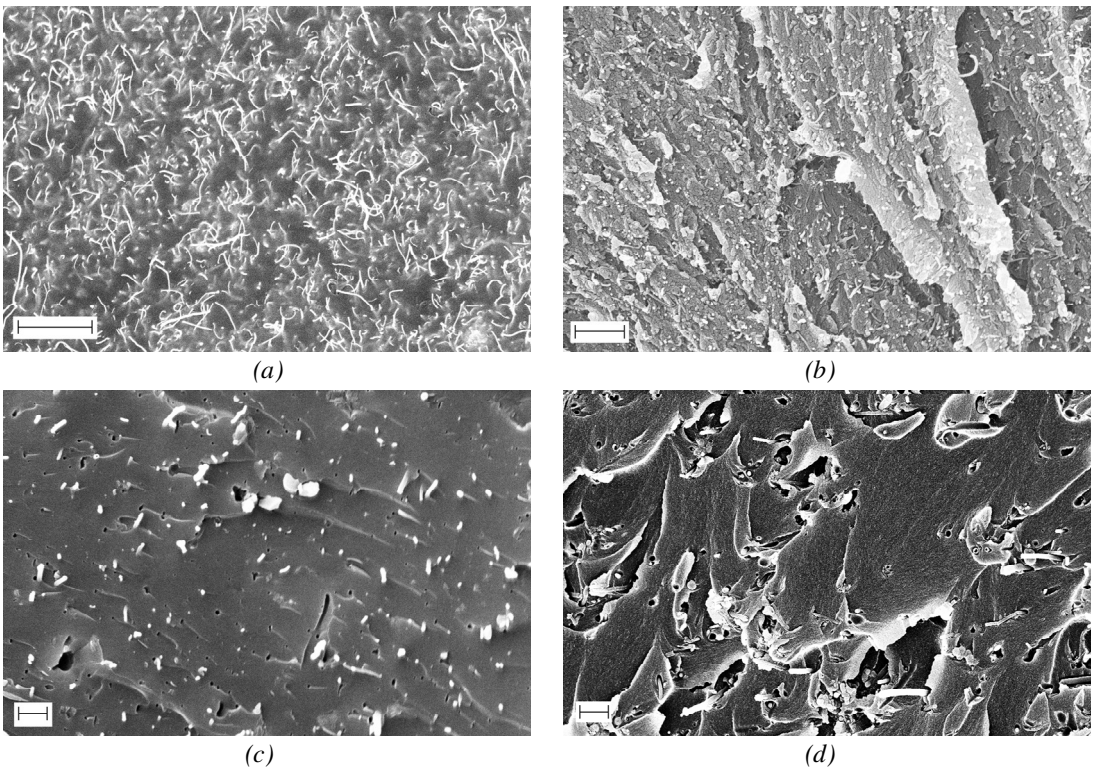

Figure 5.1: SEM images for uncured 3 wt.% MWNTs (a), cured 3 wt.% MWNTs (b), uncured 3 wt.% CNFs (c), and cured 3 wt.% CNFs (d). Uncured samples had homogeneous dispersion and distribution while cured materials exhibited increased aggregation at low filler loadings. Scale bars represent 1 µm.

determine if full cure had been achieved. For the uncured material, there was a peak at 2214 cm^{-1}, the wavenumber for phenylethynyl end groups [157]. Spectra for cured samples reflected no intensity at this wavenumber, indicating that, to the extent of sensitivity of the instrument, the end groups had reacted and the sample was fully cured. Figure 5.2 compares the spectrum for uncured and cured neat PETI-330. The cured spectrum was representative of all cured composite scans.

5.3.2 Thermomechanical Properties

Bending modulus data from DMA testing are shown in Figures 5.3, 5.4 and 5.5. During testing it was noted that applied force, displacement, and temperature initiated

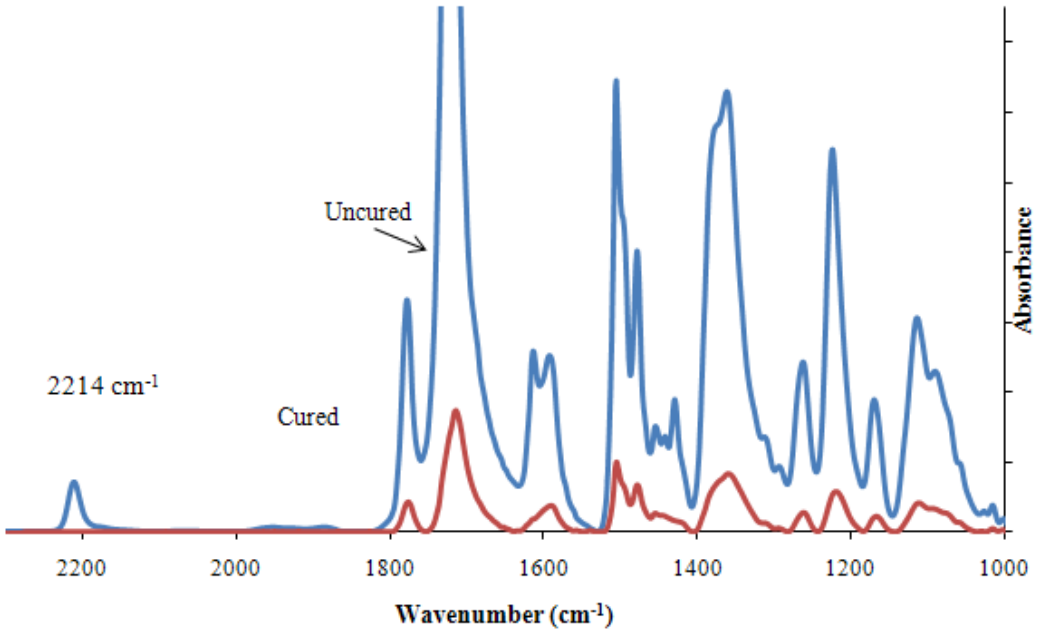

Figure 5.2: FTIR spectra for uncured and cured PETI-330. Peaks at 2214 cm^{-1} indicated phenylethynyl groups, so no peak indicated their absence and a fully cured sample. All cured nanocomposites exhibited behavior similar to the cured PETI-330 sample.

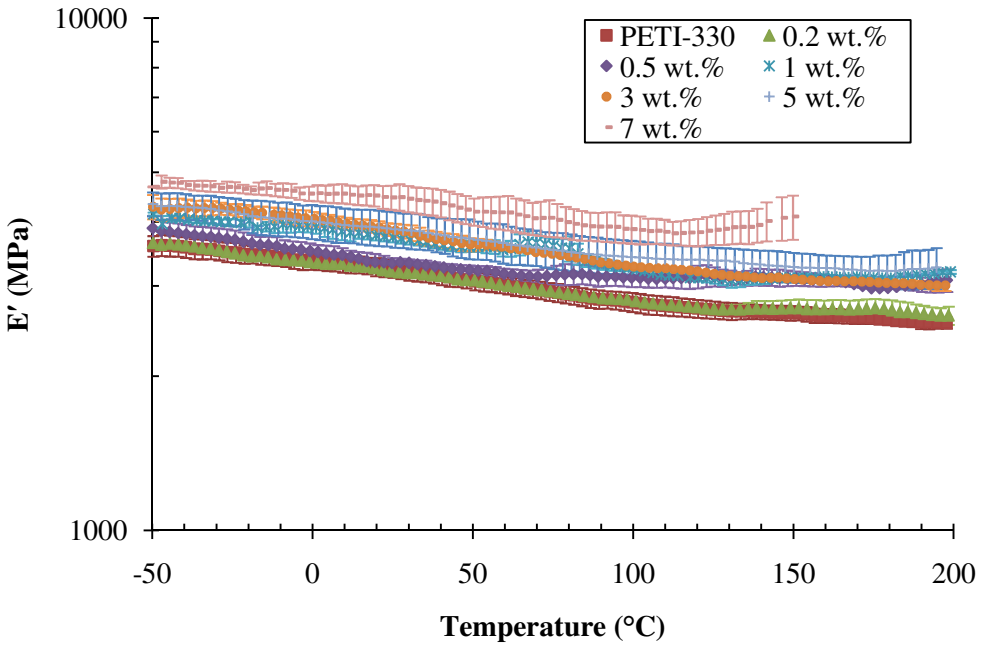

(a)

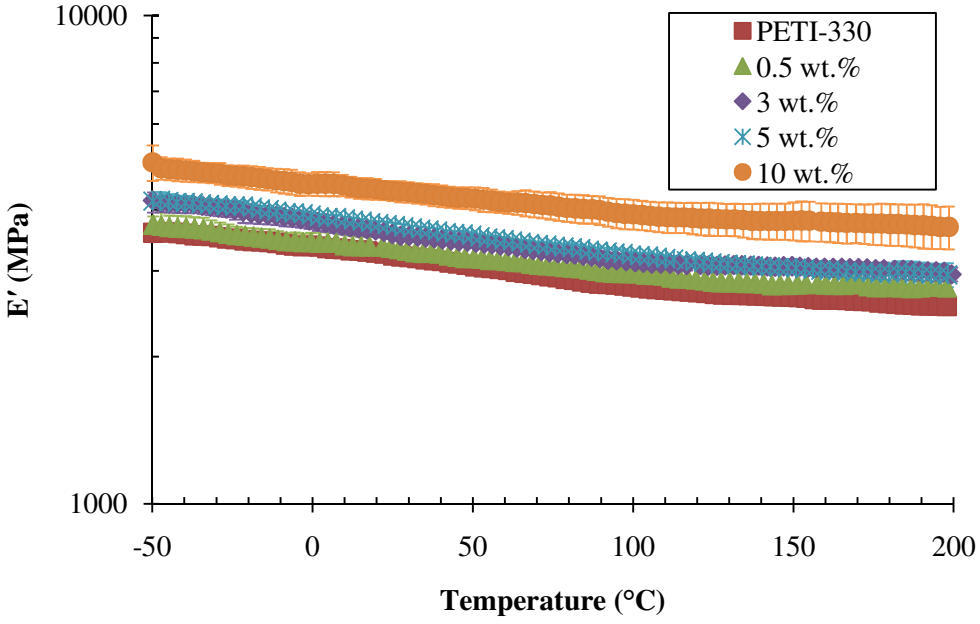

(b)

Figure 5.3: Bending storage modulus (E') as a function of temperature for MWNT composites (a) and CNF composites (b). E' values generally increased throughout the temperature sweep as the MWNT and CNF loadings increased. Error bars are shown for all data sets; some sets have a small error range that is overlapped by the markers.

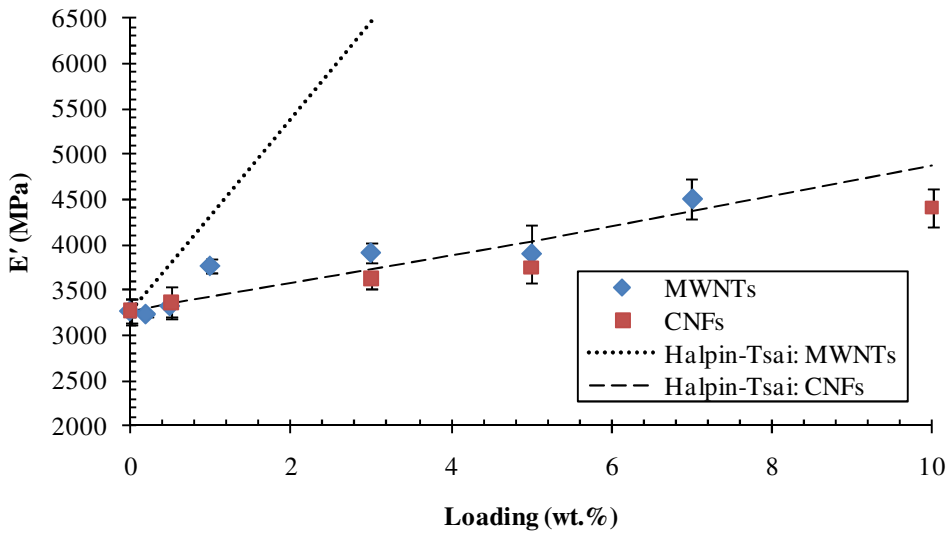

Figure 5.4: E' as a function of particle loading at 20°C. The addition of nanoparticles resulted in increased E' values for the studied fillers and loadings. Halpin-Tsai predictions are indicated by the dotted (MWNTs) and dashed (CNFs) lines. Predictions more closely matched experimental data at lower loadings.

some permanent physical changes to the sample dimensions. DMA data are dimension-dependent, so data obtained after the dimensions began to change were discarded for the analysis. The temperature at which sample dimensions began changing was signaled by a change of more than 10% in the storage modulus between repeated analyses and the average of all sample values for a given sample set. This occurred at 150°C or higher for some of the composites.

DMA data calculated for analysis were the storage (E') and loss (E'') moduli. The storage modulus is the in-phase component that indicates the elastic modulus of the sample. The loss modulus is the out-of-phase component that reflects the energy lost due to friction between polymer chains from movement. MWNT composite storage modulus values are shown in Figure 5.3 (a) as a function of temperature and in Figure 5.4 as a

function of MWNT content at 20ºC. While the 0.2 wt.% loading had approximately the same storage modulus behavior compared to the neat material, higher loadings did exhibit enhancement. The storage modulus for all samples decreased gradually as temperature increased, indicating increased polymer chain mobility. The change of behavior between 0.5 wt.% and 1.0 wt.% was an indication of percolation; the MWNTs were unable to effectively enhance the polyimide crosslinked network before a particle network was formed. This correlates with data from Chapter 4 that rheological percolation occurs at 0.93 wt.% and electrical percolation at 0.80 wt.% for this PETI-330/MWNT system. The storage modulus for the 7 wt.% had a storage modulus of 4.5 GPa at room temperature, a 38% increase from that of the neat material.

CNF storage modulus data are shown in Figure 5.3 (b) and Figure 5.4 as a function of temperature and CNF content, respectively. The first loading of 0.5 wt.% CNFs behaved similar to the neat material, while 3 wt.% and 5 wt.% composites showed an increase of approximately 11-15% from unfilled PETI-330 at 20ºC. The 10 wt.% composite exhibited a more significant storage modulus increase from 3.3 GPa of the neat material to 4.4 GPa, a 35% improvement. The CNFs used in this study were larger than the MWNTs used with diameters approximately ten times larger and similar lengths; this resulted in less available surface area for the same filler content loadings. CNF composites, then, needed higher filler content to provide the particle surface area required for the same enhancement provided by MWNT particles. The CNFs used in this study also had lower moduli than the MWNTs [43, 156, 158], which again increased the loading required to achieve the same composite elastic properties as similar MWNT

composites. This was evident from the similar storage modulus values obtained from 7 wt.% MWNT composites (4.5 GPa) and from 10 wt.% CNF composites (4.4 GPa).

While the MWNTs in this study have been shown to increase thermomechanical behavior of the PETI resin, other polyimide/MWNT studies have been able to enhance the neat polymer storage modulus by much more than 40% [159-160]. Mo *et al.* [159] used *in situ* polymerization to disperse MWNTs in a polyimide in the final form of a film; the MWNTs were 40-60 nm in diameter, 0.5-500 μm in length, and acid modified. The group found that 15 wt.% of MWNTs provided a nine-times enhancement (28.5 GPa) of the neat polyimide (3 GPa). The 7 wt.% composite provided a five-times enhancement (15 GPa), which is much greater than the enhancement from this study. This was likely due to the better dispersion as well as better interaction between particles and polymer from the MWNT acid treatment. Similarly, Wang *et al.* [160] used SWNT buckypaper to create high loading epoxy nanocomposites. The lowest studied loading, 28.1 wt.%, had a storage modulus of approximately 11.5 GPa, which was more than four-times greater than the unloaded epoxy. While the SWNTs improve the properties, the storage modulus values were much less than those predicted by the rule of mixtures. The group attributed this to poor dispersion that resulted in poor load transfer between particles and polymer-particle interactions. Both studies have identified dispersion as a key property for improving modulus values in nanocomposites. Homogeneous dispersion results in a homogeneous network of polymer-particle interactions that effectively evenly distribute stresses and response mechanisms throughout the sample. CNT aggregation results in

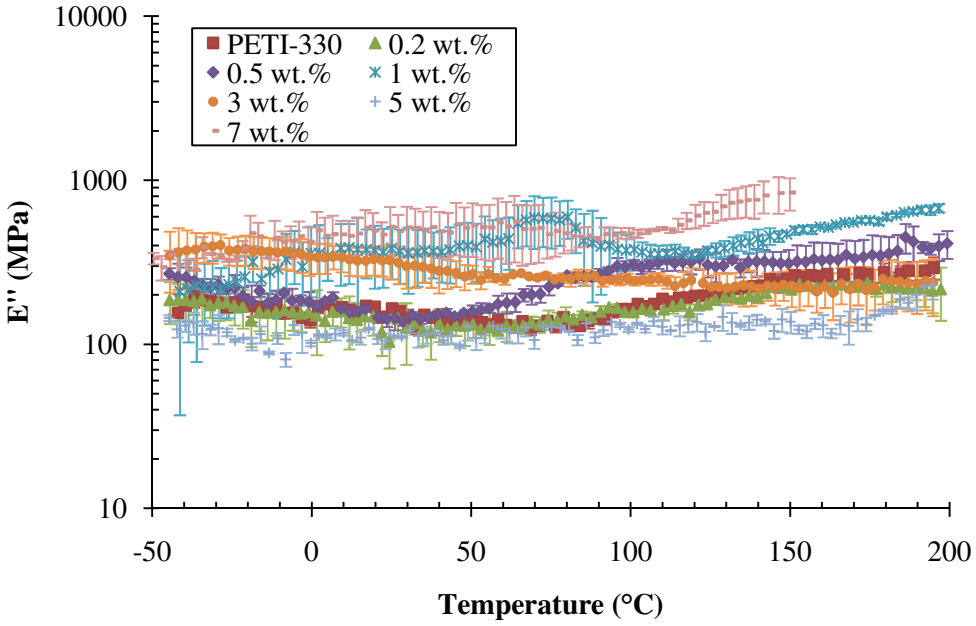

(a)

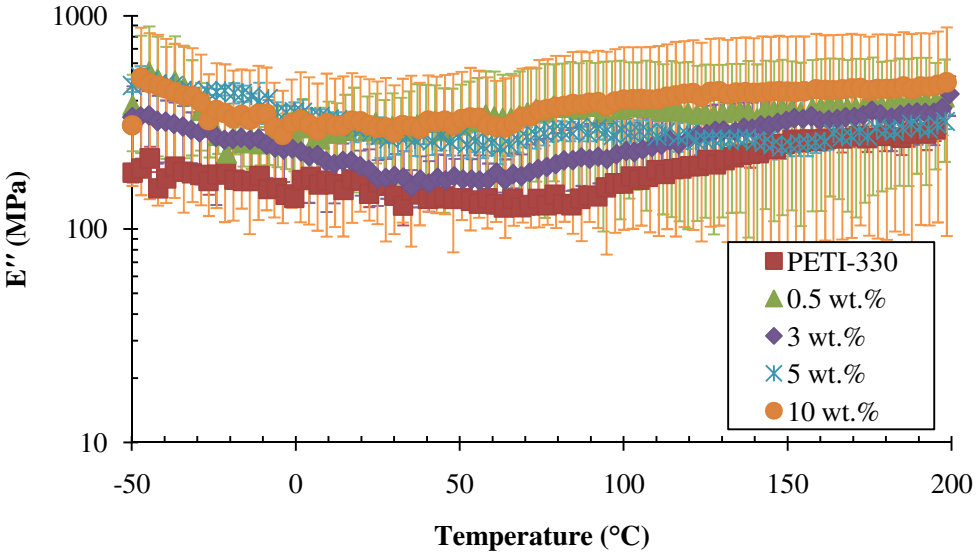

(b)

Figure 5.5: Bending loss modulus (E'') as a function of temperature for MWNT composites (a) and CNF composites (b). E'' values generally increased throughout the temperature sweep as the MWNT and CNF loadings increased.

pockets of particle-free polymer and also clumps of particles with no polymer, leading to fewer polymer-particle interactions. These interactions are also not spread throughout the composite, leaving an uneven distribution of stresses.

Loss moduli data for both MWNT and CNF composites are shown in Figure 5.5. In the range of room temperature, higher nanoparticle loadings exhibited higher loss moduli and lower loadings had behavior similar to the neat material. This trend indicated that additional energy was dissipated as the composites were deformed with increased filler loadings. There were two exceptions to these observations; 5 wt.% MWNTs exhibited a loss modulus below the neat material across the entire temperature scan. Similarly, the 3 wt.% CNFs sample had a loss modulus below all other CNF composites, including the 0.5 wt.% sample, across the temperature scan. Multiple scans were tested for both of these composites and the behavior was repeatable. It was unclear as to why there was a break in the behavior trend for these composites and future studies utilizing rheometry or other DMA sampling modes will investigate this further.

Maximum property enhancement due to particle reinforcement could be predicted using micromechanical models. While many models currently exist, several studies have used the Halpin-Tsai equations to model various polymer composite systems [43, 156, 158-167]. The Halpin-Tsai model can be used with reinforcement particles of various shapes and any general elastic composite property [168]. For a random orientation of discontinuous reinforcement, the modified Halpin-Tsai equations are [169]:

$$E_c = E_m \left[\frac{3}{8} * \frac{1+2f\eta_L v}{1-\eta_L v} + \frac{5}{8} * \frac{1+2\eta_T v}{1-\eta_T v}\right] \quad (5.1)$$

$$\eta_L = \frac{(E_f/E_m)-1}{(E_f/E_m)+2f} \quad (5.2)$$

$$\eta_T = \frac{(E_f/E_m)-1}{(E_f/E_m)+2} \quad (5.3)$$

where E_c, E_m, and E_f are the elastic properties for the composite, matrix, and fiber, respectively, f is the particle shape factor, and v is the filler volume fraction. The DMA storage bending modulus (E') was used as the elastic property for this work's analysis. The bending moduli for the MWNTs (E_{MWNT}) and CNFs (E_{CNF}) were based on previous studies using similar nanotubes with E_{MWNT}= 450 GPa [43, 156] and E_{CNF}=100 GPa [158]. In this case, the particle shape factor was the aspect ratio. While the as-received MWNTs and CNFs had aspect ratios of approximately 1000 and 100 respectively, previous work has shown that melt-mixing can cause tube shortening and a reduction in aspect ratio [77]. Analyses from Chapter 4 used modeling with rheological data to estimate a reduced aspect ratio of 250 for the melt-mixed MWNTs in this study. Using estimations from Chapter 4 and Andrews *et al.* [77], the CNF aspect ratio was estimated to have decreased by one order of magnitude to 10.

Figure 5.4 displays E' at room temperature (20°C) for MWNTs and CNFs, as well as the Halpin-Tsai predictions using the estimated aspect ratios. Predictions at low loadings (0-1 wt.%) closely matched those of the measured values, which was within 13% for MWNTs and just 2% for CNFs. At higher loadings, however, the variations became much more apparent. Previous studies have shown that nanotube reinforced composites have not achieved the properties predicted by the Halpin-Tsai models or even the rule of mixtures [30, 170-171]. The Halpin-Tsai models are based on low particle loadings, which may explain the increased deviations between predicted and actual values above percolation. Additionally, SEM images showed that higher loadings

exhibited aggregation in both uncured and cured form while lower loadings experienced aggregation only during cure. Agglomerates often contain individual nanotubes that do not interact with polymer chains, which reduce the overall interactions within the system. The aspect ratio of the aggregate, then, is the driver of the interactions that lead to mechanical reinforcement, not the aspect ratio of the nanotubes that have little or no direct interaction with the polymer matrix. A reduced aspect ratio that correlates with the aggregation in these composites would result in decreased modulus prediction by the Halpin-Tsai models and would match more closely with the experimentally obtained values.

5.3.3 Thermal analysis

Thermal analysis was used to differentiate the effects of aggregation by studying the change in T_g between homogeneous and agglomerated morphology. SEM images identified good dispersion and distribution for uncured composites after melt-mixing with small, wetted out agglomerates in higher loadings and aggregation in cured composites. Before the curing reaction could be initiated, the sample had to be fully melted to prevent air pockets or voids in the final specimen. Full melting required holding the samples at minimum viscosity for three hours. Once curing was initiated, the nanotube morphologies became “locked in” by crosslinking; it could be assumed, then, that aggregation occurred during the melt phase of the curing. To prevent aggregation a curing method with minimal melting time was needed and the DSC provided this method. Samples were heated immediately to the curing temperature, melting the entire small sample size (~5 mg) during heat up and initiating the cure reaction shortly thereafter.

SEM images in Figure 5.6 show a comparison between morphologies of uncured, press-cured, and DSC-cured samples containing 1 wt.% MWNTs. The uncured sample had small aggregates of nanotubes that were individually surrounded by polymer. Both cured samples exhibited aggregation, but the press-cured agglomerate in Figure 5.6 (c) was much larger than the DSC-cured agglomerate in Figure 5.6 (b). These images were representative of morphological behavior of composites with 1 wt.% or less MWNTs and all CNF composites. While aggregation still occurred in DSC samples, it was to a much lesser extent and was used as a best-case scenario for a comparison study on the effects of aggregation on thermal properties. Higher MWNT content composites exhibited similar morphology for both press-cured and DSC-cured samples. These samples had aggregation in the pre-cure form due to a system already saturated with particles; the sample loadings also exceeded the electrical (0.80 wt.%) and rheological (0.93 wt.%) percolation thresholds, so a network of interacting particles existed in the uncured composites. Upon curing, the pre-existing aggregates and physical interactions that restricted individual MWNT mobility may have been less susceptible to additional aggregation in the melt phase of the curing protocol than the non-interacting particles in lower MWNT loading composites. It should be noted that DSC samples were cured at 371°C, which is the typical curing temperature [89, 103], while press-cured samples were cured at 343°C. Available press equipment allowed a maximum cure temperature of 343°C. The cure was held for four hours, as opposed to one hour for the DSC-cured samples, to ensure maximum conversion for both sets of samples.

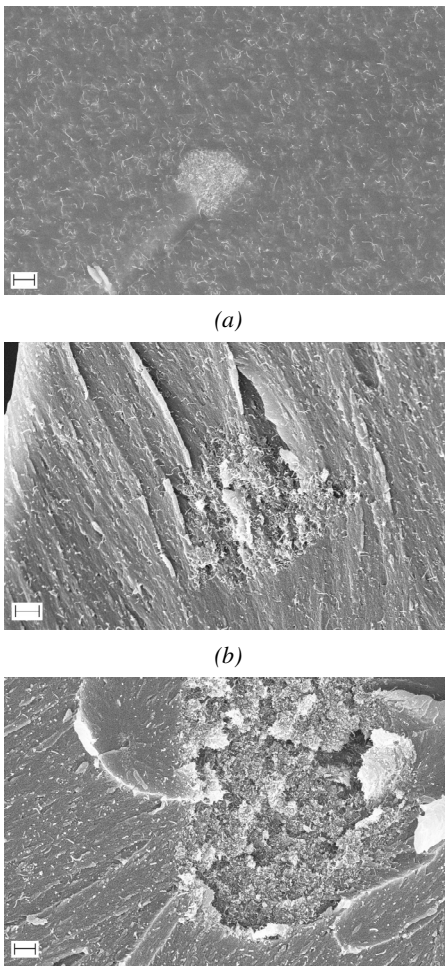

(a)

(b)

(c)

Figure 5.6: SEM images of uncured (a), DSC-cured (b), and press-cured (c) 1 wt.% MWNT composites. Small, wetted-out aggregates were found in uncured samples while larger aggregates formed during curing. The fast cure method used in DSC samples resulted in minimal aggregate size. Scale bars represent 1 μm.

Figure 5.7 shows the comparison in T_g behavior for press-cured and DSC-cured MWNT (a) and CNF (b) composites. MWNT loadings of 1 wt.% or less exhibited similar behavior for the two curing methods while higher loadings showed larger deviations. For these composites the aggregation that occurred during curing did not affect the glass transition behavior for lower MWNT loadings. The agglomerates restricted polymer motion similar to a homogeneous morphology. However, the press-cured samples for 3 wt.% and higher MWNTs had T_g values with lower values than DSC-cured by approximately 13-22°C. These samples exhibited no change in particle morphology between the two methods, so the differences could be due to cure protocol. The DSC-cured samples did not have a melt phase during cure, which could have resulted in a different network morphology which may or may not have included air pocket voids. Additionally, the different cure temperatures may have resulted in a different degree of cure. This behavior is addressed further in Chapter 6.

CNF composites did not exhibit the same break in behavior as the MWNT composites. Instead, press-cured and DSC-cured samples maintained similar T_g trends, but with press-cured values 6-18°C higher than DSC-cured. In this case, aggregation added to the reinforcement mechanism of the CNF network. The difference in size and aspect ratio of the CNFs and MWNTs here showed that the larger particles (CNFs) were less sensitive to the aggregation that occurred during curing, and CNF composites with 10 wt.% loading or less could even benefit in reinforcement from it. MWNT composites were more sensitive to the aggregation, although, as seen in the DMA analysis, lower loadings were needed for the same mechanical reinforcement as compared to CNF composites.

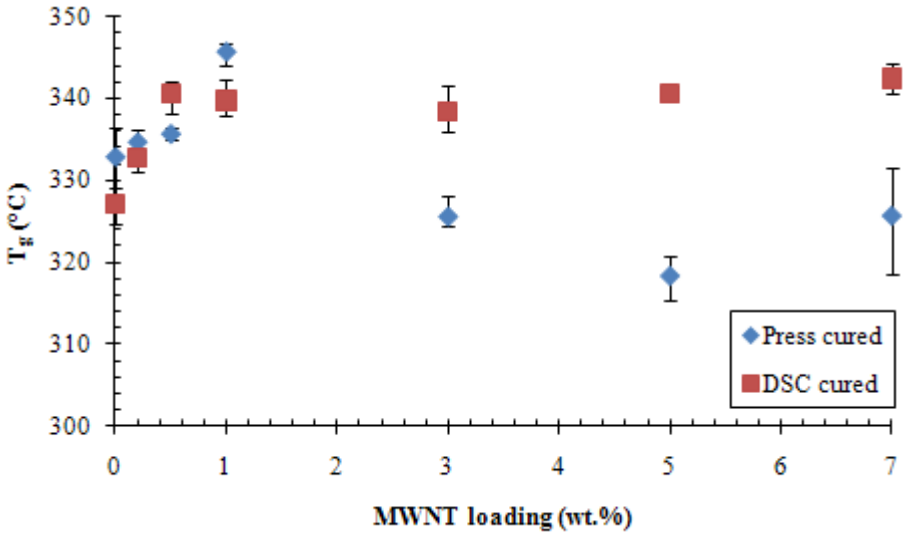

(a)

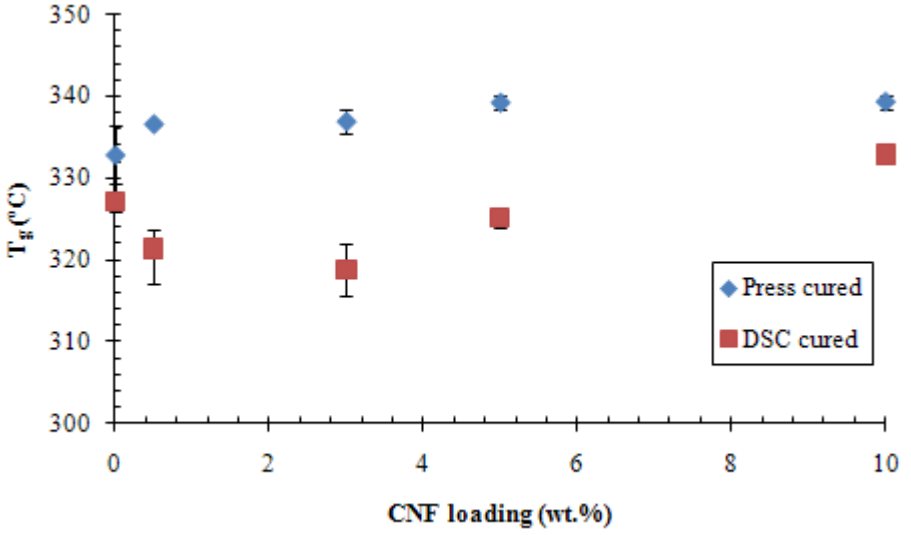

(b)

Figure 5.7: Press-cured (aggregated) versus DSC-cured (homogeneous morphology) T_g values for MWNT composites (a) and CNF composites (b). Aggregation in MWNT composites did not affect lower loadings, but loadings above 1 wt.% showed significant decrease in T_g. Aggregation in CNF composites increased T_g values for all studied loadings.

5.4 Conclusion

The purpose of this study was to monitor the influence of nanotube aggregation during cure on the reinforcement mechanisms in a polyimide network. Imaging and modeling identified that, although a good dispersion and distribution could be achieved in the uncured state, aggregation occurred during curing. Mechanical reinforcement of MWNTs and CNFs were measured using DMA and aggregates were found to limit reinforcement to only 35-38% improvement from unloaded PETI-330 resin using 10 wt.% CNFs or 7 wt.% MWNTs. DMA data were also correlated with the Halpin-Tsai model to correlate experimental data with predicted optimal behavior. Thermal reinforcement was also studied using DSC and aggregation showed little to no difference for low loading MWNT composites with homogeneous morphology. Alternatively, CNF composites exhibited improved thermal behavior with aggregation. Additional studies are required to determine the effect of cure temperature on PETI-330 network formation and PETI/MWNT interactions. These reinforcement studies have identified that aggregated MWNTs and CNFs can still provide mechanical reinforcement in cured polyimides, although improved dispersion may allow the networks to reach maximum reinforcement efficacy. Thermally, however, improving dispersions at low MWNT and CNF loadings in cured composites may not improve properties and may even lessen them.

CHAPTER 6

CURE KINETICS OF PETI-330 RESIN AND EFFECTS OF NANOTUBE FILLERS

6.1 Introduction

Since the imaging of nanotubes by Iijima in 1991 [26], nanotube technology has become more and more important to composite research. In particular, there has been great interest in high performance aerospace applications where nanotubes can simultaneously enhance the strength, electrical conductivity, and thermal stability of polymers in order to create a composite material that is lighter than metal but still retains performance. Epoxies and polyimides are two classes of polymers that have been studied for such applications and have shown some success at achieving the desired high performance properties.

The cured network formed by thermosets dictates many of the resulting system properties, so many studies have focused on the elucidation of network formation and structure-property relationships of both filled and unfilled thermoset polymers. This study attempts to further the understanding of the formation of a high performance polymer network and the effects of nanotube inclusion using thermal analysis and curing behavior.

The use of differential scanning calorimetry (DSC) for determining cure kinetics is based on the assumption that the measured heat flow is proportional to the cure reaction rate [172]. Cure kinetics can be studied through isothermal and dynamic scans, both revealing different system characteristics. Dynamic analysis uses the change in the

temperature at the exothermic peak with respect to the heating rate to estimate the system cure activation energy. However, many reaction mechanisms are activated at different temperatures, so isothermal testing is beneficial for identifying and differentiating between these different mechanisms.

The degree of conversion (α) and rate of conversion ($d\alpha/dt$) can be measured using heat of reaction:

$$\alpha = \frac{(\Delta H)_t}{\Delta H_T} \qquad (6.1)$$

$$\frac{d\alpha}{dt} = k(T)f(\alpha) \qquad (6.2)$$

where $(\Delta H)_t$ is the heat of reaction up to time t, ΔH_T is the ultimate heat of reaction, $k(T)$ is rate constant at temperature T, and $f(\alpha)$ is a function of the degree of conversion. An Arrhenius relationship can be used to describe the temperature dependence of the rate constant:

$$k(T) = Zexp\left(\frac{-E_a}{RT}\right) \qquad (6.3)$$

where Z is the pre-exponential factor, E_a is the activation energy, and R is the universal gas constant. Thermoset curing reactions can generally be described as either n^{th} order or autocatalytic. N^{th} order reactions (Equation 6.4 [173]) exhibit a maximum reaction rate at $t \approx 0$ [174]; autocatalytic reactions (Equation 6.5 [175]) do not exhibit the maximum reaction rate until approximately 30-40% of the overall reaction [176]. In this case, intermediate species are initially formed that accelerate the reaction. These reactions can be separated into two different parts, one mirroring an n^{th} order reaction while the other accounts for any secondary reactions. Combining Equations 6.2, 6.4 and 6.5, the reaction

rates for n[th] order (Equation 6.6) and autocatalytic (Equation 6.7) reactions can be expressed as

$$f(\alpha) = (1-\alpha)^n \qquad (6.4)\ (n^{th}\ order)$$

$$f(\alpha) = \alpha^m(1-\alpha)^n \qquad (6.5)\ (autocatalytic)$$

$$\frac{d\alpha}{dt} = k(T)(1-\alpha)^n \qquad (6.6)\ (n^{th}\ order)$$

$$\frac{d\alpha}{dt} = k(T)\alpha^m(1-\alpha)^n \qquad (6.7)\ (autocatalytic)$$

where *m* and *n* are reaction orders.

Dynamic thermal scans use a series of constant heating rates (β) to determine kinetic rate constants and activation energies. Thermal data can be correlated with the Kissinger [177] or Ozawa-Flynn-Wall [178] methods to determine the polymer cure kinetics. The Kissinger method is based on the assumption that the degree of conversion at the dynamic peak is constant for all heating relates; it relates the heating rate (β) with the temperature at the exothermic peak (T_p):

$$\frac{d\left(\ln\frac{\beta}{T_p{}^2}\right)}{d\left(\frac{1}{T_p}\right)} = -\frac{E_a}{R} \qquad (6.8)$$

The Kissinger method utilizes a best-fit line between $ln\ (\beta/T_p)$ and $1/T_p$ to calculate the activation energy from the slope and the pre-exponential factor from the intercept. The Ozawa-Flynn-Wall method uses a similar linear relationship between $log\ \beta$ and $1/T_p$:

$$\frac{d(\log \beta)}{d(\frac{1}{T_p})} = -0.4567 \frac{E_a}{R} \qquad (6.9)$$

This method can be used in conjunction with the Kissinger model to estimate the total cure activation energy.

The Kissinger and Ozawa-Flynn-Wall methods assume a single activation energy for all degrees of conversion. However, multiple reaction processes may exist throughout the entirety of the cure, resulting in different activation energies throughout the reaction. An isoconversional method can be used in these instances to determine the existence of additional curing mechanisms [179]. One method is to use isothermal DSC testing:

$$\ln\left(\frac{d\alpha_i}{dt}\right) = ln[Z_i f(\alpha)] - \frac{E_{a,\alpha}}{RT_i} \qquad (6.10)$$

where $E_{a,\alpha}$ is the activation energy for a specific degree of conversion. Using this method, $E_{a,\alpha}$ can be estimated from the slope of $ln(d\alpha/dt)$ versus $1/T_i$.

While there have been many studies on the curing mechanism of epoxies [179-192], fewer studies of polyimides have been published [193-198]. In this study, the cure kinetics of a phenylethynyl-terminated imide noted for its enhanced thermal and mechanical properties was studied using differential scanning calorimetry (DSC). Nanocomposites of various loadings of multiwall carbon nanotubes (MWNTs) and carbon nanofibers (CNFs) were also studied for their effect on the curing mechanisms. Empirical modeling resulted in cure activation energies that varied with nanoparticle content. Analyses identified the primary curing mechanism of the studied system, as well as a minimal secondary mechanism.

6.2 Materials and Methods

PETI-330, a phenylethynyl-terminated imide manufactured by Ube Industries, Ltd., was used as the polymer matrix for this work. PETI-330 has a reported melting temperature of approximately 185°C and a post-cured glass transition temperature (T_g) of 330°C. Elicarb PR0940 MWNTs with diameters averaging between 10-12 nm from Thomas Swan & Co., Ltd. were used as well as PR-24-PS carbon nanofibers (CNFs) with diameters averaging between 60-150 nm from Pyrograf Products, Inc. MWNT and CNF dimensions were reported by the respective manufacturers. The PETI-330 and MWNTs were used as received and the CNFs were cleaned using a method by Lozano *et al.* [98]. This method involved a five day reflux in methylene chloride followed by washing and a one day reflux in water.

Nanocomposites were made using the method outlined in Chapter 3. Nominal 50 gram batches of material were mixed at 188°C and 60 rpm for 12 minutes in an internal mixer with roller blades operated by a Brabender Intelli Torque drive unit. Samples containing 0.0, 0.2, 0.5, 1.0, 3, 5, and 7 wt.% MWNTs and 3, 5, and 10 wt.% CNFs were mixed. A LEO 1530 scanning electron microscope (SEM) was used to image the morphology of each sample as described in Chapter 3; all nanocomposite exhibited homogeneous dispersion and distribution in the imide form.

A TA Instruments Q200 DSC was used to perform dynamic and isothermal testing on all samples. For dynamic testing, samples were ramped from 40°C to 400°C at 10, 6, 4, and 2°C/min. Neat PETI-330 samples were isothermally tested by equilibrating at 280°C and holding for 30 minutes, ramping at 50°C/min to the isothermal testing temperature, and holding again until the cure was complete. Samples were held initially

at 280°C to ensure a complete melt of the sample; it has been previously shown the PETI-330 does not cure at 280°C and the viscosity remains unchanged when held at that temperature for at least two hours [89]. Neat samples were isothermally tested at 10°C intervals between 340°C and 400°C in addition to 343°C; this last temperature was added as a reference to the curing temperature of samples mechanically tested as described in Chapter 5. Nanocomposite samples were isothermally tested in a similar fashion but only at 343°C and 370°C. All analyses were performed at least twice to ensure reproducibility.

6.3 Results

6.3.1 Dynamic kinetics

Dynamic testing allowed for initial characterization of the cure kinetics of PETI-330 and isothermal testing produced a more detailed overview of the behavior. First, dynamic data were analyzed with the Kissinger and Ozawa-Flynn-Wall methods to estimate activation energy. The Kissinger method assumes that the exothermic peak in a dynamic peak is isoconversional and is dependent on degree of conversion, not heating rate [199-200]. To test the validity of this assumption with this study's data, the degree of conversion at the temperature of the exothermic peak was obtained for all heating rates for PETI-330. Figure 6.1 shows these data. All degrees of conversion were in the range of 49%, concluding that the Kissinger method did apply to this system.

Using Kissinger's method in Equation 6.8, a plot of $ln\ (\beta/T_p^2)$ versus $1/T_p$ was constructed, as seen for selected samples in Figure 6.2 (a). Similarly, the Ozawa-Flynn-

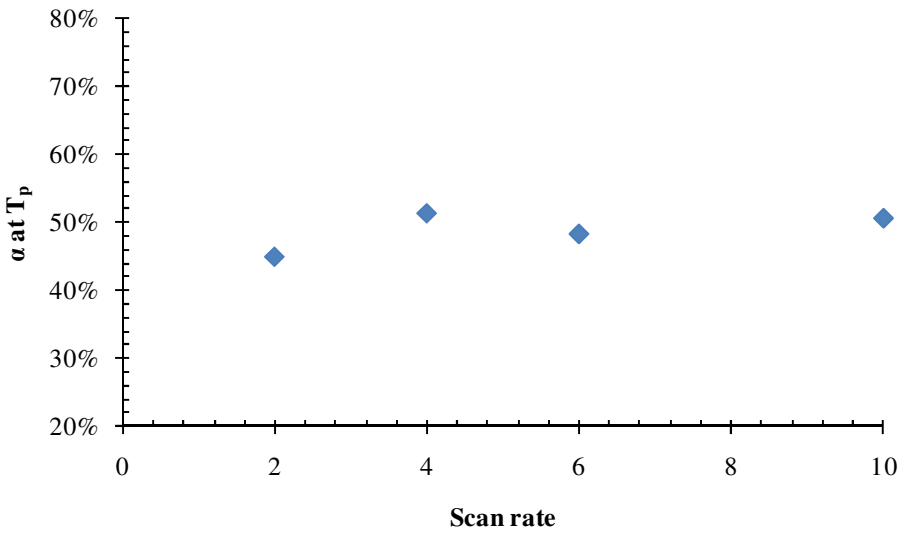

Figure 6.1: The degree of conversion of neat PETI-330 at the peak exothermic temperature for different scan rates. Approximately constant values indicate that the Kissinger method for determining the cure activation energy was appropriate for this system.

Table 6.1: Activation energy values as calculated by the Kissinger and Ozawa-Flynn-Wall methods.

	Loading (wt.%)	E_a (kJ/mol)	
		Kissinger	Ozawa-Flynn-Wall
Neat	0	166.0	168.0
MWNT	0.2	147.3	150.3
	0.5	171.7	173.4
	0.8	154.1	156.8
	1	166.1	168.0
	3	160.7	162.9
CNF	3	152.3	155.2
	5	130.6	134.4
	10	151.6	154.5

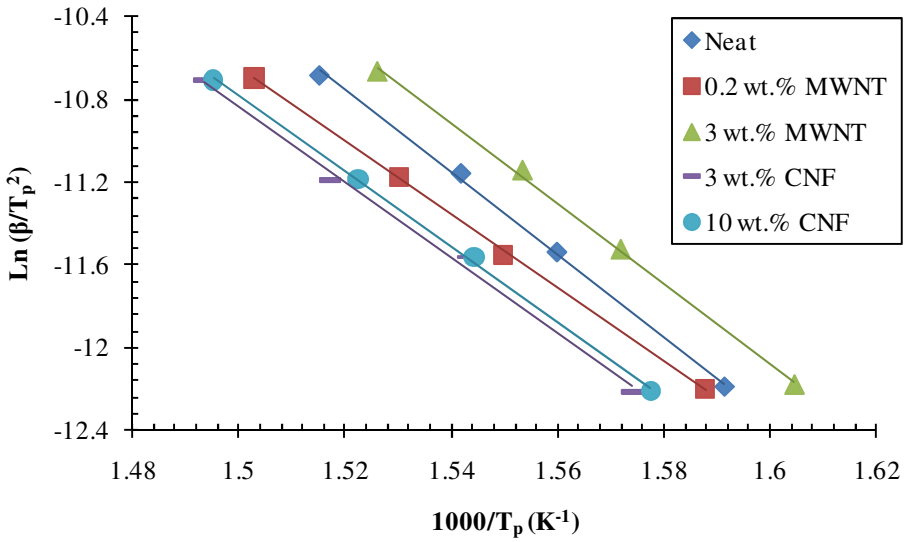

(a)

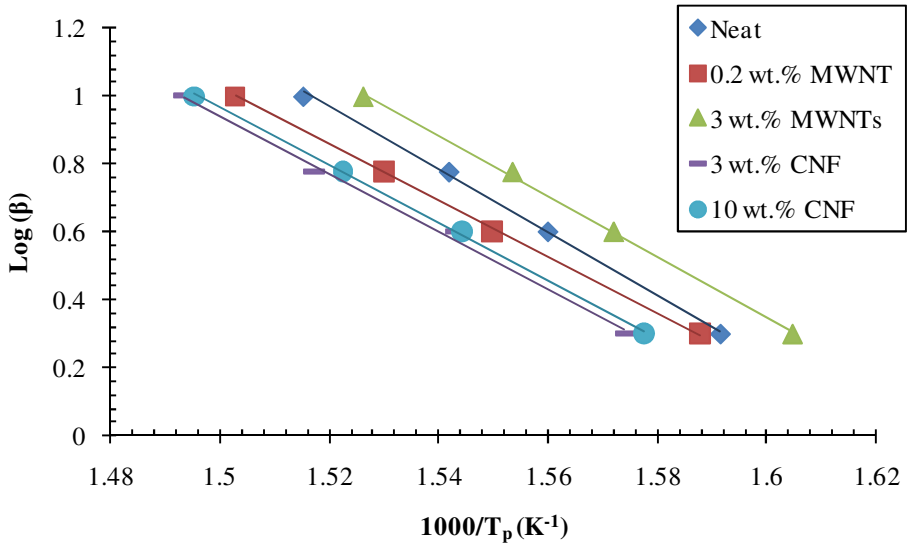

(b)

Figure 6.2: Activation energy calculations for neat PETI-330 and select composites using dynamic data and the Kissinger (a) and the Ozawa-Flynn-Wall methods (b).

Wall method in Equation 6.9 was used to construct Figure 6.2 (b) with $log\ \beta$ versus $1/T_p$. The activation energy was calculated from the slope of the best linear fit for all composites. Table 6.1 displays the E_a values for all neat and composite samples calculated using both the Kissinger and Ozawa-Flynn-Wall methods. Although the Ozawa-Flynn-Wall method consistently predicted higher E_a values, variation between the two values was less than 3% for all samples.

For the most part, the addition of MWNTs or CNFs reduced or did not affect the E_a of the resin. This indicates that the nanoparticles were accelerating the cure reaction. Lower energy was required to initiate and carry out the cure of PETI-330 in the nanocomposites. Similar behavior for nanotubes composites has been noted previously [192, 201], and it may be due to the high thermal conductivity of the nanoparticles [201]. The nanotubes may have improved overall thermal conduction, which would result in lower T_p and, thus, E_a at the same scanning rates compared to the neat samples. Dispersion could have also played an important role; effective thermal conduction would be achieved when the nanotubes are homogeneously dispersed and distributed. Chapter 3 identifies good morphology for all the studied composites in the pre-cure imide form. However, it is unclear as to why the E_a values varied inconsistently with addition of MWNTs or CNFs, particularly for the 0.5 wt.% MWNT composite. It is possible that this sample, as well as other loadings, experienced a loss of morphological properties as the experiments were performed, particularly at the slowest heating rate. Previous work from Chapter 4 shows that both fillers tend to aggregate during curing for this system. The aggregates could then cause inhomogeneities in thermal distribution, resulting in varying activation energies.

Table 6.2: Heat of reactions for different cure temperatures of PETI-330.

Cure temperature (°C)	ΔH (J/g)		
	Average	+	-
340	217.1	3.0	3.0
343	224.3	2.7	2.7
350	216.6	7.7	5.8
360	255.7	0.2	0.2
370	256.3	5.5	5.5
380	251.6	1.4	1.4
390	244.9	4.1	4.1
400	234.6	16.0	14.2

6.3.2 Isothermal kinetics

Isothermal testing was used to identify additional temperature dependent curing mechanisms. PETI-330 was isothermally cured at temperatures ranging from 340°C to 400°C. The heat of reaction for the total cure at each temperature was obtained by integrating the exothermic peak with respect to time; these values are available in Table 6.2. As the isothermal cure temperature increased, the total heat of cure approached a maximum value. Within error, the heat of cure for samples cured at 360, 370, and 380°C are approximately the same. The ultimate heat of reaction (ΔH_T) for PETI-330 was taken as 256.3 J/g, which was the maximum averaged value in that temperature region. High temperatures yielded lower total heat of cure values, which was most likely due to limitations of DSC sensitivity and has been reported previously [183, 202]. The polymer cures very rapidly at these high temperatures and the full exothermic peak may not have been fully recorded while the system equilibrated at the cure temperature.

Using 256.3 J/g as ΔH_T, the conversion of PETI-330 at different times and

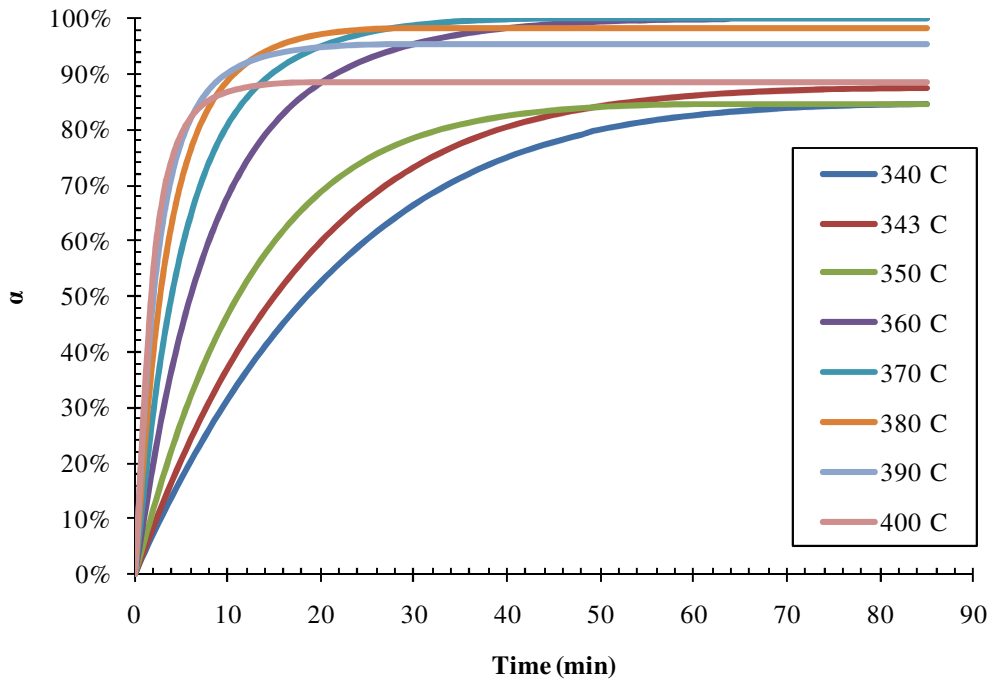

Figure 6.3: Conversion with time for neat PETI-330 cured isothermally at various temperatures. 370°C was taken as the maximum degree of cure.

temperatures was calculated with Equation 6.1 and displayed in Figure 6.3. Because maximum conversion was based on the heat of reaction at 370°C, the neat sample cured at 370°C was the only one to reach 100% conversion as defined here. However, samples cured at 360℃ and 380℃ came close at 99.9% and 98.1% conversion, respectively. Nanocomposites were tested at two temperatures: 370℃ to reflect the maximum cure characteristics and 343℃ to model the cure behavior of mechanically tested composites in Chapter 5. Only the polymer weight in each composite was considered in the integrations to determine ΔH. Figure 6.4 displays conversion for MWNT and CNF composites cured at 370℃ and Figure 6.5 displays data for composites cured at 343℃. All neat and composite samples exhibited a rapid increase in conversion at the start of the

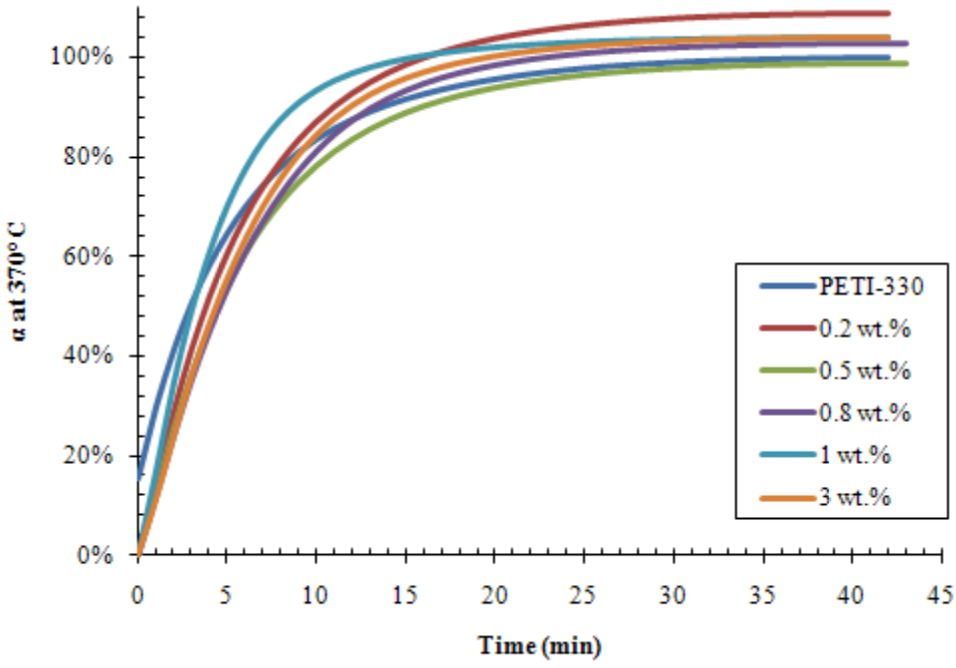

(a)

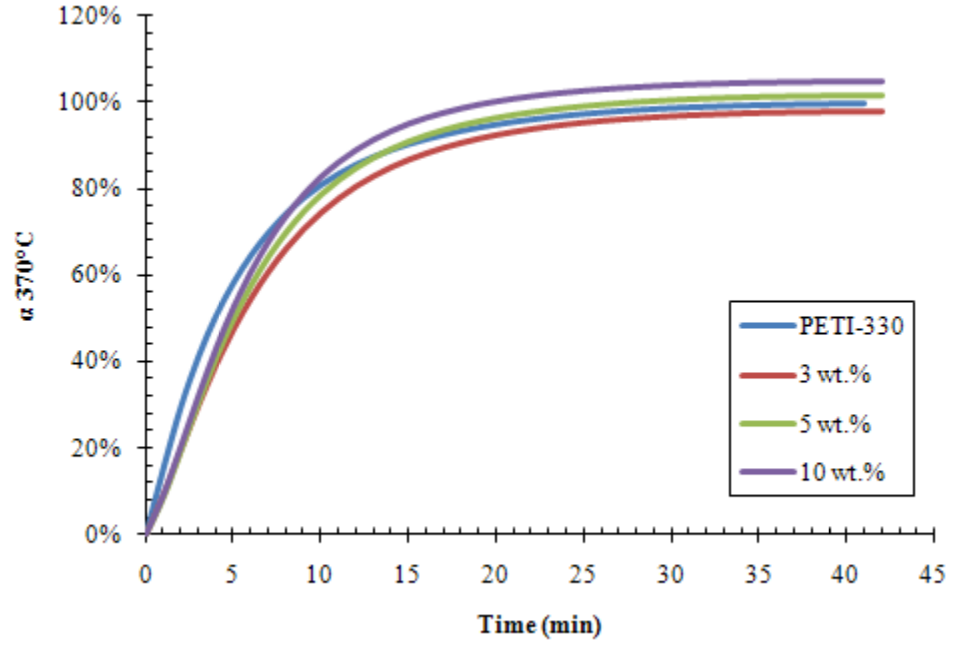

(b)

Figure 6.4: Conversion with time at 370°C for MWNT (a) and CNF composites (b).

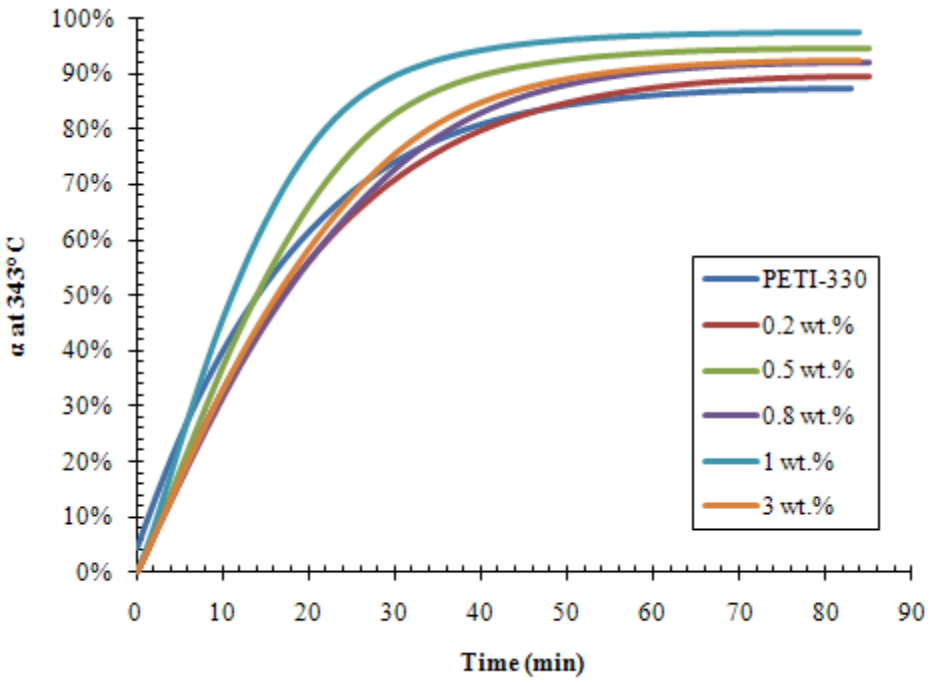

(a)

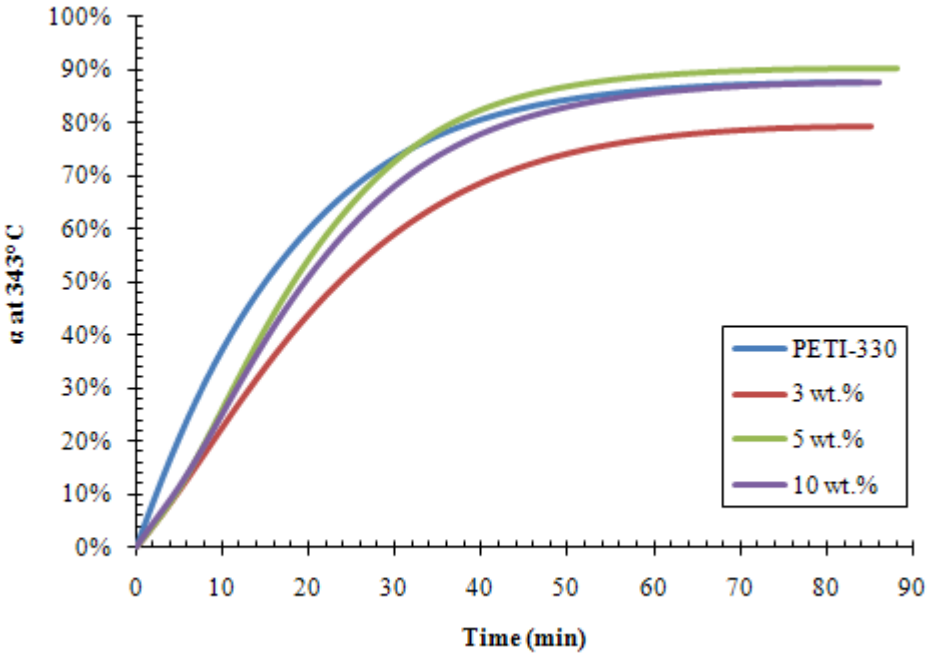

(b)

Figure 6.5: Conversion with time at 343°C for MWNT (a) and CNF composites (b).

cure but then leveled out to a nearly constant conversion for the remainder of the cure. At 370℃, all nanoparticle loadings aided in enhancing conversion with time with the exceptions of 0.5 wt.% MWNTs and 3 wt.% CNFs. In both cases, the degree of cure was less than 2% under that of the neat material. At 343℃, all MWNT particle loadings enhanced overall conversion, but 3 wt.% CNF still remained below the neat. In enhancing conversion with nanoparticles, ΔH was actually higher for most of the nanocomposites, resulting in α>100%; these values are displayed in Table 6.3.

As previously noted, an n^{th} order reaction is defined as the maximum cure rate occurring at approximately t=0, which also correlates to $\alpha \approx 0$, while an autocatalytic cure has a maximum conversion rate at 30-40% of the total cure. To classify the curing mechanism of PETI-330, the rate of conversion was plotted against the degree of conversion in Figure 6.6. The rate of conversion peaked at well under 20% for all studied temperatures, indicating an n^{th} order reaction. This conclusion could be further verified by plotting *log (dα/dt)* versus *log (1-α)*. According to Equation 6.6, an n^{th} order reaction

Table 6.3: Heat of reactions for nanocomposites at 370°C and 343°C.

Particle	Loading (wt.%)	ΔH at 370°C(J/g)			ΔH at 343°C(J/g)		
		Average	+	-	Average	+	-
None	0	256.3	5.5	5.5	224.3	2.7	2.7
MWNT	0.2	279.1	6.4	6.4	230.0	5.9	5.9
	0.5	252.7	3.3	3.3	243.0	0.7	0.7
	0.8	264.1	1.8	1.8	235.7	7.6	7.6
	1	266.9	2.6	2.6	250.2	7.6	7.6
	3	266.5	0.5	0.5	235.8	14.9	12.8
CNF	3	262.9	14.2	14.2	203.1	5.3	5.3
	5	260.5	6.0	6.0	231.4	3.0	3.0
	10	268.6	3.6	3.6	224.2	2.3	2.3

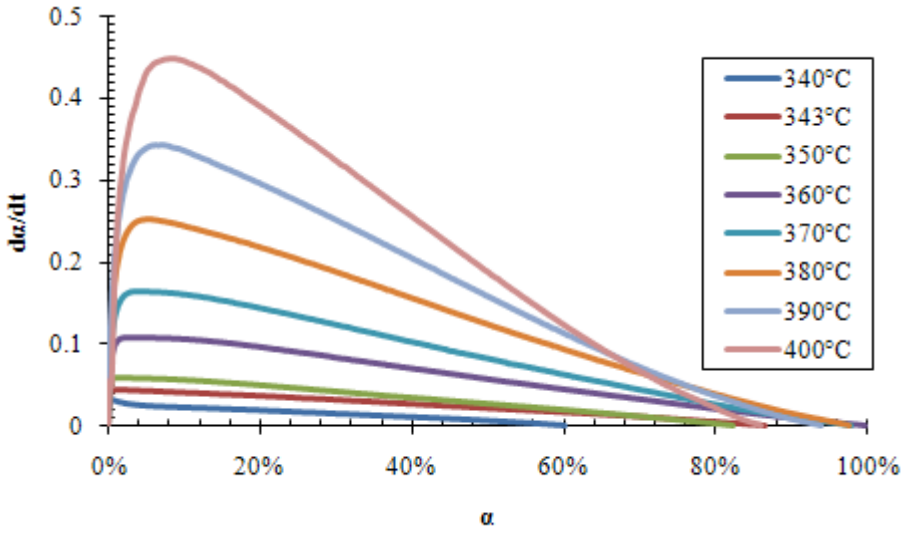

Figure 6.6: The rate of reaction with the progression of conversion for neat PETI-330 isothermally cured at various temperatures. The maximum rate of conversion occurs at less than 30%, indicating an n^{th} order reaction.

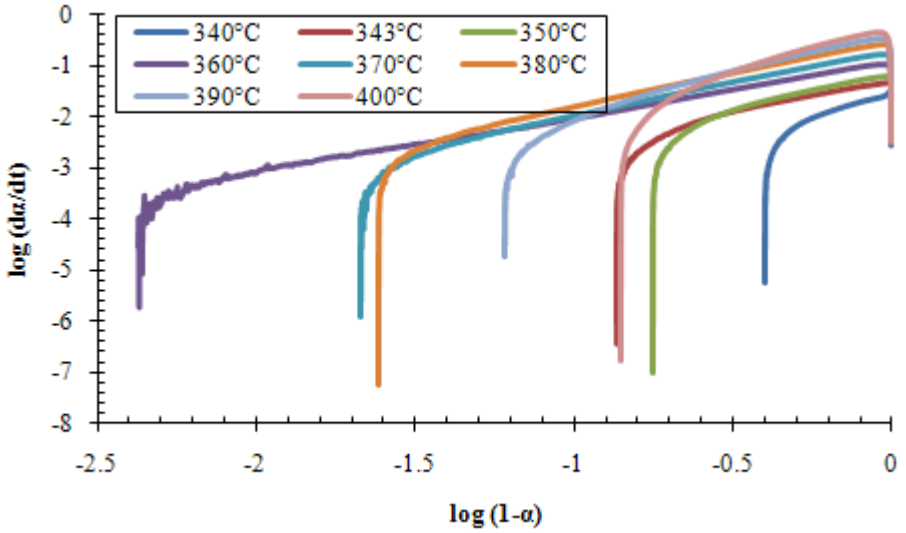

Figure 6.7: Neat PETI-330 plotted using the definition of n^{th} order reactions, as outlined in Equation 6.6. The linear behavior above the vertical drop for each studied temperatures indicates n^{th} order behavior.

would result in linear behavior on this plot; Figure 6.7 shows that all temperatures exhibited two distinct regions. The first included the start of the cure and continued until the second region, which included a characteristic vertical drop. This asymptotic behavior indicated that the rate of reaction rapidly decreased at the maximum extent of cure, which is expected at the full degree of cure.

At degrees of conversion less than each temperature's maximum, Figure 6.7 shows linear behavior, which agrees with the previous conclusion that the PETI-330 curing mechanism was n^{th} order. Linear regression was used to fit data from each temperature, and the rate constants (k) and reaction orders (n) could be determined using Equation 6.6. These values are listed in Table 6.4. By taking the natural log of the Arrhenius relationship in Equation 6.3, Equation 6.11 could be used with data in Table 6.4 to calculate the activation energy from isothermal testing.

$$\ln k = \ln Z - \frac{E_a}{RT} \qquad (6.11)$$

Table 6.4: Rate constants and orders for neat PETI-330 at various temperatures.

Temperature (°C)	k (sec^{-1})		n	
	Average	+/-	Average	+/-
340	4.94E-04	6.83E-06	1.90	0.15
343	1.01E-03	6.05E-05	1.50	0.13
350	1.41E-03	5.44E-05	1.64	0.05
360	1.78E-03	1.92E-04	1.02	0.06
370	3.18E-03	4.37E-04	1.15	0.19
380	5.28E-03	3.26E-04	1.31	0.07
390	9.38E-03	2.98E-04	1.70	0.13
400	1.20E-02	3.91E-04	1.92	0.18

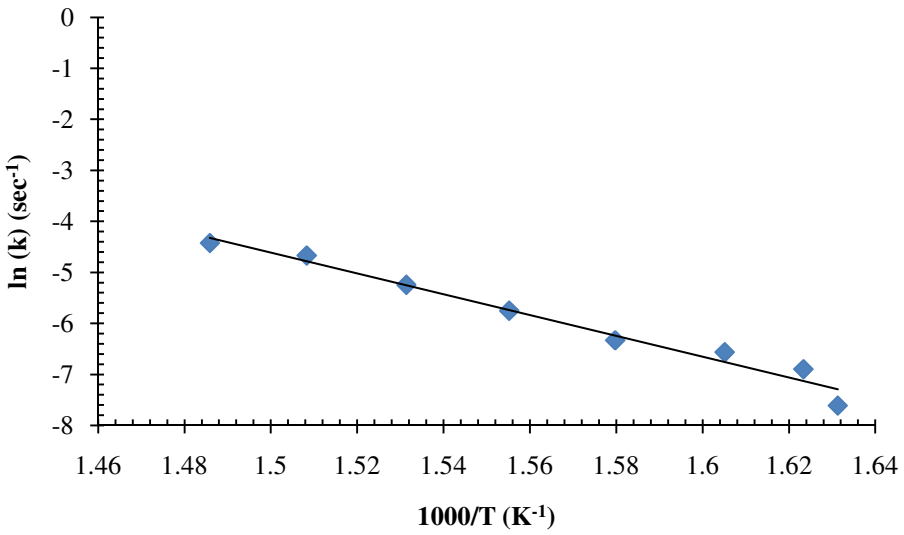

Figure 6.8: Determination of cure activation energy using the Arrhenius relationship in Equation 6.3.

Figure 6.8 shows *ln k* versus *1/T* and a best fit line for the data. The activation energy could be calculated from the slope, resulting in a value of 169.7 ± 1.4 kJ/mol. The intercept of the best fit line could also be used to calculate the pre-exponential factor (*Z*) and resulted in a value of 2.06×10^{11} min^{-1}.

The curing mechanism of PETI-330 shifted with the inclusion of MWNTs and CNFs, as illustrated in Figure 6.9 for samples tested at 370°C and Figure 6.10 for samples tested at 343°C. At 370°C, the maximum rate of conversion for MWNTs was below 20% conversion and at approximately 20% for CNFs. There was a greater shift at 343°C with MWNTs exhibiting a maximum rate of conversion at approximately 20% and CNFs at approximately 25% conversion. The PETI-330 curing mechanism was clearly n^{th} order and, although the nanoparticles caused a shift in the conversion rates to higher

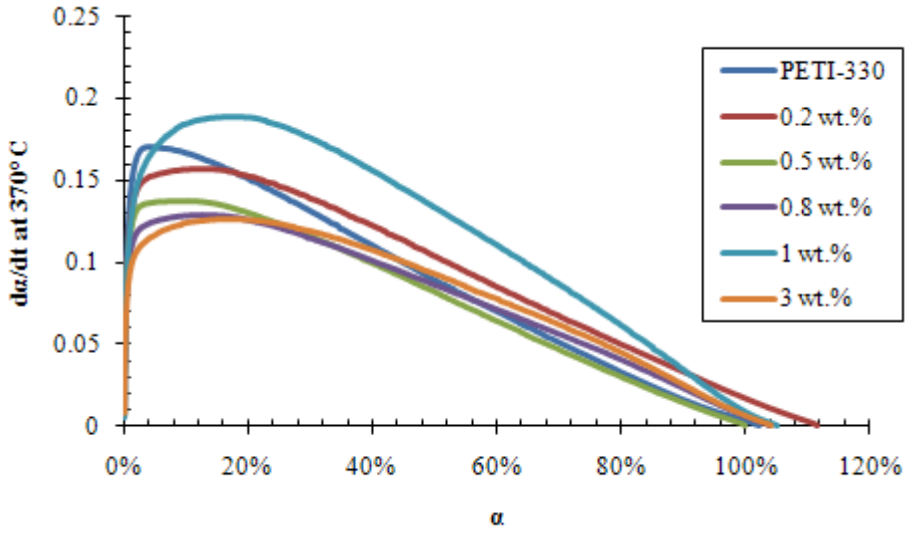

(a)

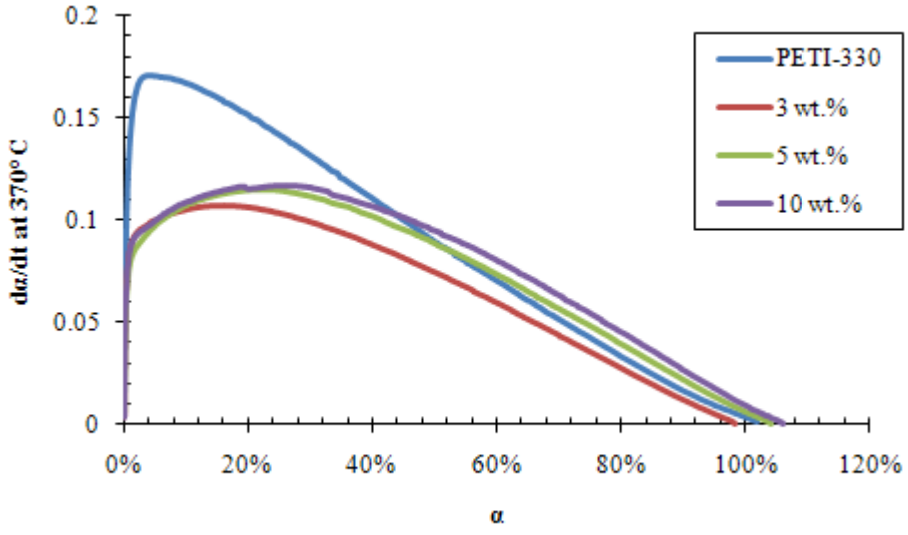

(b)

Figure 6.9: Rate of conversion with the progression of conversion at 370°C for MWNT (a) and CNF composites (b). A shift in the maximum rate is seen with the addition of particles to PETI-330.

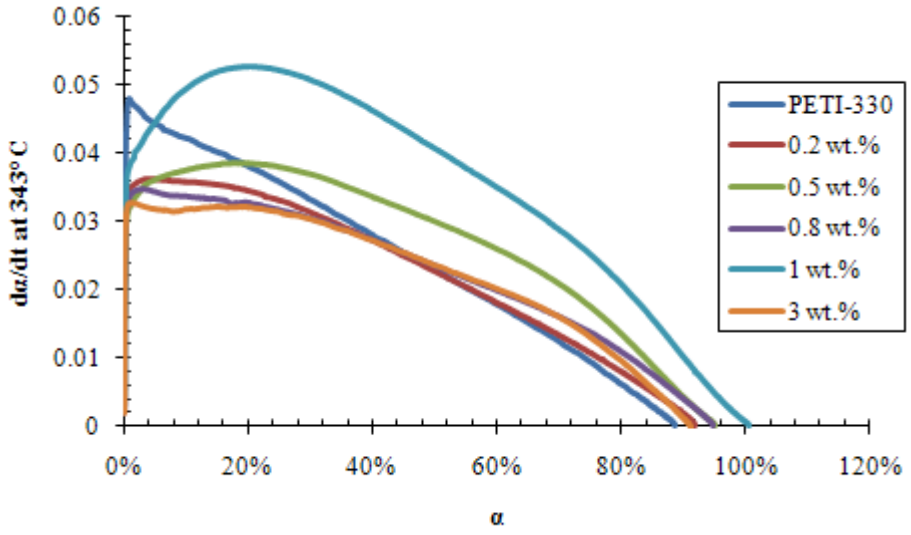

(a)

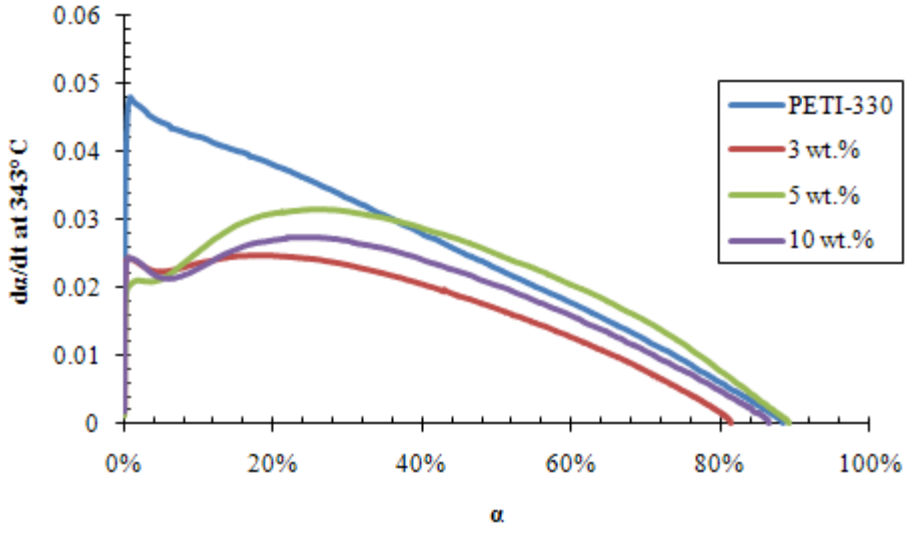

(b)

Figure 6.10: Rate of conversion with the progression of conversion at 343°C for MWNT (a) and CNF composites (b). A shift in the maximum rate is seen with the addition of particles to PETI-330.

conversions, all composites still maintained maximum rates below 30% conversion. It could be concluded that PETI-330 had an n^{th} order reaction both with and without nanoparticles, although with some delay in the nanocomposites. The difference in the shift of MWNTs and CNFs might have been caused by the differences in the particles sizes. The MWNTs were much smaller with diameters of 10-12 nm and the CNFs much larger with diameters of approximately 100 nm. The larger particles may have inhibited or impeded the curing mechanism as the network had to form around them. The smaller MWNTs would also have had the same effect, but on a smaller scale.

As previously discussed, inconsistencies in kinetic parameters may have been due to the existence of multiple cure processes of PETI-330. One method of identifying the existence of multiple cure processes is by using an isoconversional model, such as Equation 6.10. For this model, data at each degree of conversion of neat PETI-330 were taken at each studied temperature. Due to incomplete cures at some studied temperatures, data from all temperatures were obtained for only 10-60% conversion while curing temperatures of 340-400°C achieved up to 80% conversion and only 360-390°C achieved 90% or higher conversion. This decreased the number of data points for higher conversions and resulted in high variability for 90%, which was omitted from the analysis due to the inconsistencies. These data were then plotted as $ln\ (d\alpha/dt)$ versus $1/T$ in Figure 6.11 (a) for 10-80% conversion. A line was fit to each α, and E_a could be calculated from the slope of that line. The resulting E_a values are shown in Figure 6.11 (b). The activation energy was consistent from 10-50% conversion, but decreased and remained constant for 60-80% conversion.

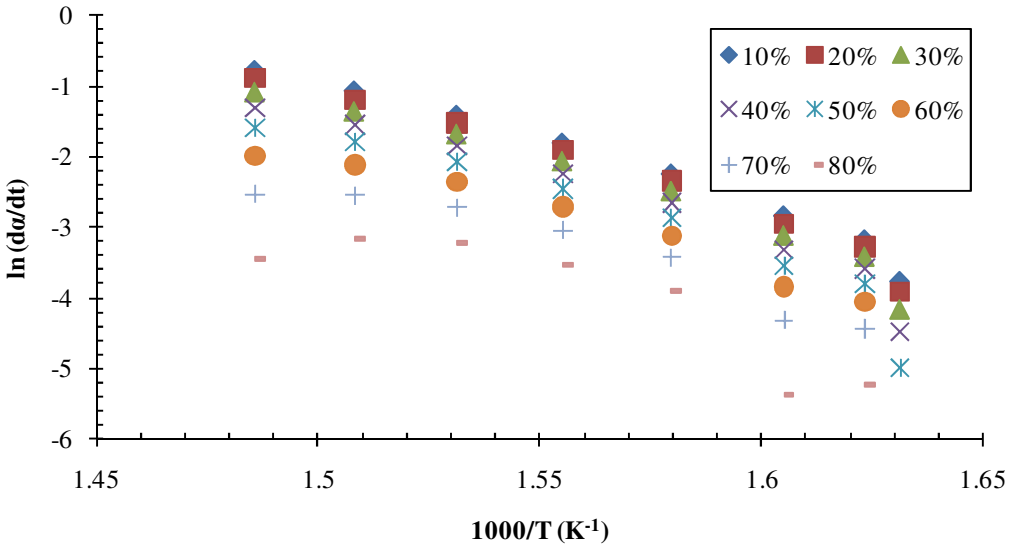

(a)

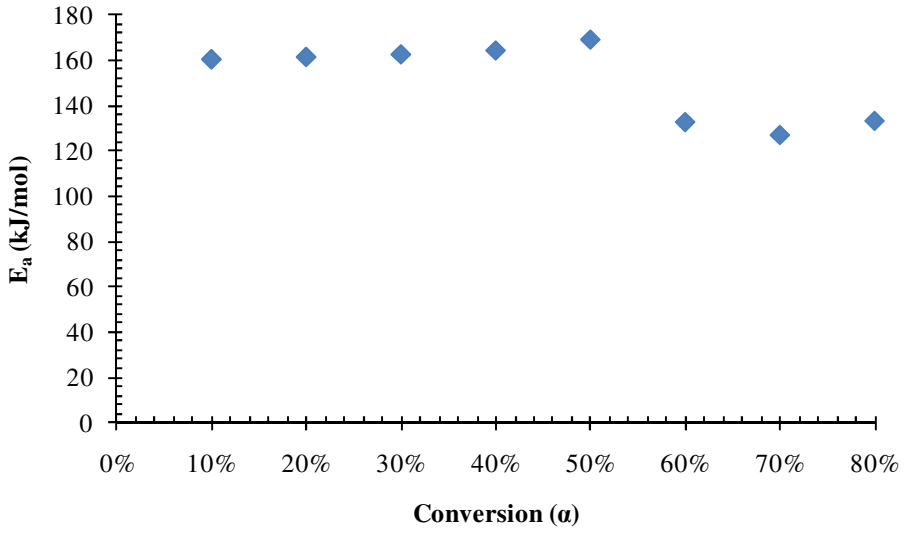

(b)

Figure 6.11: Calculations for the cure activation energy of neat PETI-330 using an isoconversional method. (a) Using a constant degree of conversion, fitting the rate of conversion to the isothermal cure temperatures. E_a could be calculated from the slope of each set of data. (b) Activation energy as a function of conversion. The data show two regions of constant values of E_a, indicating two cure mechanisms.

6.3.3 Comparison of calculated activation energies

The activation energy of PETI-330 was calculated in three different manners in this study and can be compared to one another. Using dynamic scans, values were obtained using the Kissinger method (166.0 kJ/mol) and the Ozawa-Flynn-Wall method (168.0 kJ/mol). The second method utilized isothermal testing at various temperatures and n^{th} order kinetics to estimate E_a to be 169.7 kJ/mol. These three values were obtained under the assumption that the curing occurred via a single step reaction. The third method instead assumed that E_a could change with conversion. This isoconversional method identified that PETI-330 transitioned to a very slow rate of reaction at higher extents of cure. The cure reaction of PETI-330 has been proposed to initially form polyenes through chain extension, branching, and crosslinking, which is then followed by Cope rearrangements and Diels-Alder intra- and inter- molecular reactions of the polyenes [203]. The isoconversional E_a values in Figure 6.11 (b) indicate two different curing mechanisms, with an average E_a of 163.7 kJ/mol for 10-50% conversion and an average E_a of 131.2 kJ/mol for 60-80% conversion. The initial region may indicate the formation of the polyenes while the second region indicates the intra- and inter- molecular polyene reactions.

The calculated E_a values are comparable to other phenylethynyl terminated imide studies [193-195]. Several studies have concentrated on PETI-5, which has a similar structure to PETI-330 but a number average molecular weight of 5000 g/mol. Hinkley used the Ozawa-Flynn-Wall method at various conversions during dynamic DSC scans (isoconversionally) and calculated an average activation energy of 139.0 ± 3.3 kJ/mol [193]. Fang *et al.* supplemented Hinkley's work by studying PETI-5 conversion using an

isoconversional method with infrared (IR) spectroscopy and a one step DSC analysis with the DiBenedetto equation [194]. The group reports an E_a value of 170.4 ± 11.3 kJ/mol from IR analysis and 141.5 ± 8.4 kJ/mol from thermal analysis. It is interesting to note that methods utilizing the same analysis method (DSC) from Hinkley and Fang's work end in similar results, while IR analysis was 20% higher than the average of the DSC results; this may be due to the basis of the methods, where cure kinetics using thermal analysis concentrate on the heat of reaction or glass transition temperature as measured by DSC and IR follows the ratio of absorbance of chemical bonds with time. Another study by Boswell *et al.* used a phenylethynyl-terminated imide that had been modified from PETI-5 by adding a plasticizer to reduce the overall viscosity, which behaved more similar to PETI-330 [195]. This study used the Ozawa-Flynn-Wall method as done in this study and identified the resin as n^{th} order with an activation energy of 164.5 kJ/mol. This value matches well with the E_a values obtained for PETI-330 using dynamic and isothermal testing; it could also indicate the importance of the value of viscosity in initiating the curing mechanism.

6.4 Conclusion

The cure kinetics of PETI-330 and its composites were studied using different methods by DSC. The polymer was shown to exhibit n^{th} order behavior, although nanocomposites did show a slight delay in initial polymerization. The cure activation energy was estimated as approximately 167 kJ/mol using dynamic temperature scans with the Kissing and Ozawa-Flynn-Wall models and also estimated as 131 kJ/mol using an isoconversional method. These values were shown to match closely with E_a values of

other studies. The isoconversional method also aided in identifying the existence of multiple curing mechanisms, although secondary mechanisms had minimal impact on the overall activation energies. In general, nanoparticles reduced the activation energy required to initiate cure which accelerated the cure reaction. This study has characterized the curing mechanism of PETI-330 as well as identified the influence of nanoparticles on that mechanism.

CHAPTER 7

BUSINESS PLAN

7.1 Introduction

Technology developed in a research lab is often overlooked as a potential commercially produced product due to a lack of experience or market understanding by the scientists that develop the technology. Because of this, many patents and potentially market-changing products sit collecting dust on university shelves; however, with the establishment of the Bayh-Dole Act[1] and an increase in academic opportunities that lead to more well-rounded educations, these technologies are becoming more available and have a greater impact on society. As more and more STEM (Science, Technology, Engineering, and Mathematics) students are introduced to entrepreneurship or technology commercialization, the developing scientists themselves will have and know the opportunities for moving their technology from the labs to the market place and to generate income from this productization. The purpose of this chapter is to take the graduate work presented in this dissertation and determine if there is market potential and, if so, the best method for moving it to market. It also addresses common concerns that customers have with material suppliers.

Much of this work was done under the guidance of the TI:GER fellowship program. TI:GER, Technological Innovation: Generating Economic Results, is an NSF-sponsored program that teams together a Georgia Tech PhD student and an MBA student

[1] The Bayh-Dole Act (PL96-517) of 1980 gives the control and rights of inventions arising from federally-funded research to the US universities, small business, and non-profit organizations that performed the research.

with two Emory law students. Each team then works together for two years toward understanding all the aspects required for commercializing the PhD student's research. While general concepts of the process, such as intellectual property or market analysis, are taught in the classroom by a variety of guest speakers, the development of the commercialization and business plans are mostly self-directed by the teams due to the uniqueness of each PhD project. TI:GER has produced several companies as a result of the program, including DiagNano[2], Sentrinsic, and Syzygy Memory Plastics.[3]

As part of a commercialization strategy it is also important to analyze what future customers may require. For example, customers of material suppliers will be interested in factors such as shelf life, heat and light stability, process parameter windows, influence of minor contamination, or warehouse environments. With this in mind, a series of experiments was performed to help establish such parameters.

7.2 Commercialization plan

Written with Melissa Johnson, Michelle Louie, and Andres Velarde

Nanovate was founded under TI:GER guidance by the author, Michelle Schlea, Michelle Louie (Georgia Tech MBA), Melissa Johnson (Emory Law), and Andres Velarde (Emory Law) and the group worked as a team from fall 2008 until spring 2010. Nanovate's technology is identified as a polymer material with advanced properties coupled with an ease of processing and custom design. This material product is targeted for the aerospace market.

[2] http://www.nanohc.com/about.html
[3] http://www.thesyzygy.com/

***NOTE: This commercialization plan is written toward a non-technical audience. This audience is typical among potential investors.*

7.2.1 Why aerospace?

The primary industry for Nanovate's material is aerospace. Aerospace was chosen for several reasons; this market is one of the few that would be willing to pay for the technology. Both the polyimide and nanotubes are expensive (approximate $1500 per kg and $1-100 per gram, respectively) relative to metal alternatives. The aerospace industry is also known as the initial showcase of many technologies. While there are potential future customers in the sports and health industries, aerospace would be the first to take advantage of all of Nanovate's material properties. Nanovate also possesses an advantage with an existing relationship with NASA. NASA funds the research and development of this material; while this means it will have free use of the technology, it also will provide an advertisement of the material's capabilities. This will result in a real-world demonstration of the final application of the material for other potential customers.

7.2.2 Product definition

Nanovate provides a high performance material by combining two materials known for their exceptional properties: polyimide polymers and carbon nanotubes (CNTs). Polyimides are extremely strong, temperature resistant, and easily processed. With heat treatment, this plastic structure is chemically "locked" into place, which provides an additional reinforcement mechanism. Carbon nanotubes are the strongest material measured to date, have high temperature stability, and are electrically

conductive. The small ("nano") size allows the CNTs to share their properties with the surrounding polymer when only a small amount is added. Larger particles with similar properties that must be added in larger quantities to produce similar enhancement often have a negative effect on the polymer's properties, resulting in decreased strength or processability. These negative effects may include particle clumping, increased viscosity, or poor binding between the polymer and particles.

A drawback of using CNTs is their propensity to clump together. Separating these clumps into individual particles and scattering them throughout a polymer is difficult, resulting in processing methods that require additional chemicals or significant amounts of time (hours to days). While these methods have been used previously to manufacture similar materials, only a few grams could be produced at a time. Our technology incorporates basic processing principles with material characteristics to produce a high performance material that can be manufactured in minutes and in large quantities without additional chemicals.

Our material is classified as a nanocomposite, which is a basic material used for manufacturing. Our nanocomposite, then, can be used to create a composite, which includes fiber or fabric reinforcement, and is in the final form for the given application. Overall, our product can be classified as an evolutionary incremental technology.

One of the ways in which our technology is innovative is in its processing. The processing method used with our material is one that can be used on a large-scale with common industrial equipment. The biggest issue in productization, however, is the availability of raw materials in the quantities needed. Once materials are available in the necessary quantities, productization as a materials supplier is very feasible in that

processing is readily available and takes negligible set-up and running time. Customers, then, could use our material for their own range of products, and as they see fit. As a parts supplier, however, productization would be more difficult: additional engineering and design expertise would be needed in order to design mechanical components.

7.2.3 Prior art and intellectual property

7.2.3.1 Prior art

There is published literature regarding the mixing of carbon nanotubes with high performance polymers. Currently, there are two patent applications and one published article that may indicate that our application is obvious to one in the art. These are:

- Connell, PCT/US2007/067,386 (2007) [204]. A patent application that describes a method for mixing carbon nanotubes with polyimide using a dry mixing technique. The range of nanotube loadings recommended is 3 weight percent or greater. This patent is partially based on the article by Ghose *et al.* [91].
- Fischer PCT/US05/031,041 (2005). A patent application that shows preparation of conductive thermoset precursors containing carbon nanotubes. It recommends a preferred thermoset precursor of bisphenol A derivative but also discusses polyimide. It claims a conductive thermoset where the carbon nanotube loading is from 0.5- 30 weight percent [205].

- S. Ghose, K. A. Watson, D. M. Delozier, D. C. Working, E. J. Siochi, and J. W. Connell, "Incorporation of multi-walled carbon nanotubes into high temperature resin using dry mixing techniques," Composites Part A-Applied Science and Manufacturing, vol. 37, pp. 465-475, 2006 [91].

7.2.3.2 Intellectual property plan

Due to these publications and the unique aspect of our technology, we decided to utilize trade secrets as our intellectual property strategy. However, the following intellectual property routes were considered.

7.2.3.2.1 PATENTS

While our current CNT concentrations in the polyimide and the mixing technique are not covered by any one of these relevant prior art explicitly, a patent examiner may deem that our method and carbon nanotube concentrations can be concluded from the prior art. For this reason, there have been no patents filed. Any attempt to patent would be potentially patenting a species within a genus. To do this, Nanovate will need to show that current patents do not teach our method.

Also, once a patent is granted, Nanovate would need to police the patent. Since a published patent teaches the method, patenting would expose our knowledge without giving us a method to prove infringement. Once revealed, many competitors could modify the process to use Nanovate's method while circumventing our patent. Finally, due to the rapid development of high performance polymers, our patent may not be granted before the life cycle of our material expires.

A potential future strategy would be to file several very specific patents, creating an intellectual property “minefield” for competitors to wade through. This would take a significant amount of time and money initially, but could be continuously built upon for future endeavors should Nanovate continue beyond the theoretical stage.

7.2.3.2.2 TRADE SECRETS

Nanovate has decided to use trade secrets and strong licensing agreements to protect our technology. Keeping the technology a trade secret will allow us to produce and sell material to second and first tier suppliers without disclosing our technology to end customers. By using protective licensing agreements, Nanovate will provide a strong disincentive to its suppliers who may consider reverse engineering the material. The licensing agreements will document the specific individuals in our customer’s company who are allowed to be exposed to our process, contain appropriate grant back clauses on new developments, and lay out potential damages if the customer breaks the license. The only concern with this route is that some suppliers may decide to break the agreement because we would be a small supplier and may not be able to challenge them adequately in litigation.

Nanovate has chosen this route because of the cost of policing the process and also with the knowledge that publishing the method will allow others to make small changes and claim that they are not infringing. Finally, due to the short shelf life of the technology, patenting may only lead to publishing our process and receiving a patent once the material is obsolete.

7.2.3.2.3 EXIT ROUTE OPTION

Due to the competitive landscape, another option is to seek a patent for the purpose of selling it to a larger competitor. Selling the rights to the process will allow Nanovate to profit from the technology and assure that the process has the potential to be policed. However, again, the current state of the art in the polymer composite industry may surpass our product before a patent is issued, making it obsolete before it can be sold to a larger company.

7.2.4 Market analysis

7.2.4.1 Target market

Our selected market is the global aerospace and defense market. The global aerospace and defense market has several main segments: commercial aircraft, maintenance, repair and overhaul (MRO) services, space equipment, and military equipment [206]. We will initially target the military aircraft and the space equipment segments.

We chose to concentrate on military aircraft and exclude naval craft at this time because (1) naval craft could not take advantage of our material's heat resistance properties and (2) additional research and development would be needed to determine the impact of water on the nanocomposite. Furthermore, since the nanocomposite is unique and its properties are novel, the MRO services segment will not be an initial point of focus, but may become a sizable market in the future.

7.2.4.1.1 AIRCRAFT SEGMENT

In 2008, aircraft industry market size, as measured in terms of total units to be produced and the value of deliveries from 2008-2012, was estimated to be $808 billion [207]. The aircraft industry can be segmented as illustrated in Figure 7.1.

For our selected segment, military aircraft, the market is $108 billion. We chose the military aircraft segment because it is not as affected by market forces and is less likely to be as cost-sensitive as the commercial aircraft segment [207-208]. There are always safety issues when integrating new materials and technology into new applications, which may restrict use in commercial applications; while safety is an issue for military customers, performance is still the primary concern in the pursuit of being on the leading edge of technology. Polymer composites are used today in commercial airplanes (such as the Boeing Dreamliner) because the composites were used first in military and defense applications [209]. Thus, the military aircraft segment is more likely to experiment with new composites than is the commercial aircraft segment.

7.2.4.1.2 SPACECRAFT SEGMENT

In 2008, the Space Foundation released a report that revealed more than $251 billion in global space activity in 2007 [210]. The space industry can be segmented as illustrated in Figure 7.2.

Nanovate will also focus on the government-funded segments of the space industry (domestic and international). For these segments, the market is $77 billion. Government programs for space exploration and travel are more concerned with

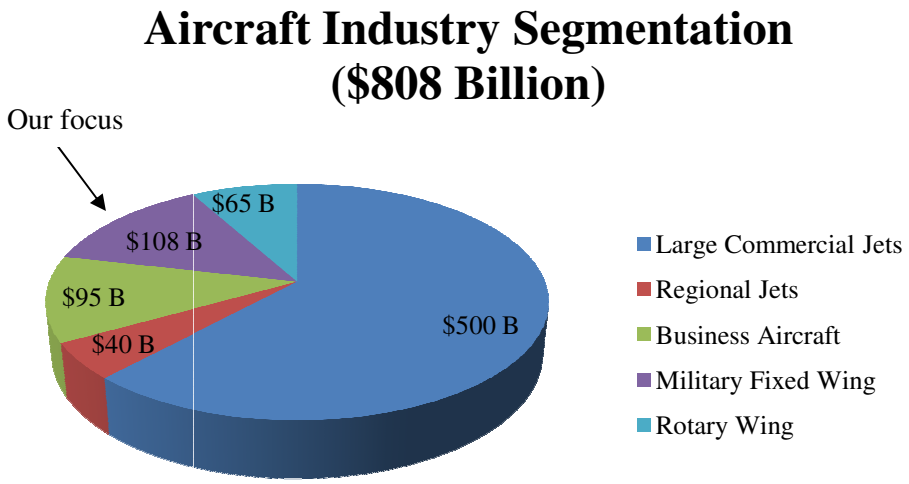

Figure 7.1: Aircraft industry segmentation as of spring 2008 [207].

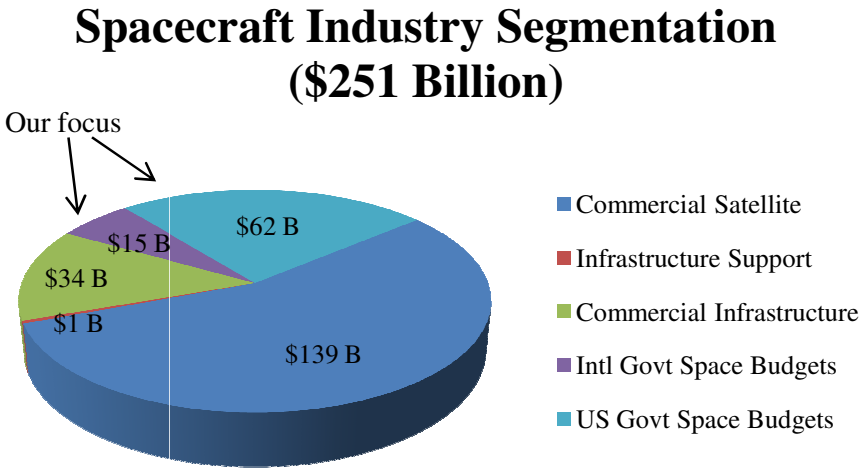

Figure 7.2: Space industry segmentation as of spring 2008 [210].

performance than cost, opening a venue for our product to first be tested and used. Reusable launch vehicles are of particular interest because they undergo extreme conditions by traveling through the earth's atmosphere multiple times; the weathering that these vehicles must withstand gives our product an application where its properties can be fully utilized. Most importantly, focusing on this segment will allow Nanovate to leverage its existing relationship with NASA to establish a reputation in the space industry. This reputation will go a long way in facilitating sales to NASA contractors.

7.2.4.2 External influences on market and industry

External influences affect both our market (global aerospace and defense) and industry (aerospace composites); these influences are particularly felt downstream in the aerospace composites industry.

7.2.4.2.1 POLITICAL: U.S. DEFENSE BUDGET

In mid-2007, the Defense industry as well as the Boeing 787 and the Airbus A380 were expected to drive aerospace's need for composite materials over the next 20 years [211]. In 2010, the White House proposed to spend $533.7 billion on the Pentagon, a 4% increase over 2009. Spending on Iraq and Afghanistan would be another $130 billion (for a total of $664 billion) [212].

The recent restructuring of the Department of Defense budget cuts production of military aircraft that would benefit from increased high performance polymer composites, such as the F-22. On the positive side, this restructuring has now opened a window for the complete redesign of military aircraft, creating an opportunity for cutting edge

technology such as Nanovate's nanocomposite. However, the current 4% funding increase for the Pentagon trails the 6.7% overall increase in the 2010 budget. More ominously, the White House budget has overall defense spending falling sharply starting in future years - to $614 billion in 2011, and staying more or less flat for a half decade. This means that relative both to the economy and especially to domestic priorities, defense spending is expected to decline.

7.2.4.2.2 POLITICAL: SPENDING ON SPACE EXPLORATION

Space applications currently represent a small, but growing percentage of the market for composites [213]. NASA has begun a major initiative to reduce costs and lighten payloads through increased use of composites in future space structures [214].

The good news for growth in composites is that the White House's plan for fiscal year 2010 gives NASA $18.7 billion, an increase of $2.4 billion over 2008 when money from the economic stimulus package is included, and stresses research into climate change and space exploration [215].

7.2.4.2.3 SOCIAL AND TECHNOLOGICAL: PUSH FOR FUEL EFFICIENCY

Standard & Poor's believes the long-term trend in energy prices will be upward, and that fuel efficiency, as well as environmental "friendliness," will remain major factors driving aircraft purchases [206]. This is a good indicator of increased composite purchases for the aerospace market because composites are directly tied to increased fuel efficiency and reductions in operating costs.

7.2.4.3 Future market potential

Although we believe Nanovate's current technology has approximately a three year window of opportunity, we expect the technology to trickle down from the military to the commercial aircraft sector. Therefore, we believe that looking at longer term trends in the commercial aircraft sector is relevant to our commercialization plan.

7.2.4.3.1 LONG-TERM GROWTH FOR COMMERCIAL AEROSPACE COMPOSITES

Composite content is increasing on new commercial airframes. The use of composites over the last 30 years has evolved from less than 5% in the Boeing 737 and 747. The Boeing 787 Dreamliner, which is scheduled for delivery in late 2011, will use about 50% composites by structural weight, and will be 20% more fuel efficient than similar-sized planes, due, in part, to advancements in composite materials technology [211, 216]. The next generation of commercial aircraft will have most of their structural parts made from composite material.

There are multiple drivers of this trend towards increased composites content. First, up to 20% - 30% in operating costs per commercial airplane seat can be saved by flying higher composite-content aircraft. Secondly, as jet fuel prices remain elevated and volatile, airlines look to replace old, less efficient aircraft with a more fuel-efficient fleet utilizing high levels of composites. Lastly, composite parts are usually easier to mold and assemble than metal airframes, and require no rivets.

The long-term growth predicted by commercial aircraft manufacturers will have a

2008 –2018 Aerospace Composites Demand (Millions of Pounds) "Buy" Weight

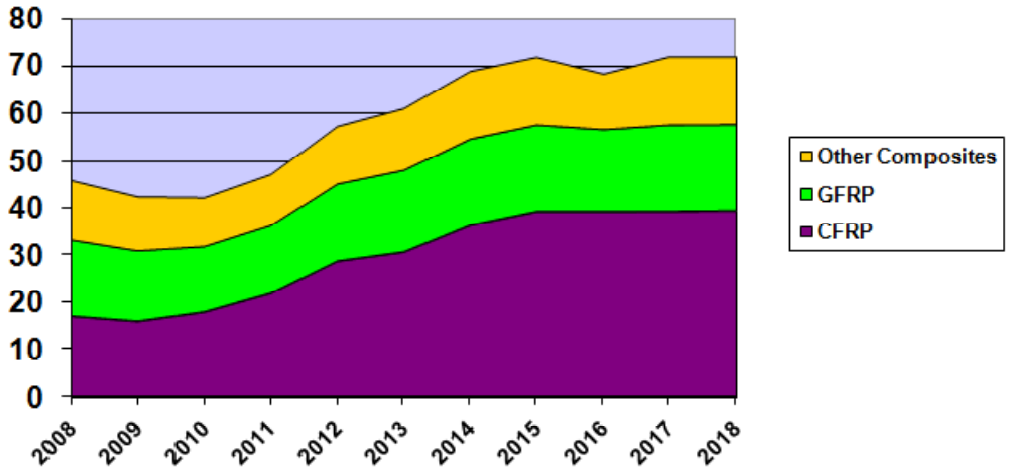

Figure 7.3: Aerospace composites demand in the next decade, as predicted by Aerostrategy, LLC, February 26, 2009 [217]. *Note: GFRP – Glass Fiber Reinforced Plastics; CFRP – Carbon Fiber Reinforced Plastics*

positive effect on the demand for composites. In its Current Market Outlook 2008–2027, Boeing predicts its fleet growth projections on a global GDP growth rate from 2007 to 2027 averaging 3.2% per year. These projections are based on a growth in worldwide air traffic driven primarily by economic growth [206].

7.2.4.3.2 GROWTH IN NEW MARKETS

Globalization of business and growth in developing economies, including China, India, the Middle East, and Latin America, will drive growth in global demand for new aircraft, and demand for new aerospace composites. Approximately 65% of the Boeing 787 orders are from airlines in emerging markets, such as Asia and the Middle East [218].

Boeing estimates that China's fleet of commercial aircraft stands at about one for every 1 million people. The fleet size in Southwest Asia, which includes India, Pakistan, and Bangladesh, is one aircraft for every 3.3 million people. In contrast, North America has one aircraft for every 62,000 people, and Europe has one for every 159,000 people. Thus, significant expansion in aircraft fleets in Asia and other emerging regions is expected over the next 20 years [206].

7.2.5 Industry analysis

7.2.5.1 Major industry trends

As a composite manufacturer for the aerospace market, our industry will be aerospace composites. Overall, the major trends in the aerospace composites industry point to long-term growth for the industry even though it will be affected by the current global economic downturn. Part of this long-term growth prediction is due to the aforementioned interest in fuel efficiency as well as ease in assembly, which is driving aerospace manufacturers to increase composite content per aircraft. More details on this key trend that is shaping the industry are presently discussed.

7.2.5.1.1 INCREASED COMPOSITE CONTENT FOR AEROSPACE APPLICATIONS

"Given the higher composite content, even if the industry stays flat, there's still going to be growth for [the aircraft composites industry]", says the Chairman and CEO of

Cytec Industries [218]. In five to 10 years, even engines will be made of high-strength, high temperature-resistant polymers [218].

7.2.5.2 Barriers to entry

There are few barriers to entering the aerospace composites industry because Nanovate intends to enter as a materials supplier. Expected barriers to entry are shown in Table 7.1 and include developing adequate manufacturing capabilities, establishing relationships with Tier 2 aerospace suppliers as well as end users like the U.S. military and NASA, and meeting the certification standards for various regulating authorities, such as the Federal Aviation Administration (FAA) and NASA [218].

7.2.5.3 Industry threats

7.2.5.3.1 THREAT OF NEW ENTRANTS

The barriers to entry for the aerospace composites industry would help protect Nanovate from new entrants to the market. Additionally, IP protection through the use of trade secrets for Nanovate's technology could also help prevent direct competition. The weakness of using trade secrets, however, is that there are no mechanisms for preventing companies from reverse-engineering to create a competing product and no recourse for Nanovate to take action on the infringers.

Because of these factors, we believe that Nanovate will have only approximately a three-year time period to fully exploit the competitive advantages of this particular

Table 7.1: Barriers to market entry and subsequent implications for Nanovate.

Barrier	Description	Implications for Nanovate
Manufacturing Capability	In dealing with specialty composites, heavy capital and technology requirements usually present high barriers to entry [219].	One of the advantages of Nanovate's composite is that it is more easily processed than most comparable materials, which make the capital investment less expensive than what is typically seen in the market.
Relationships	Would-be aerospace composites suppliers are "significantly disadvantaged by not having the relationships and the technology in-house today [220]." Companies must have a lot of experience in the space industry to be considered for a space vehicle [221].	NASA has a free license to use Nanovate's technology. This relationship will greatly benefit Nanovate in establishing our reputation as a high-quality materials provider, which will in turn lead to the development of profitable relationships between Nanovate and other government contractors.
Qualification Processes	There is also a long qualification process for parts used in military aircraft. The process is much more difficult than on the commercial side [222]. Our customers' need to meet tough qualification standards creates another barrier to new competition, because consumers of materials such as ours are often reluctant to change suppliers or alter their raw materials [219].	Nanovate will use the relationship with NASA to establish our product standards. NASA will perform significant testing on our materials to ensure it meets standards. This will enhance our attractiveness to customers who are bound by government qualification processes. Partnering with an existing materials provider may also facilitate military and eventually FAA approval.

technology. In order to continue to have a presence in the aerospace composites industry, Nanovate will have to continually invest in research and development to combat the continuing threat of newer, more sophisticated technologies.

7.2.5.3.2 THREAT OF SUBSTITUTES

From a substitutability standpoint, aerospace composites could be replaced with metals, which, until now, were the "traditional" materials used in the aerospace industry. For customers to switch from using composites back to metals, there could be substantial switching costs involved, depending on the application and material. Also, using metals as a substitute material could have downstream impacts from a weight/fuel efficiency standpoint, depending on the application [223]. However, metals may be considered a more sustainable option because they can be reprocessed while polymer composites generally cannot be reformed or reused once damaged. Some manufacturers may hesitate to switch to composites because of relatively high fabrication costs; however, composite fabrication costs are considerably lower than a decade ago and are expected to continue to decline [217].

The enhanced properties of polymer composites (reduced weight, high strength, high temperature resistance, and ease of processing and assembly) in comparison to metals make the threat of substitution low once a manufacturer has made the decision to switch.

7.2.6 Competitors

Understanding our competitive environment is also essential to commercializing Nanovate's technology. First, we must understand the technologies that compete with our material. Also, we must understand the competitive environment for high performance polymers catering to the Tier 2 and Tier 1 suppliers to the aerospace industry.

7.2.6.1 Major competitive forces and competitors

A plane is made of five main types of materials: aluminum, steel, titanium, composites, and other materials [207]. The range of material varies by plane. Nanovate's technology could potentially compete with each of these materials, which necessitates our understanding of the trends affecting their sourcing and manufacture.

As for overall trends, technological innovations, including three-dimensional design techniques, a greater reliance on composite materials, and improved "lean" production processes are being adopted across the industry [207]. The desire to create a lightweight, fuel efficient plane has resulted in steel becoming the least used material [207]. Titanium and aluminum are the two preferred metals. With improved processing and manufacturing, composites demand has grown and cut into the aluminum and titanium market as a lightweight material for the aerospace industry.

7.2.6.1.1 TITANIUM

Titanium is a common mineral. In aerospace, it constitutes a large percentage of the structural weight and propulsion systems of current advanced tactical aircraft [224]. Aerospace, in combination with industrial, automotive and sporting good applications,

consumes 84% of domestic production [224]. Even though titanium is a common mineral, its availability represents a severe constraint in the industry since its supply has been predetermined for years in advance [207].

7.2.6.1.2 ALUMINUM

The United States aluminum industry produces about $40 billion in products and exports [225]. The production of aluminum is energy intensive, so the price of aluminum is highly correlated with the price of crude oil and natural gas [226]. Large transport aircraft such as the C-17 use significant quantities of aluminum (73% aluminum) [224]. High aluminum prices and tight supply conditions, coupled with the entrance of China into the market as a supplier, has put pressure on U.S. aluminum producers [224].

7.2.6.2 Polymer composites versus metals

Polymer composites are being used as substitutes for metals such as titanium and aluminum due to a 25% to 50% reduction in weight and a better strength to weight ratio. Polymer composites will allow the aerospace industry to reduce weight while creating stronger airplane components. Nanovate offers a high performance nanocomposite which can be made into various parts by Tier 2 or Tier 1 suppliers. Nanovate's nanocomposite can be used at temperatures above 340 degrees Celsius (°C) and allows for easier processing. Unlike competing materials, our nanocomposite does not utilize compression molding or require a vacuum for manufacturing. For this reason, we will compare our product to other high performance polymers. Various polymers are used in composites. Unlike other high performance polymers, Nanovate also uses carbon nanotubes. In the

coming years, the increased production and supply of carbon nanotubes will lead to improved costs both for the airplane producers and the consumer in the aerospace industry.

7.2.6.2.1 COMPARABLE HIGH PERFORMANCE POLYMER SUPPLIERS

The main suppliers of high performance polymers are DuPont, Solvay, and Cytec. Of these, two offer polymers which can be used in applications greater than 300°C. The industry is very competitive. Materials are sold through authorized vendors that must comply with company standards. Overall, DuPont is a clear market leader that is constantly developing new products and has products covering the entire high performance temperature range. Table 7.2 identifies the characteristics of Nanovate's primary competing products.

Table 7.2: Comparison of Nanovate's material characteristics with those of main competitors.

	Nanovate	DUPONT The miracles of science	CYTEC
Product Name	SRB2009	Vespel SCP	Avimid N
Operating Temp °C	342	370-430	332
Ease of Process	No machining or vacuum required	Must be machine cut into shapes	Uses vacuums or machine cut
Material Form	Powder	Rods	Pellets/powder
Electrically Conductive	Yes	No	No

Cytec Engineered Materials produces a variety of materials, including high performance polymer composites, specialty thermoplastic materials, and carbon fibers [227]. Thermoplastic polymers have the added benefit of being re-processable; however, they do not have the ability to "lock in" a chemical-particle structure formation. This creates a loss in strength and reinforcement which limits their use. Cytec's products are used on nearly every modern commercial transport aircraft, military aircraft and rotorcraft in production. Of their products, Avimid most closely resembles our composite. Avimid boasts a wet service capability up to 332°C and is sold in resin form [228].

DuPont is a fully integrated chemical company and the market leader in high performance polymers. With over 40 years of experience, DuPont's Performance Materials division had over $6.4 billion in sales in 2008 [229]. The company offers a fully integrated line of polymers which span a broad temperature range. Their highest performance polymer is the Vespel line. Vespel SCP-5000 and SCP5050 are the newest additions to the Vespel line. SCP 5000 is sold in rods and can withstand operating temperatures between 370-430°C [230]. This year, DuPont is launching the SCP5050 product line which the company will mold to customer specifications for large orders directly to DuPont.

7.2.6.3 The Nanovate advantage

Nanovate will sell a powdered, uncured high performance nanocomposite. The ability to easily mold parts is very desirable. Currently, DuPont is preparing to launch SCP5050 which will also be molded by DuPont. However, our product allows Tier 2 suppliers to mold their own products. Table 7.3 summarizes how Nanovate's technology

addresses our customers' needs, which includes processing, performance, and safety mechanisms. While other companies may be able to provide a material with similar thermal and mechanical properties, Nanovate's material is uniquely easy to process into wide variety of shapes and also provides an additional safety mechanism through its electrical properties.

Future product extensions include applying our manufacturing processes to other polymers to enhance their performance while maintaining end customer ease of processing.

7.2.7 Potential customers

In the aerospace market, a tiered system of suppliers service major players, who are represented by final assemblers and designers. Figure 7.4 illustrates the basic tiered supply chain, and Figure 7.5 outlines the pros and cons of supplier positions in each tier. Tier 1 suppliers are contractors who supply engineering and manufacturing services to the main players, are well established, and have gone through major qualification processes. They generally supply large vehicle components or systems such as wings, cockpits, fuselages, etc. Tier 2 suppliers, in turn, supply services and smaller parts to Tier 1 that help to build the larger parts, which are sent for final vehicle assembly. Lower tiers are known as basic suppliers; this is where most players enter the market. As companies establish themselves as high quality and price competitive suppliers, they are

Table 7.3: Nanovate product values meeting customer needs.

Customer Needs	Value Provided
Easy Processing	• Processing requires minimal labor and uses common plastics and composite processing equipment. • Low melt viscosity allows use in many injection processes. • Highly customizable final component designs.
High Temperature Resistant	• Temperature resistance up to 342°C. • Stability at high temperatures for prolonged periods of time (2+ hours).
Structural Strength	• High strength. • Can withstand vibrations with carbon fiber reinforcement.
Minimized Weight	• Results in increased fuel efficiency. • Enhanced aerodynamic performance.
Increased Component Safety	• Electrically conductive to aid in lightning strike mitigation. • Structural health monitoring- changes in conductivity can indicate component damage (see Appendix A). • Can be used for electrostatic dissipation.

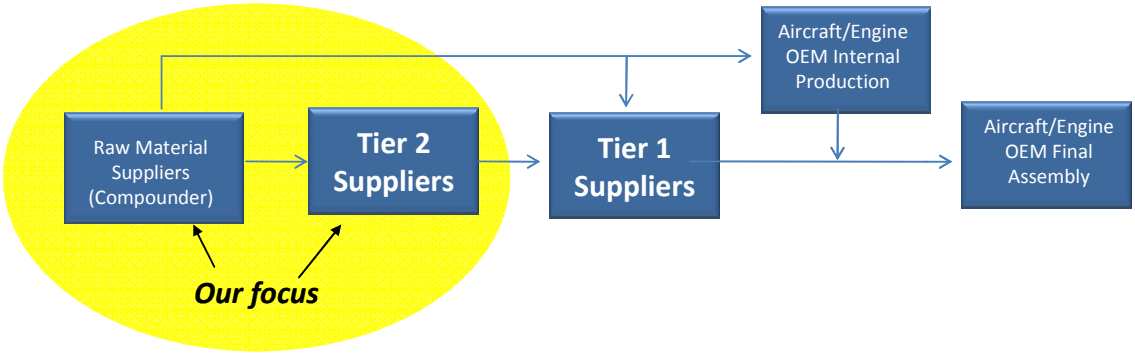

Figure 7.4: Tiered supply chain for the aerospace industry.

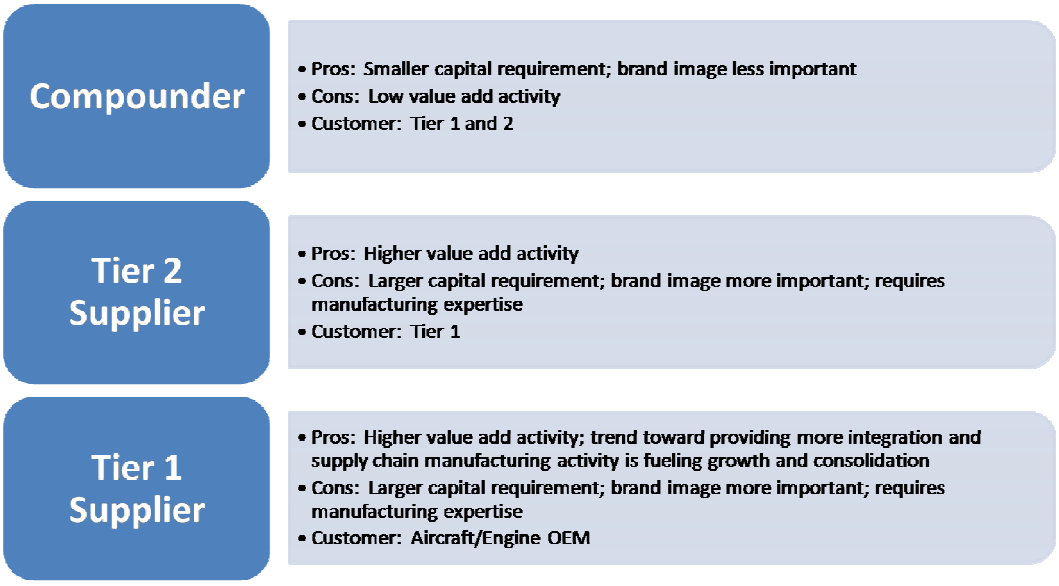

Figure 7.5: Summary of tiered supply chain pros and cons.

able to expand their core competencies and move into higher tiers. The higher tiers have increased profit margins because it is difficult for new entrants to acquire significant market share.

Nanovate will create a corporation to enter the market as a materials supplier to lower tiers. Being a materials supplier will allow us to establish our name without having to go through the difficult qualification processes required by higher tiers. Nanovate's current relationship with NASA can also be leveraged to break down another difficult barrier to entry: relationships with government contractors and reputation in the industry.

7.2.7.1 Customer needs

Polymer composites can be used in both structural applications (e.g., bushings, bearings) and wear applications (e.g., wear pads and strips, seals). The desired qualities for each material vary in importance by both market and application [209]. Figure 7.6 graphically depicts the relative importance of each attribute by market.

7.2.7.2 Sales and marketing strategy

The main elements of Nanovate's sales and marketing strategy consist of segmenting and positioning (which were addressed previously) and the proposed marketing mix, which is addressed in Figure 7.7. The importance of Nanovate's values in properties and performance can be seen throughout these elements.

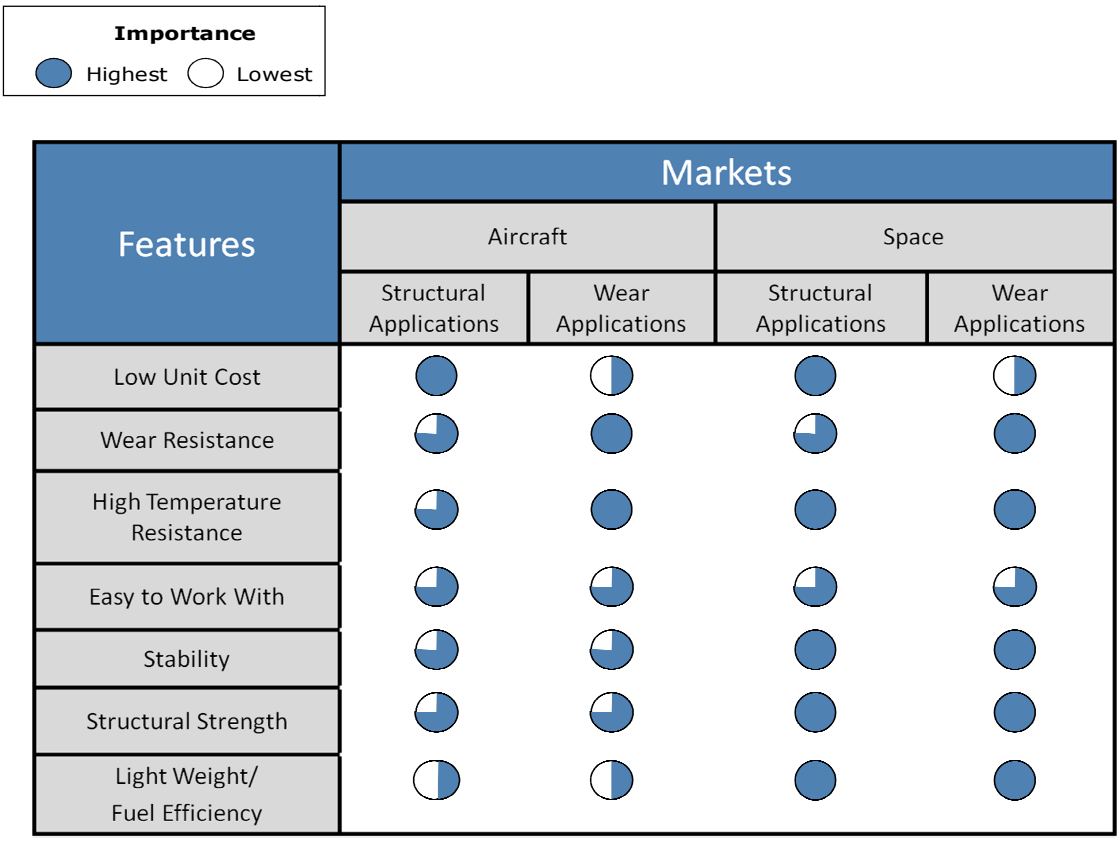

Figure 7.6: Relative importance of material attributes by market and application.

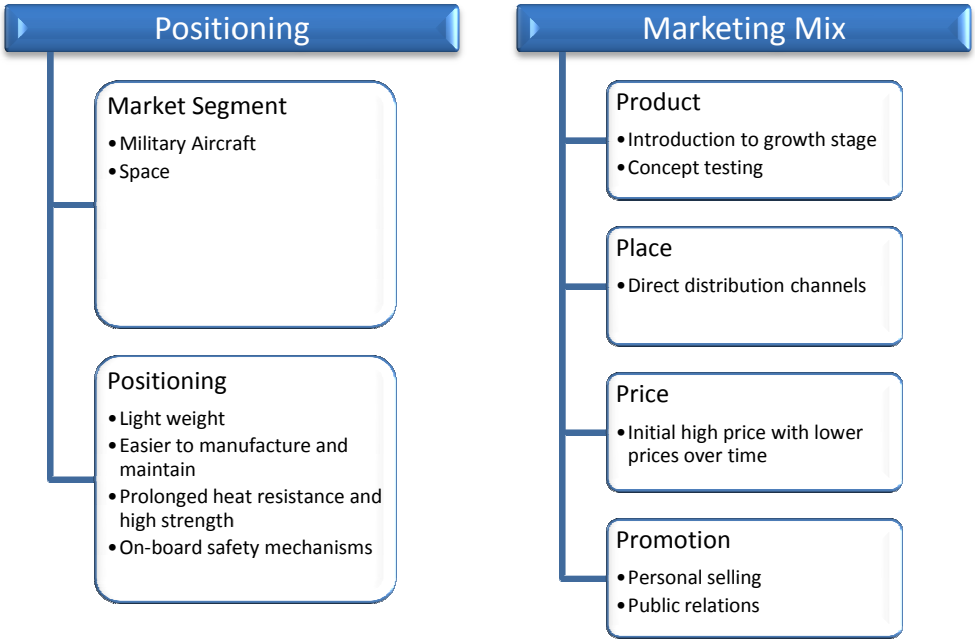

Figure 7.7: Summary of marketing and sales strategy.

7.2.7.2.1 PRODUCT

Nanovate's product is currently in the development stage. The polymer composite industry, as a whole, is fairly mature. In contrast, the use of polymer composites in aerospace is in a growth stage. Our particular polymer nanocomposite is in an even earlier stage in the product lifecycle. A concept test will need to be done with the product. This will occur before final prototypes are designed to incorporate customer feedback. During concept testing, Nanovate will also develop a brand which customers can use to remember our product.

7.2.7.2.2 PLACE

Regardless of Nanovate's position in the value chain, we would use direct distribution channels. Our customers are geographically grouped in aerospace regions in the country, such as Ohio, California, and Florida, and are businesses, rather than consumers. Direct distribution channels are also key because extensive technical knowledge would be required in promoting our product.

7.2.7.2.3 PRICE

Nanovate would utilize a price skimming approach for pricing our product. Price skimming involves setting a relatively high price for a product at first, then lowering the price over time. Our product offers a significant performance advantage over existing products, and its ease of manufacture using some existing equipment means that customers would have low switching costs in many cases. Because our polyimide is considered a specialty product, its cost is currently high. Once synthesizing raw material

costs for this polyimide have been addressed and economies of scale increase, the price of this polymer and, thus, our material can be lowered [230].

7.2.7.2.4 PROMOTION

Nanovate plans to use personal selling as our primary means of promotion. Although this could be expensive, it is necessary because (1) a great deal of technical knowledge would be required to effectively communicate the benefits of our product to the customer and (2) we anticipate having long sales cycles. Our secondary means of promotion would be through public relations such as inviting political figures as well as the general public to view demonstrations of the technology. Public relations will help us to build credibility and a brand image. As an added benefit, it could promote our company to the venture capital/angel community, which would help with funding.

7.2.8 Financial analysis

We believe that Nanovate has a product that can be sold at a marketable price, and that we will have positive cash flow. Our initial analysis indicates that we could potentially realize revenues of $9.27 million in the first year, and, based on modest penetration and revenue forecasts, that this could reach $37.1 million by the third year. We used conservative values for penetration and quantity estimates because although we believe that our material has a competitive advantage, we realize that it is expensive, and that this could dampen overall demand for our product.

Because our material is easily processed, our capital requirements are relatively low. Therefore, our main financial criteria for moving forward would be based on

Nanovate being able to raise the money needed for capital equipment and working capital. Another key milestone would be having a customer pipeline so that we can estimate funds needed for working capital, as our raw materials are expensive.

Based on revenue and expense projections as outlined in Table 7.4, as well as capital equipment requirements, we believe that we could potentially generate positive EBITDA (earnings before interest, taxes, depreciation, and amortization) of $269,000 in the first year and $2.16 million by the third year.

Table 7.4: Three year revenue and expense projection.

	Year		
	1	**2**	**3**
Revenues	$9.27 million	$27.8 million	$37.1 million
Expenses and Capex	$9.00 million	$26.2 million	$34.9 million
EBITDA	$269,000	$1.61 million	$2.16 million

7.2.8.1 Determining revenues and expenses

We began the financial analysis of our technology by determining the total size of our potential market. Aerostrategy estimates that there are 20-25 Tier 1 suppliers, with annual revenues of several hundred million dollars each [217]. Estimating Tier 2 suppliers is more difficult, however. Aerostrategy estimates that there are "hundreds and possibly thousands" of Tier 2 suppliers, each with annual revenues under $100 million [217].

We used this information as a basis for estimating the total number of potential Tier 1 and Tier 2 customers. Then for the next 3 years, we used penetration rates of between zero and 7.5% for Tier 1 suppliers and between 0.5% and 1% for Tier 2

suppliers to estimate our customers per year. We then projected the total amount of material sold per year by estimating the amount of material required (by weight) for projected quantities of small, medium, and large parts. Estimates of projected quantities of parts were based on customer interviews [209].

Based on these quantity projections, and margins of 18%, we were able to forecast our revenues by year. We assumed a cost per kilo of $1045, which is based on:

- Polyimide, $900/kilo
- Carbon nanotubes, $35/gram
- 0.5% nanotubes by weight, ideal formulation for composite

Our preliminary financial analysis also included a projection of capital equipment requirements and expenses by year. Ease of manufacture means that our production, capital equipment, and facilities expenses are expected to be relatively modest. We expect that the bulk of total yearly expenses will be comprised of cost of materials and licensing fees (to Georgia Tech). At this time, monthly working capital requirements have not yet been determined.

Details supporting our financial analysis can be found in Appendices C and D.

7.2.8.2 Funding

In order to commercialize this technology, Nanovate must raise funds to cover capital expenditures for production equipment, as well as working capital needs (to cover

monthly expense outlays for such items as cost of materials, facilities rental, salaries, marketing and other Selling, General and Administrative (SG&A) expenses.

Possible sources of funding for Nanovate include friends, family, and personal savings. Funding may also be available from the United States Small Business Association Office of Technology through its Small Business Innovation Research (SBIR) and Small Business Technology Transfer (SBTT) programs. SBIR and SBTT funding is generally solicitation based, so ability to raise funds through this approach would depend on the technology needs of various federal government agencies, including DARPA and the Department of Defense. Based on this difficult economic climate, the probability of raising funds from angel investors is fairly low. The probability of raising funds from venture capital is even lower, as this economic climate has made them extremely risk averse and has impacted the amount of money they are willing to invest in a potential venture.

7.2.9 Valuation

Two methods were used to determine the value of Nanovate technology: discounted cash flow (DCF), and discounted cash flow using Monte Carlo analysis. Based on these results of these methods, we believe that Nanovate has a likely valuation in the range of $1.21 to $1.80 million. This is based on revenue and expense projections for a three-year timeframe beginning once prototypes are completed and we are confident that the product performs as expected. We believe that we can reasonably project revenues and expenses (within a range) during this timeframe. However, we also believe that because of technological innovation in this industry, we cannot reasonably project

revenues and expenses beyond this time period. In fact, because our intellectual property protection relies on the use of trade secrets and licensing, we feel that this three-year timeframe could represent the full lifecycle of this particular nanocomposite. We also did not incorporate lifecycle and replacement analysis into this valuation. Our research indicates that parts made from Nanovate nanocomposites will be extremely durable, and thus will not require replacement within our three-year timeframe for analysis. However, looking beyond this timeframe, we would expect to find alternative uses for our nanocomposite, perhaps in other markets. Also, we plan to apply Nanovate technologies and processes to other composites. Both of these factors would impact our valuation.

7.2.9.1 Discounted cash flow analysis

Based on three-year revenue and expense projections and a 40% discount rate, basic DCF analysis values our technology at $1.8 million, as shown in Table 7.5. This is based on projected EBITDA and thus does not account for taxes, interest, and depreciation.

Table 7.5: Discounted cash flow analysis.

	Year		
	1	**2**	**3**
Revenues	$9.27 million	$27.8 million	$37.1 million
Expenses and Capex	$9.00 million	$26.2 million	$34.9 million
EBITDA	$269,000	$1.61 million	$2.16 million
EBITDA, Present Value	$192,000	$821,000	$787,000
DCF Valuation (Total NPV)	**$1,800,000**[4]		

[4] NPV is based on 3 year timeframe beginning after prototype completion

We also performed a basic sensitivity analysis on the impact of discount rate and margin on this discounted cash flow model (see Appendix C). Varying margins from 5% to 35% and discount rate from 25% to 50% provides a wide range of valuations – from $(2.13 million) to $8.21 million.

7.2.9.1.1 ASSUMPTIONS

We made several assumptions when determining our valuation using the DCF model. These assumptions are detailed in Appendix C and are summarized here:

- Projected revenues:
    - Raw material costs (based on the ideal formulation of Nanovate composite)
    - Total number of potential Tier 1 and Tier 2 customers
    - Penetration rates for Tier 1 and Tier 2 customers, by year
    - Weight (quantity of material required) for different sizes of finished parts
    - Quantity of material demanded, by part size, customer type, and year
    - 18% margin (performed sensitivity analysis)
- Projected expenses and capital equipment requirements
- 40% discount rate (performed sensitivity analysis)

7.2.9.2 Monte Carlo analysis

In order to test the sensitivity of our DCF model to our assumptions, we performed a Monte Carlo analysis[5] on Nanovate's basic DCF model. Monte Carlo analysis on our DCF model indicated a range of possible valuations from $1.21 million to $1.59 million. It also indicated that the probability of having a valuation of at least $1 million is between 64.8% and 96.8%.

The goal of this analysis is to determine the sensitivity of our valuation to various assumptions. Thus, we analyzed the impact of varying the range of values (using a normal distribution) for the following variables:

- Raw material costs
- Tier 2 and Tier 1 penetration rates
- Weight (quantity of material required) for different sizes of finished parts
- Number of parts sold, per size, per year, and per customer type
- Discount rate
- Margin

This Monte Carlo analysis indicates that our overall valuation of Nanovate is particularly sensitive to:

- Margin (62.7% of our valuation is determined by our margin)
- Raw material cost (16.4% of our valuation is determined by our raw material cost)

[5] 20,000 trials for each simulation

Although our model is particularly sensitive to these variables, the Monte Carlo analysis does indicate that our DCF model is robust and has a high probability of having a positive net present value. Please see Appendix D for additional details regarding the Monte Carlo analysis.

7.2.9.3 Other valuation models

Other commonly used valuation methods, such as decision tree analysis, real options analysis, and comparable firm analysis did not apply to our technology. Decision tree analysis did not apply because the probability for success for our technology is not based on multiple stages with decision criteria and corresponding probabilities of success, but rather on our estimates of annual revenue and expenses once we commercialize our technology. Real options analysis did not apply because the standard deviation for our technology is unknown. Finally, although there are many raw material suppliers in the aerospace composites industry, financial information is not publicly available for those who are of comparable size and who sell a comparable technology.

Table 7.6: Summary of valuations of Nanovate technology by different methods.

Valuation Methodology	Valuation
DCF Model	$1.8 million
DCF Model, Sensitivity to Margins and Discount Rate	$(2.13 million) to $8.2 million
Monte Carlo Analysis	$1.21 million to $1.59 million

7.2.9.4 Valuation summary

The various valuations of Nanovate technology are summarized in Table 7.6. Differences in valuation can largely be attributed to:

- The impact of margin and discount rate on the DCF model
- The impact of applying probabilities to our assumptions instead of using static values
- The impact of varying distributional assumptions when applying Monte Carlo analysis to the DCF model

7.3 Sample conditioning for customer use guidelines

As a material supplier, it is important to know the sensitivity of the material to the various conditions that it might encounter during manufacturing, transit, and storage. Further, it is also important to know the process windows in which the resulting product still maintains its optimal properties. These concerns can be studied by basic laboratory experiments and also by applying previously recorded material properties.

Two common issues in material packaging, shipping, and storage are water contamination and light exposure. Water contamination can lead to processing issues during final component manufacturing, and usually results in discontinuities or air pockets due to evaporation at high temperatures. Water can also cause erosion and degradation over time. Similarly, if material is packaged incorrectly, it may be exposed to light for a prolonged period. Light can break down the chemical structure of the material and may result in reduced properties and processability.

7.3.1 Experimental

For this work, processing studies were limited due to raw material limitations. Experiments, then, were based on material property change over time using thermal analysis. Future work would include processing studies as material becomes more available. For light exposure studies, neat, 0.5 wt.% MWNT, 5 wt.% MWNT, 3 wt.% CNF, and 10 wt.% CNF samples were powdered and packaged in sealed polyethylene bags. The bags were then placed less than one foot below a fluorescent lamp. Exposure was continuous over 175 days. Samples were taken at periodic intervals and tested using differential scanning calorimetry (DSC) and thermal gravimetric analysis (TGA). For water contamination samples, 1 gram each of neat, 0.5 wt.% MWNT, 5 wt.% MWNT, 0.5 wt.% CNF, and 10 wt.% CNF samples were placed in capped glass vials with 20 drops, approximately 40 mL, of water. Contamination was in one discrete quantity on the first day. The vials were placed in a dark drawer at room temperature and all samples were removed periodically and tested using DSC and TGA.

A TA Instruments Q200 DSC was used to determine the post-cured glass transition temperature (T_g) of all samples. Each sample went through a one hour cure at 371°C and followed by a temperature ramp at 10°C/min to 700°C. Degradation temperatures at 95% and 75% of original weight were identified and compared.

Basic cure processing windows were studied through DSC. Neat, 0.5 wt.% and 5 wt.% MWNT, and 3 wt.% and 5 wt.% CNF samples were prepared for cycles of varying time and temperature. For cure time studies, each sample was ramped to 371°C, held for 10, 30, 60, and 120 minutes, and followed by a temperature sweep to determine T_g on cooling. For cure temperature studies, each sample was ramped to 350°C, 371°C, and

390°C, held for 60 minutes, and followed by a temperature sweep to determine T_g on cooling.

7.3.2 Light study results

Overall, the light studies show that filler particles help to stabilize fluctuations in T_g, as illustrated in Figure 7.8. The neat material experienced an overall loss of 6°C in T_g over 175 days of exposure. Composites with 0.5 wt.% and 5 wt.% MWNTs fluctuated 9°C and 2°C in T_g, respectively, over the 175 testing days, but had an overall loss of 1°C or less. In these composites, the MWNT particles are helping to reinforce and stabilize the crosslink network, counteracting degradation due to light. The 3 wt.% CNF composites fluctuated by 18°C and exhibited an overall loss of 17°C in T_g, while the 10 wt.% CNF composite fluctuated by 12°C and experienced a small increase in T_g. While

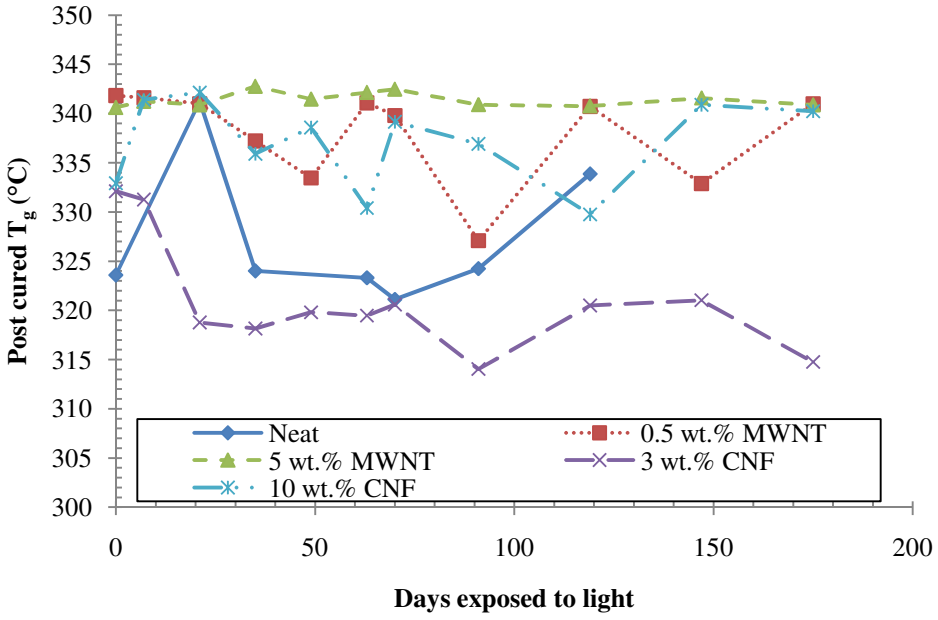

Figure 7.8: Post-cured T_g of select composites as a result of light exposure.

both CNF composites had fewer fluctuations than the neat material during the testing period, their reinforcement effect was less than that of the MWNT composites.

Figure 7.9 illustrates TGA data for samples taken throughout the sampling period and their respective temperatures for 95% and 75% of original mass during the heat scans. The onset for degradation for all samples occurred in the region of 95% of original mass, and 75% occurred after significant degradation was initiated. For 95% original mass, all samples exhibit an initial loss in temperature during the first 21 days. However, after those 21 days the loss began to stabilize. Like the T_g data, higher particle loadings had less variability between testing days. Data taken at 75% original mass was much more variable due to the dramatic loss in sample mass in that region of the TGA graph. Trends at 75%, however, are similar to those for 95% original mass although more pronounced.

7.3.3 Water study results

DSC Results from the water contamination studies can be seen in Figure 7.10. The neat material experienced up to 9°C fluctuations in T_g, but ultimately only lost 1°C over the studied 70 days. MWNT composites fluctuated by as much as 19°C for the 0.5 wt.% sample and 12°C for the 5 wt.% sample. Like the neat material, the 0.5 wt.% MWNT sample experienced only a 1°C loss in T_g over the whole testing period; however, the 5 wt.% sample exhibited the most stable T_g until day 56, after which it decreased by 10°C. CNF composites also fluctuated throughout the testing period, but only lost 1-2°C over the entire testing period. TGA data for the water contamination

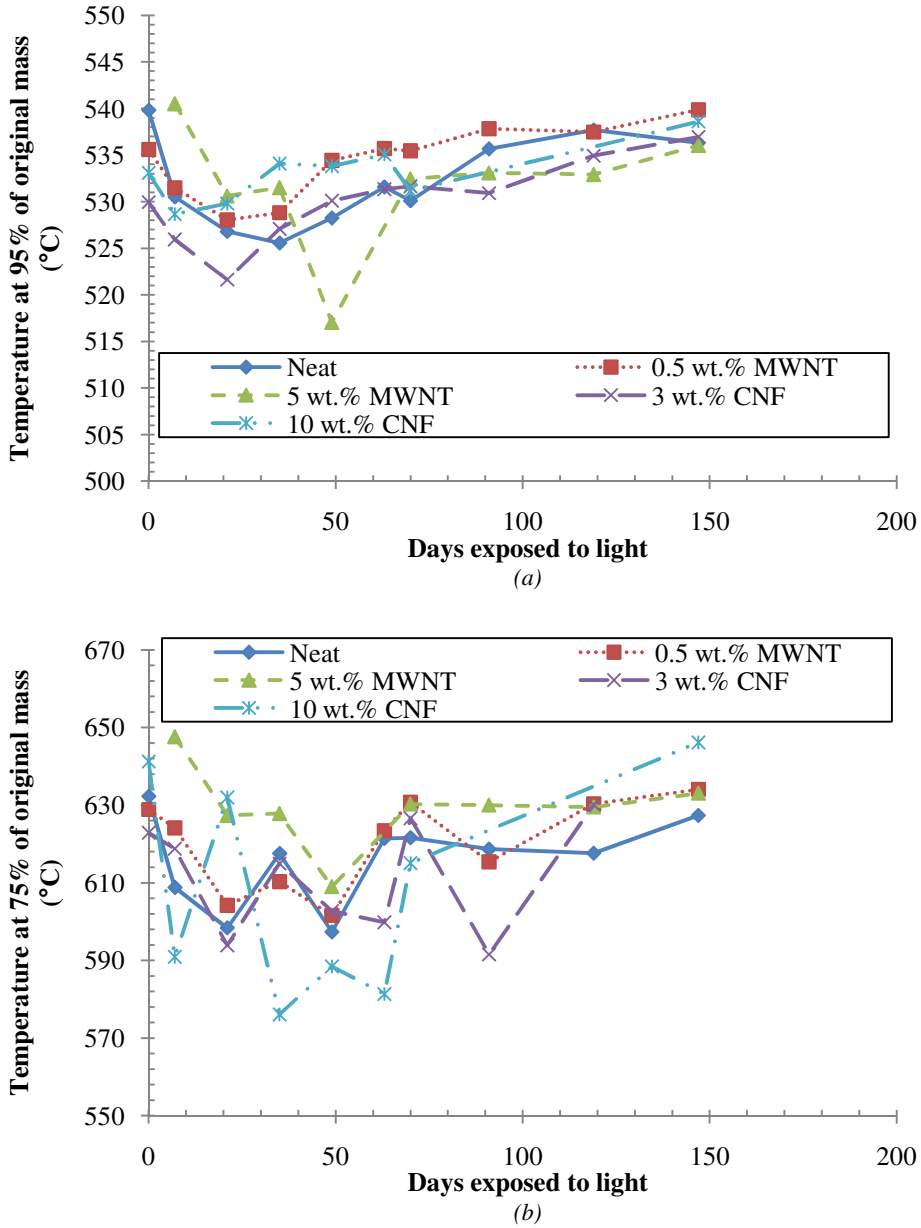

Figure 7.9: Temperatures at 95% (a) and 75% (b) original sample mass for select composites as a result of light exposure.

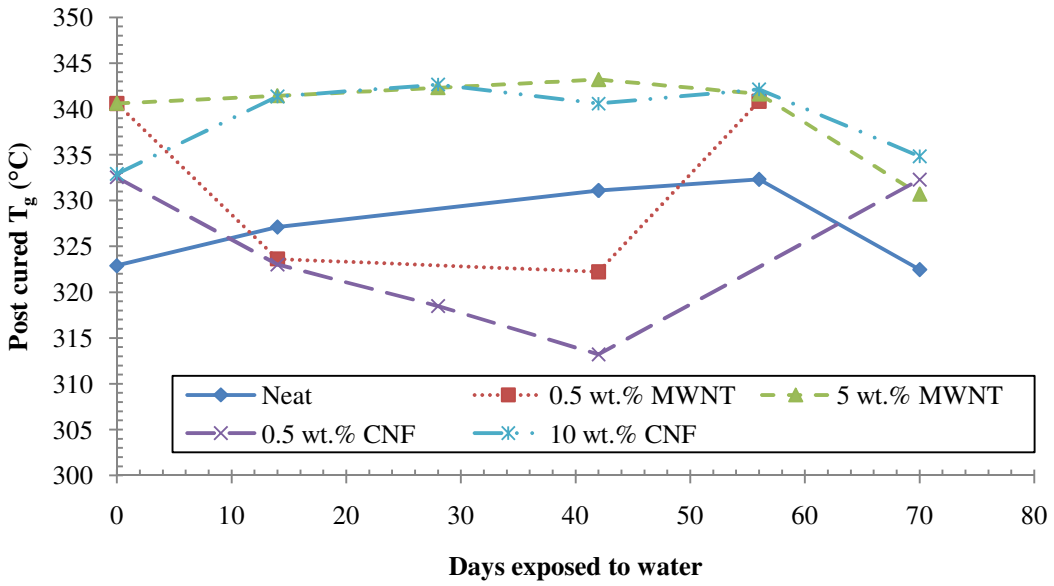

Figure 7.10: Post-cured T_g of select composites as a result of water contamination.

studies are shown in Figure 7.11. All samples had minimal loss in the temperature at 95% original mass after 56 days, although the MWNT composites fluctuated by 15-35°C during that time.

Overall, water affected T_g and weight loss characteristics only negligibly. Within the first 1-2 weeks the water caused a loss in T_g, most likely from voids that formed during curing. After that time period, however, the water seemed to be evaporated out and no longer affected the system. Water contamination will cause more trouble for customers who cure the composites into a final form. If the water is not evaporated out before the curing reaction begins, voids will form in the structure where the water droplets were trapped and evaporated. This causes a loss in macroscopic reinforcement, as seen in the data from these studies in the first 7-14 days. Suggested counter measures for these users would be to dry the material prior to use at approximately 100-110°C to

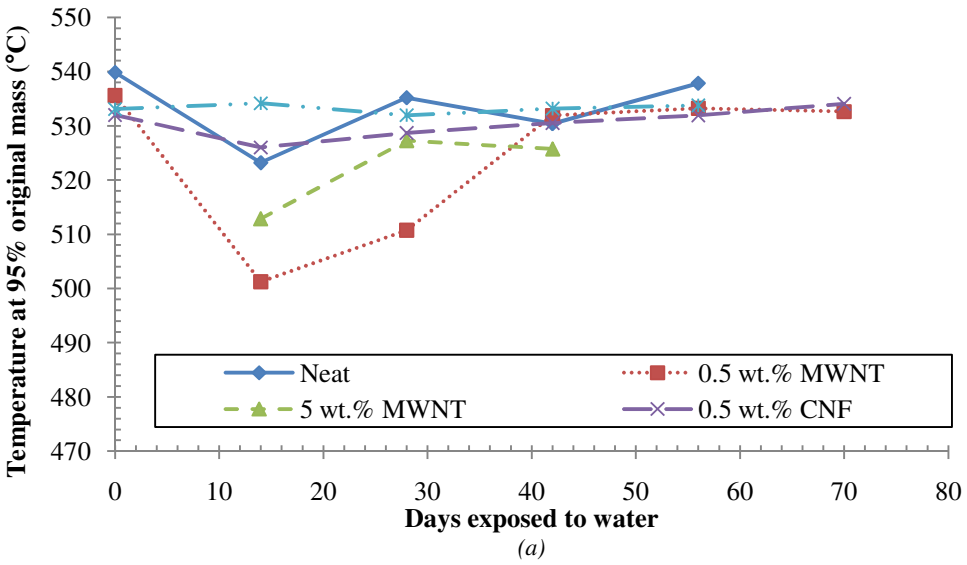

(a)

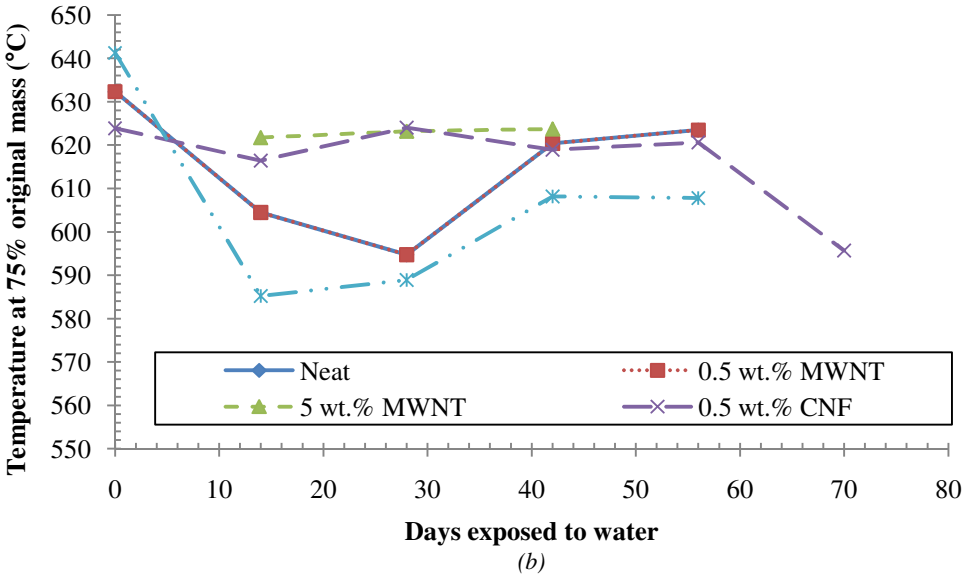

(b)

Figure 7.11: Temperature at 95% (a) and 75% (b) original sample mass for select composites as a result of water contamination.

evaporate the water but keep the oligomer in solid form. The melting temperature of the material is approximately 185°C and rheological studies [92] have shown that prolonged exposure at 280°C does not affect the end material properties, so drying the material at these lower temperatures will not affect other final properties. Also, composite molders can degas the material in its fully melted state under vacuum or with a mold vent in order to remove the water contamination prior to the cure reaction.

7.3.4 Cure condition results

DSC cure temperature and time studies are shown in Figures 7.12 (a) and (b), respectively. As examined in Chapter 6 with degree of cure studies, the cure temperature greatly affects the final degree of cure which, in turn, affects the final composite T_g. By comparing composites cured at 350°C, 371°C, and 390°C for 60 minutes, it is evident that 350°C does not provide sufficient thermal energy to result in a maximized T_g for composites with one exception. The 5 wt.% MWNT composite exhibited less than 0.5°C change at all curing temperatures. In this case, enough MWNTs are in the system to allow a reinforced network to be established even with less thermal energy for cure. The neat sample had little change in T_g when the curing temperature was raised from 371°C to 390°C although 0.5 wt.% MWNTs and CNFs both experienced a small loss in T_g. This may be due to the polymer network curing too quickly around the particles and resulting in fewer crosslinks and particle/polymer interactions.

Cure time studies show that longer curing time results in higher T_g for all composites. There is a dramatic increase in T_g for all composites between 10 minutes and

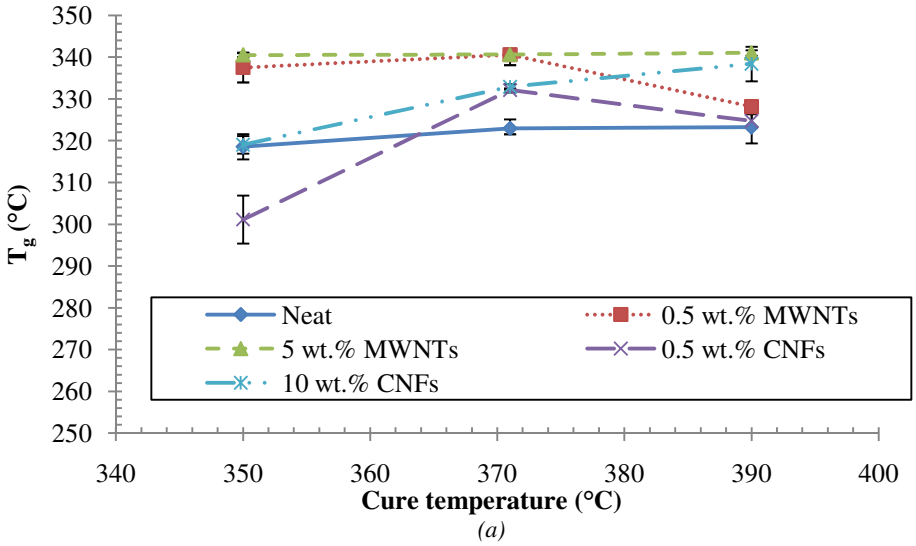

(a)

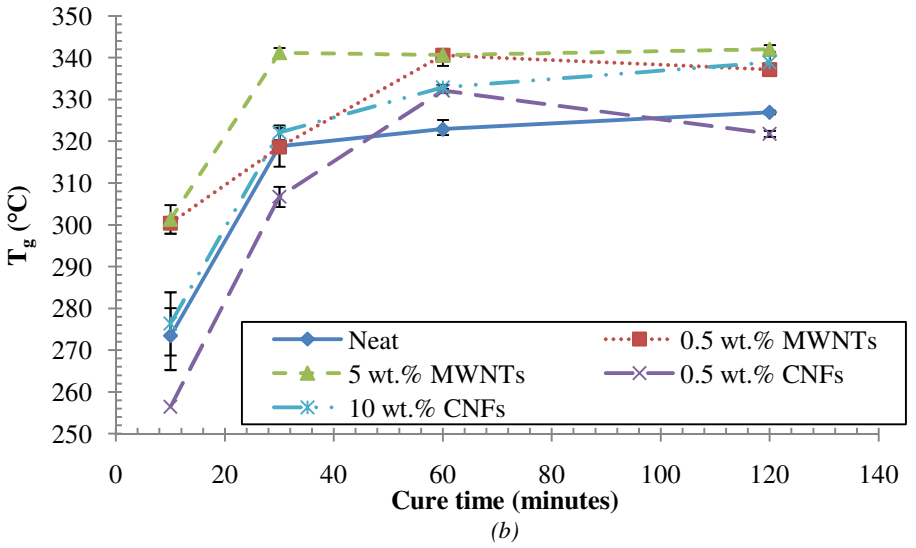

(b)

Figure 7.12: Post-cured T_g for select composites as a function of cure temperature (a) and cure time (b).

30 minutes, and another increase between 30 minutes and 60 minutes. However, after 60 minutes, there is little to no change in T_g. These behaviors can be used to help material users to determine optimal processing temperatures and times. Users will want to use the lowest process temperature for cost savings involving thermal energy, and the shortest possible cycle time for quicker product turnaround. For the studied cases, 371°C and a 60 minute cure cycle is sufficient. In some case, a 30 minute cure cycle may also reach the user's final product requirements.

Using data from these experiments as well as those from Chapter 3, a suggested processing and troubleshooting guide was formed and is shown in Table 7.7.

Table 7.7. Customer processing and troubleshooting guide.

Pre-cure Melt Processing	• Optimal properties will be maintained when any pre-cure processing is performed at 188°C. Higher processing temperatures may result in additive clumping and a loss in properties. • Material may be processed at temperatures up to 288°C without initiating cure. • For injection processes, minimum viscosity may be required to inject and infiltrate a preform. In this case, the material showld be melted at 280°C prior to injection.
Cure Processing	• Optimal mechanical properties are retained when the material is cured at 371°C for 60 minutes under pressure. • Specific pressures are dependent on the user's quantitiy and processing method. The user will need to adjust to his/her own set-up, but a suggested starting point is 9 MPa.
Alternative Cure Processing	• For customers with lower property requirements that desire faster turn-around times, the material can also be cured at 371°C for 30 minutes. • However, component properties will be lower than those cured for 60 minutes.
Contamination: Water	• Nanovate material is delivered in packaging for hygroscopic materials and will repel water. However, once opened and if it is not resealed properly, water can infiltrate the product. • If water contamination is suspected, it is recommended that the material be dried at 110°C for 2-4 hours prior to use. • Additional time may be required for severe contamination.
Contamination: Light	• Nanovate material is delivered in opaque packagine that prevents degradation due to light. However, should the material experience light exposure, it is recommended that it is repackaged immediately to prevent further damage. • Prolonged exposure may result in some property degradation and the user should be aware of this during component dsign.

CHAPTER 8

CONCLUSIONS AND FUTURE WORK

8.1 Conclusions

A summary of the conclusions for the studies and experiments presented in this work follows. These conclusions are presented by their respective chapters and are based on the PETI-330/MWNT and PETI-330/CNF composites used in this work.

8.1.1 Processing PETI-330 nanocomposites (Chapter 3)

- Homogeneous dispersions and distributions of MWNTs and CNFs in PETI-330 were obtained using melt-mixing with the processing parameters of 188°C, 60 rpm, and a 12 minute mixing time. The nanoparticle morphology was shown to be temperature dependent where a 12°C increase in processing temperature resulted in a loss in dispersion which was indicated by the presence of agglomerates, and a 42°C increase resulted in a loss in distribution with particle rich and particle void areas throughout the polymer matrix.
- The melt-mixing torque curves were analyzed for total mixing energy and different regions of the curves were classified as loading and steady state. The steady state torque and total mixing energy increased with increasing nanoparticle content and also with decreasing process temperature.
- Additional mixing studies showed that the loading and steady state energy contributions as well as the value of the steady state torque significantly affected

dispersion. When comparing energy contributions, dispersion and distribution were better when the steady state portion was close to ½ of the total energy. The value of the steady state torque was also shown to be more important for dispersion than the value of the total mixing energy.

- Thermal analysis showed that the nanoparticles had no effect on the oligomer T_g, but 10 wt.% CNFs exhibited a post-cured T_g of 333°C and 0.5 wt.% MWNTs had a post-cured T_g of 341°C. Additional MWNTs did not increase the T_g by more than 1°C.
- Rheological studies on MWNT composites showed that minimum viscosity increased with increasing MWNT content and with decreasing melt-mixing temperature. The only MWNT composite that exhibited rheological properties that would qualify for RTM use was the 0.5 wt.% sample that was mixed at 230°C and, thus, had poor dispersion and distribution.

8.1.2 Network behavior of PETI-330/MWNT composites (Chapter 4)

- SEM images showed that aggregation occurred during curing for composites with MWNT loadings less than 1 wt.%. This was thought to be due to the reduced viscosity that allowed for increased nanotube mobility.
- Rheological studies showed that 0.2 wt.% and 0.5 wt.% MWNT composite behavior was dominated by matrix effects with primarily liquid-like responses. Higher loadings of 1 wt.% and 3 wt.% MWNTs exhibited pseudo solid-like behavior. The highest loadings of 5 wt.% and 7 wt.% MWNTs were dominated by the CNT network with solid-like responses.

- Impedance spectroscopy studies shows that low loadings of 0-0.5 wt.% MWNTs exhibited frequency-dependant conductivity over the studied frequency range while higher loadings of 1-7 wt.% had frequency-independent conductivity values. The frequency-independent regions indicated DC conductivity values.
- Power law relationships were used with rheological and conductivity data to estimate percolation thresholds. The rheological percolation threshold was estimated as 0.93 wt.% using the storage modulus at a low frequency. DC conductivity values were used to estimate an electrical percolation threshold of 0.80 wt.%. Electrical percolation was dependent on the maximum allowable distance required for electron hopping and rheological percolation depended on the polymer size; the electrical percolation threshold was lower than the rheological percolations threshold, so the radius of gyration could be estimated as roughly less than 5 nm.
- The Guth model was used with rheological data to estimate an effective aspect ratio of 250 for the MWNTs. The as-received MWNTs were reported to have aspect ratios of approximately 1000, so it was assumed that some nanotube shortening occurred during melt-mixing.
- A geometric percolation threshold was estimated as 0.47 wt.% using the Celzard model with MWNT dimensions and the effective aspect ratio. Geometric percolation was based on a network of particle-particle interactions, so the geometric percolation threshold should be higher than both rheological and electrical percolation thresholds. However, the geometric percolation threshold was less than the rheological and electrical percolation thresholds for these PETI-

330/MWNT composites. This was most likely due to aggregation or inhomogeneities in the composite morphology.

8.1.3 Thermomechanical properties and morphological effects on cured nanocomposites (Chapter 5)

- Cured MWNT and CNF composites were tested for thermomechanical properties. The storage modulus increased with nanoparticle loading and decreased with temperature. A MWNT loading of 7 wt.% resulted in a storage modulus of 4.5 GPa, which was a 38% improvement from the neat PETI-330. A CNF loading of 10 wt.% resulted in a storage modulus of 4.4 GPa, a 35% enhancement.
- The Halpin-Tsai models were used to model and predict the nanocomposite behavior. The predictions matched actual composite behavior for all CNF loadings and MWNT loadings of 1 wt.% or less. The Halpin-Tsai models are for non-interacting particles, so predictions for MWNT loadings above the percolation thresholds were less accurate.
- To test the effect of aggregation on the cured composite thermal properties, samples were cured rapidly in the DSC to prevent any reaggregation. SEM images showed that some aggregation still occurred in the DSC-cured samples, but were much smaller than those in the press-cured samples.
- Thermal analysis of the DSC-cured and press-cured samples showed that aggregation had little effect on the T_g of lower MWNT loadings. However, above 1 wt.%, DSC-cured samples exhibited higher T_g values. The aggregates in the DSC-cured and press-cured samples of these higher loadings were similar in size,

so it was likely that the curing protocol resulted in polymer networks with different morphologies for the two sets of samples. This was further explored in Chapter 6.

- Thermal analysis of DSC-cured and press-cured CNF samples showed that aggregates affected all studied CNF loadings. However, samples with larger aggregates had higher T_g values than those with more homogeneous morphologies.

8.1.4 Cure kinetics of PETI-330 resin and effects of nanotube fillers (Chapter 6)

- The Kissinger and Ozawa-Flynn-Wall methods were used with dynamic temperatures scans to determine the cure activation energy for the composites. The presence of MWNTs and CNFs reduced or had no effect on E_a; this could have been due to the high thermal conductivity of CNTs that aided in distributing thermal energy during curing.
- Isothermal testing was performed on PETI-330 and the total heat of reaction was calculated at each tested temperature. The cure temperature of 370°C resulted in the maximum ΔH of 256.6 J/g, which was taken as the ultimate heat of reaction for PETI-330.
- Nanocomposites were cured at 371°C and 343°C; in both cases, the nanocomposites achieved a higher degree of conversion than PETI-330. The rate of conversion of the neat material and nanocomposites was then used to classify the reaction as n^{th} order.

- Isoconversional studies identified the activation energy required for each degree of conversion for PETI-330. The results showed that a secondary reaction was occurring at high degrees of conversion (60-80%).

8.1.5 Business plan (Chapter 7)

- A business plan was formed for the fictional company Nanovate, which would provide an uncured nanocomposite as its product. The product would have custom formulations based on customer requirements, where the type of additive (CNF or MWNT) would be adjusted as well as the additive content.
- The main IP strategy would be trade secrecy. The life of the technology would most likely be shorter than the time it would take to patent it and policing a patent would be very difficult.
- The target market of the technology would be the military fixed wing sector and the international and U.S. government space sectors. The potential customers in these sectors would be raw material and Tier 2 suppliers.
- The sales and marketing strategy would include direct distribution, price skimming, and personal selling. The technical knowledge required for selling the material and the long sales cycles result in optimal profits through direct sales techniques.
- The material was valued as $1.21 to 1.80 million using discounted cash flow analysis for a three year projection. Forecasting beyond three years was not completed due to the volatility of the market and evolution of the current technology.

- Environmental studies were completed to identify potential issues in manufacturing and distributing the nanocomposite material. Light studies showed that prolonged exposure to fluorescent light could cause permanent damage to the oligomer, which would result in a loss in cured composite properties. Water studies showed that water contamination could cause problems, but could be solved by drying the material. A processing and troubleshooting guideline was written for future customers to reference.

8.2 Recommendations for future work

This work included processing and characterization studies, both of which left experimental gaps that could be addressed in future work. Melt-mixing was shown to be an effective processing method for CNT composites, but additional processing parameter studies could improve on the results by studying the effect of motor speed. This work also showed that melt-mixing was potentially shortening the nanoparticles, so a study to determine the parameters that affect this shortening the most would be beneficial in maintaining nanoparticle aspect ratios. Cured composites in this work also experienced aggregation, and further studies could concentrate on limiting this aggregation or determining the root cause.

Morphology was studied here using microscopy and micromechanical models with rheological behavior; morphological characterization would benefit from a molecular level method such as ultra-small angle x-ray scattering. Additional thermomechanical testing using a different testing method, such as shear, would

supplement the three point bending data presented here. The electrical conductivity studies could also be expanded to include experiments that detect changes in conductivity with the onset of damage. If the nanocomposites could repeatedly detect damage through changes in conductivity behavior, they may have additional applications in structural health monitoring (SHM); SHM is briefly discussed in Appendix A. Additional electrical testing could include electromagnetic interference (EMI) shielding efficacy, which is another beneficial property for applications where EMI can distort or destroy signals (i.e. aircraft navigational systems). EMI is also briefly discussed in Appendix B.

The curing mechanism of PETI-330 was thoroughly studied here, but additional studies could elucidate the full effects of the nanoparticles on that mechanism. These studies could cure the nanocomposites with varying concentrations and types of nanofillers at a range of temperatures to determine if the optimal curing temperature remained at 370°C for all, or if the cure mechanism itself changed or shifted due to the fillers.

Finally, the characterization in this work is for the nanocomposites alone; the properties of the nanocomposites within a carbon fiber reinforced composite should also be characterized to better understand performance in a final application.

APPENDIX A

STRUCTURAL HEALTH MONITORING

A.1 Introduction

For any structural component, it is important to have the ability to detect significant failure. Structural health monitoring (SHM) is the process used by the aerospace industry to detect such failures and to determine whether a vehicle can go back into service or if further maintenance is required. SHM can be a major problem for the industry as it contributes to long vehicle downtime and can be complicated for determining the type and degree of failure that may have occurred.

Some SHM methods are difficult to put to use because some require intricate equipment while others may actually cause additional damage. A few examples of current crack and corrosion detection methods for composite structures include acousto-ultrasonics, comparative vacuum monitoring, or imaging ultrasonics [231]. These methods utilize changes in acoustic waves, pressure, or stress distribution to determine the presence or degree of structural degradation caused by cracks and corrosion. However, each method requires sensitive equipment for testing, such as sensors and acoustic or ultrasonic wave emitters and also requires significant vehicle downtime to fully test structural integrity. These methods can be improved by reducing aircraft downtime, the frequency of reviews required, and the equipment needed for monitoring. This may be accomplished by taking advantage of an inherent property of the composites, which would reduce the amount of equipment needed for monitoring as well as allow for online monitoring of structural integrity.

Methods using electrical conductivity as a measure of damage are growing in popularity in SHM. Initial electrical resistance monitoring in polymer composites came from utilizing the properties of carbon fiber. Chung studied the change in resistivity of carbon fiber in carbon fiber reinforced composites (CFRCs) [232]. He found that minor matrix damage or disturbances in fiber arrangement were indicated by irreversible decreasing resistivity both in the longitudinal direction and through the thickness. Delamination or interlaminar interface degradation was indicated by irreversible increases in through-thickness resistivity. He also found that major fiber breakage damage was indicated by irreversible increasing resistivity. Chung showed that resistivity could be used as an effective tool in measuring damage, but it accounts for mainly major failure. A more sensitive way of measuring might allow for detection of the onset of damage before failure occurs.

Scheuler *et al.* took damage detection by electrical resistivity in CFRCs and extended it through the use of electrical impedance tomography (EIT) [233]. In EIT, electrodes are placed along the edges of a sample and currents are ejected by two of the electrodes with the remainder measuring the potential difference. Using the characteristics of the conducting carbon fiber, the group showed that EIT could be an effective tool in detecting and mapping the location of a structural failure. The method was used differently for isotropic and anisotropic samples, but both had good predictive results. EIT aids in precise mapping of damage detection with high sensitivity although it does require an intricate initial set-up to establish the system of electrodes.

Recently, scientists have been investigating CNTs as strain and damage sensors by studying the instantaneous changes in resistivity of the composite as it experiences

stress [234-236]. Li, Thostenson and Chou published a comprehensive review of CNT strain sensors [237]. Carbon nanotubes form a percolated network that effectively conducts electricity in a resistive matrix. When the connection between nanotubes is severed, the entire composite experiences a decrease in conductivity. Thostenson and Chou [238] studied the change of resistance in glass fiber reinforced epoxy composites with tensile and bending forces. MWNTs were initially mixed into an epoxy precursor using a calendaring method, and laminates were made using vacuum assisted resin transfer molding (VARTM) with the epoxy nanocomposites and glass fibers. Tensile testing with unidirectional laminates in which all fibers were aligned with the direction of testing showed that there was a linear increase in resistance with the initial deformation; the slope of the response increased gradually as testing continued, exhibiting increased sensitivity at higher strains. Cross-ply laminates were also tested, which is important because failure usually initiates at 90° plies when these patterns are used [239]. Figure A.1 was taken from the study and is displayed here; it illustrates the electrical resistance response of the cross-ply laminate with the evolution of tensile testing. While the cross-ply laminates initially had similar behavior as the unidirectional laminates with a gradual linear increase in resistivity with loading, additional loading resulted in two more regions. A sharp increase in resistivity occurred with the initiation of microcracking in the 90° plies, and another sharp increase occurred with microcrack accumulation. More importantly, the sample was unloaded and reloaded (Figure A.1 (c)), showing minimal hysteresis but a sharp increase in resistivity at lower strain level during the reload cycle.

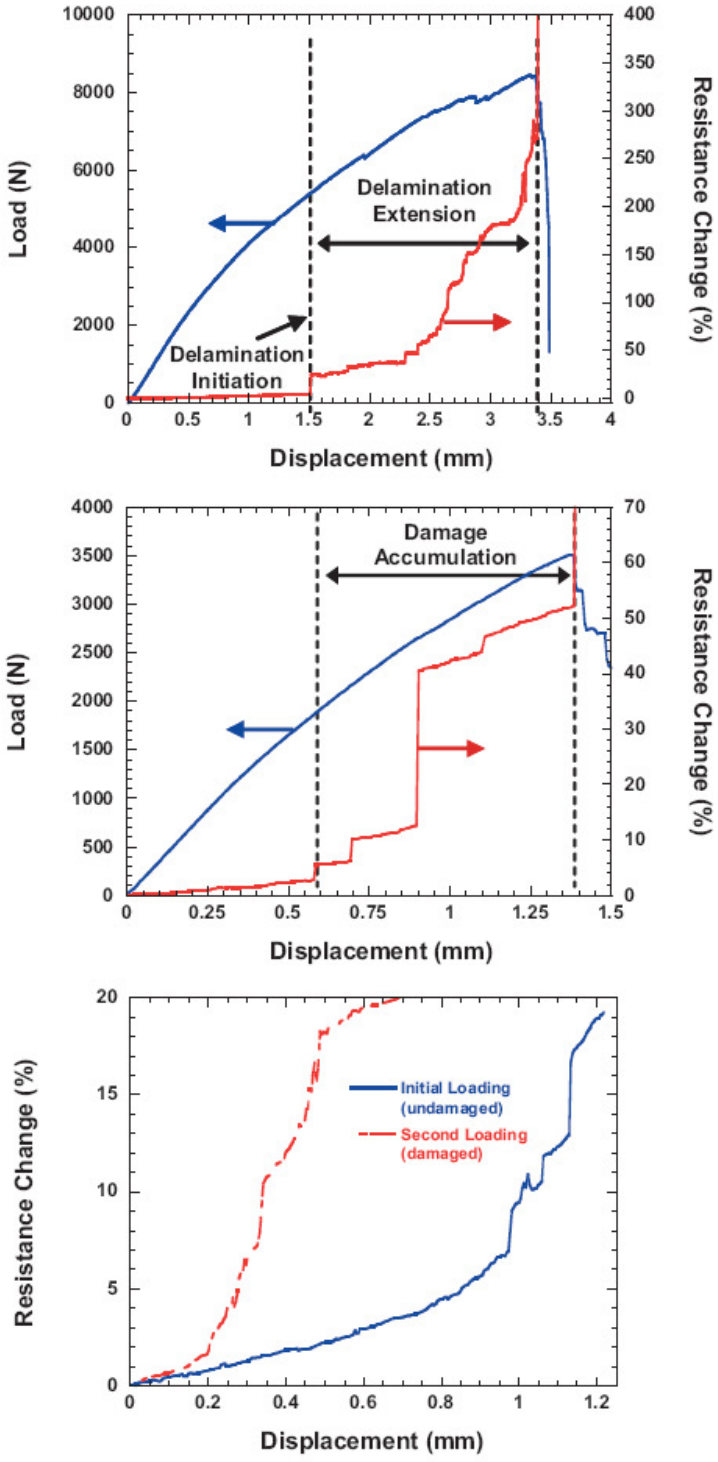

Figure A.1. Change in resistance with load application for (a) 0 specimen (b) 0/90s specimen and (c) laminate loaded and unloaded. Taken from [238].

This indicates permanent damage. The group concluded that monitoring the shifts in resistivity during applied loads can be an effective SHM method in determining permanent damage.

The study went on to look at electrical resistivity changes due to bending, which was testing using a three point bending test set up and unidirectional laminates [238]. Thostenson and Chou determined this study was important because failure often occurs at ply interfaces and bending promotes delamination. Data showed sharp increases in resistivity, indicating complete delamination. Upon reloading, large spikes in resistivity indicated friction and establishment of new conducting networks. The bending study concluded that incremental changes in resistivity correlated to accumulated damage.

Chou expanded on this study with Li by creating a mathematical model and utilizing finite element modeling [236]. The study used finite element modeling with the electrical current flow over a range of conductivities; the lower bound resistance was taken as 100 kΩ, which was the lowest contact resistance between nanotubes, and the upper bound was taken as the resistance when nanotubes do not touch but can still tunnel. A critical strain of 0.4% was identified as the strain in which multiple damage spots became visible. Another critical strain of 1.2% indicated the strain in which damage spots began to merge to form microscopic cracks. The critical strains could, in future studies, be correlated back to experimental data to determine accuracy.

A more precise view of the electrical monitoring mechanism of CNTs can be seen in studies concentrating on only nanotube-polymer nanocomposites. Kang *et al.* compared the effectiveness of SWNT buckypaper and SWNT/polymethyl methacrylate (PMMA) composites as strain sensors [240]. Although buckypaper is more conducting

because it consists of only metallic and semi-metallic elements, the composites include a binding element that prevents tube slippage during strain applications. The group placed the film sensors on a cantilever beam and measured resistivity as the beam deflected in tension and compression; results are shown in Figure A.2. While both samples recorded a linear decrease in resistivity for negative strains (tension), only the composite recorded a linear increase in resistivity for positive strains (compression). The buckypaper had a nonlinear response in this region, most likely due to tube slippage. The composites were further tested at different loadings and the group concluded that loadings closer to the percolation threshold were more sensitive to changes in strain. This study showed that nanocomposites can be effectively used as strain sensors, and are actually more accurate in prediction than nanotubes alone.

Another film study reviewed the effects of two different loadings, 0.56 vol.% and 1.44 vol.%, of MWNT/polyethylene oxide (PEO) composites [241]. The group attached composite films to dogbone polycarbonate samples for tensile testing. The change in film resistance was measured as a function of strain and both composites exhibited an initial linear response followed by a nonlinear response; the 0.56 vol.% composite film responded linearly from strains of 0 to only 0.008 while the 1.44 vol.% film responded linearly from a strain of 0 to 0.02. The two regions were explained as direct contact conduction for linear responses and electron tunneling for nonlinear responses. The group showed with imaging that the nanotubes began to align with added strain, so the smaller loading lost direct particle contacts much more quickly than the larger loading, which had more nanotubes to maintain contacts despite particle alignment. The study was completed

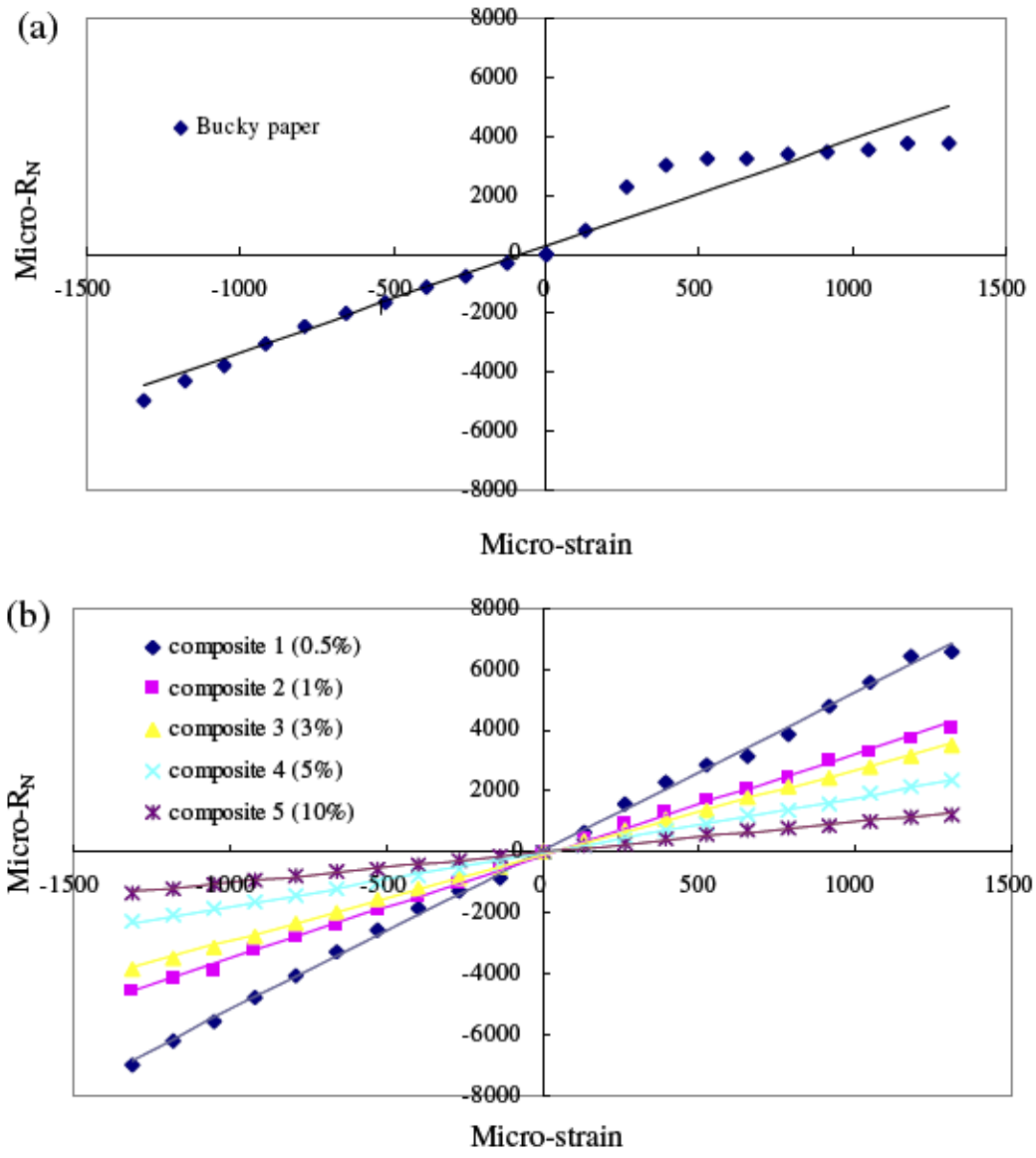

Figure A.2. Change in resistance as a function of strain for (a) buckypaper and (b) SWNT/PMMA composites. Composite sensors exhibit more predictable, linear behavior, while nanotube slippage in buckypaper yields nonlinear behavior. Taken from [240].

with a model that combined the power law scaling rule with tunneling resistance to account for both the linear and nonlinear responses; this model was shown to accurately predict the measured behavior. This study is another good example of the use of nanotube composites and the efficiency in strain prediction; while many of the other studies could accurately model linear behavior, this one accounts for nonlinear behavior that covers a wider range of strain values.

A study of amino-functionalized MWNT/polyurethane-urea films by Zhang *et al.* measured both linear and exponential responses in resistivity when tensile tested [242]. Like Park's study, the group identifies an initial area that can be modeled by a linear response, correlating to changes in the direct contact of nanoparticles. This response occurred up to approximately 5% strain; above that value, resistivity responded exponentially to correlate with tunneling effects. The group was also able to remove the dependence of nanotube content on the responses in resistivity by normalizing the change in resistivity with respect to the original resistivity. This resulted in a more universal model for composites with similar properties and particle morphologies. Additional studies that may look at universality will aid in improving behavior prediction for strain sensors made of nanotube composites.

For this work, it was hypothesized that the electrical properties of PETI-330 composites could be utilized for SHM purposes. Experiments were performed on cured MWNT samples to determine if any kind of damage accumulation could be detected by changes in electrical conductivity. Results showed that the electrical behavior did change after discrete damaging events; however, results also indicated that further analyses were required to classify the different types of damage.

A.2 Materials and methods

Discrete damage testing was performed in two manners. In the first set of experiments, MWNT composites were subjected to micro-indentation using the highest setting of 1000 g. The samples, surface treated with silver paint to act as electrodes, were measured for conductivity behavior both before and after indentation. Limited materials were available for all experiments, so the second set of experiments was done concurrently with other testing. Data for undamaged melt-mixed and cured samples was available from analyses in Chapter 4. Samples were then mechanically damaged during a temperature ramp in dynamic mechanical analysis (DMA) in Chapter 5. These samples were then coated with silver paste and frequency scans were performed on 1 mm parallel diameter plates. For both sets of experiments, real (Z') and imaginary (Z'') components of impedance were measured using a Solartron SI 1260 impedance-gain analyzer with a Solartron 1296 dielectric interface. Conductivity was calculated using Equation 4.1. None of the samples experienced complete fracture during testing, but shifts in electrical conductivity may serve as indications of internal stresses or crack formation and propagation.

A.3 Results

Change in composite conductivity due to damage caused by micro-indenting is shown in Figure A.3. These results show that there was no change in electronic behavior due to a 1000 g impact force on the 1 wt.% and 3 wt.% samples. The highest loading did experience a loss in conductivity, indicating some crack initiation and growth. All samples were tested under the same conditions, so the increased sensitivity of the highest

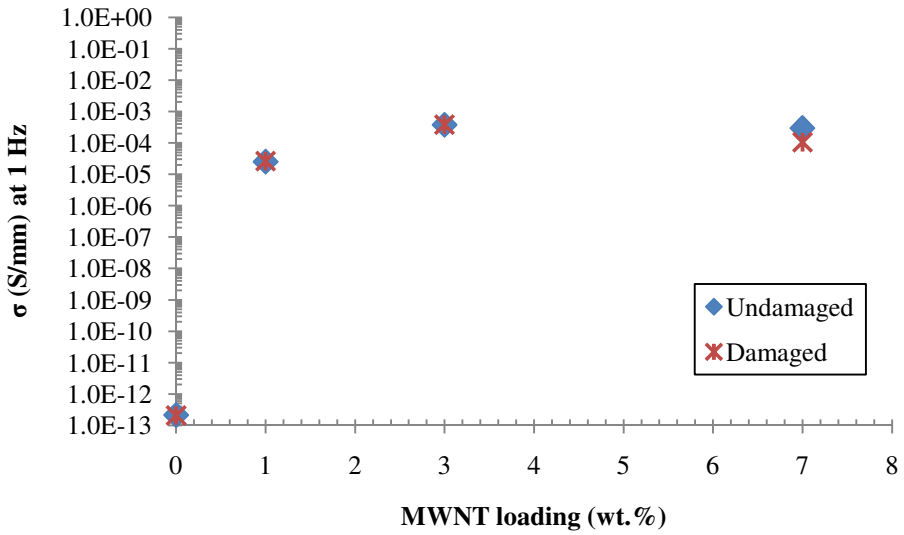

Figure A.3. Conductivity of PETI-330/MWNT composites before and after micro-indentation at 1 Hz. The highest loading, 7 wt.%, was the only sample to experience property change.

loading may be due to specific structure-property relationships. As more nanotubes are included in a composite system, there is an increase in polymer-particle surface area interactions. These additional interactions may result in increased mechanical reinforcement, but may also lead to increased brittleness if adhesion between the nanotubes and polymer chains is less than the adhesion amongst polymer chains alone. The brittle behavior could lead to crack initiation at lower forces that composites with fewer nanoparticle interfaces present.

The change in conductivity for the micro-indented samples was small or negligible, so a method with more force was needed. Because of limited material availability, samples were tested for conductivity before and after three-point bending during DMA testing. While many studies have noted a loss in electrical conductivity with the onset of damage [238, 241, 243-245], data from post-DMA testing exhibited an

increase in conductivity from before testing. Results in Figure A.4 show an increase of 1-2 orders of magnitude with damage accumulation. This has happened less frequently in the literature, but Kang also noted similar behavior under certain conditions [240]. For some studies, cracks formed during damaging terminated conducting pathways and reduced the overall conductivity. However, for samples undergoing tension and compression stresses, cracks can be forced shut to reestablish conducting pathways, establish new ones, or reopen and extinguish those pathways in tension.

For this work, samples were permanently damaged during DMA testing and went from completely flat specimens to curved one. The outermost thickness layer experienced the most tension forces while the innermost experienced the most compressive forces. It

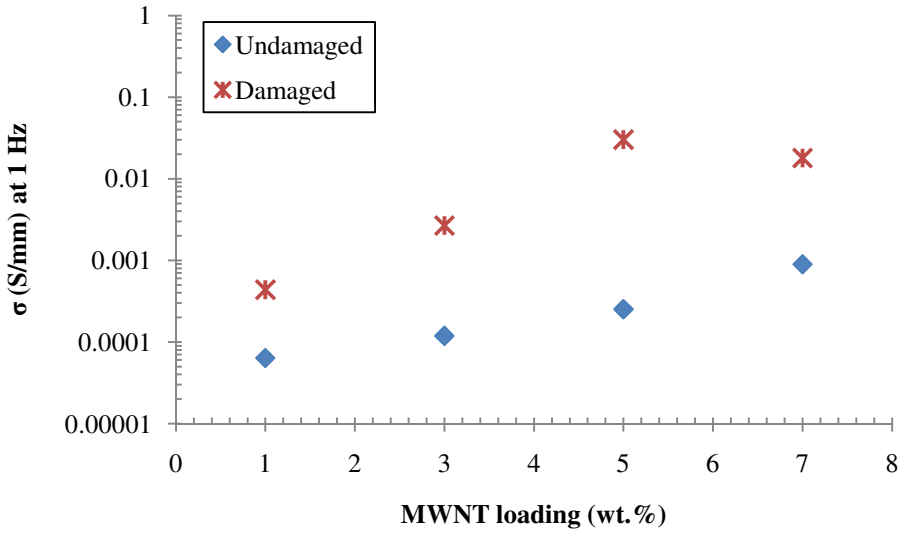

Figure A.4. Conductivity of PETI-330/MWNT composites before and after DMA testing. Damaged samples experienced an increase in conductivity, and only low MWNT loadings had proportional conductivity changes due to damage.

is possible, then, that, although tension caused a reduced number of conducting pathways, compression closed cracks and established new networks, resulting in increased conductivity. In comparison, the 7 wt.% sample experienced a loss in conductivity in the micro-indentation experiment. However, the micro-indenting force was applied perpendicular to the sample surface; this suggested that the type and angle of force and damage onset may have different effects on the overall conductivity. Additional studies are needed to isolate and confirm the mechanism of different forces.

Figure A.4 also shows that conductivity after damaging remained proportional between filler loadings to undamaged conductivity for lower loadings. The 5 wt.% composite however, exhibited a larger change in conductivity than all other samples. Chapters 3 and 4 showed that higher loadings resulted in more aggregation due to saturation, which may have led to disproportionate conductivity changes for the higher loadings. This followed with previous studies that showed nanoparticle loadings closer to the percolation threshold were more sensitive and had linear responses to damage accumulation [240].

A.4 Discussion and conclusion

This test studied the change in conductivity due to discrete damaging events. A dynamic testing method that studies the evolution of different types of damage may be a better solution for applying these nanocomposites toward SHM principles. Dynamic data can then be correlated to different damage thresholds and used in discrete on-board conductivity testing. Dynamic testing can be done in several ways, the most basic in conjunction with a strain sensor and damage mechanism. The strain sensor can be

attached to the test specimen and then both can be damaged using stress. Electrodes attached to the test specimen collect real-time conductivity while the strain sensor measures real-time strain. Repeated samples can be correlated to model behavior.

Another useful study would isolate different conductivity behaviors with types of damage. Damage can occur under many different types of stresses, the main kinds being tensile, bending, compression, and thermal fluctuations. These tests can then evolve from the nanocomposites alone to carbon fiber reinforced composites where the nanocomposites act as the binding agent.

This work has shown that the PETI-330/MWNT composites do detect damage accumulation through electrical conductivity properties. However, the extent and accuracy of this detection mechanism evolved into a very extensive study, as shown above, and went beyond the purposes of this dissertation. It has, in fact, become a thesis in and of itself, and is now being studied by Materials Science and Engineering Masters student, Cait Meree.

APPENDIX B

ELECTROMAGNETIC INTERFERENCE SHIELDING

Additional characterization of electrical properties could be used to investigate the shielding efficacy of the nanocomposites against electromagnetic interference (EMI). EMI is created when electromagnetic waves from different sources interact and form a new wave pattern, causing disruptions in the performance of the original sources. This is a critical issue in aircraft communication and navigation equipment, and is most commonly treated by reducing the number of signals in close proximity (i.e. turning off cell phones, lap tops, and other entertainment electronic devices). With the number of sources ever rising, alternative methods of EMI shielding are of growing interest.

EMI shielding efficacy (EMI SE) is directly related to electrical conductivity [246]. The composites in this work were tested for EMI SE using conductivity values measured for experiments in Chapter 4; CNF composites were also measured for electrical conductivity behavior using the same method. These values could then be compared with the threshold value required for EMI shielding [112, 246], as shown in Figure B.1. It should be noted that conductivity values were taken at 0.1 Hz; for samples above percolation, this was equal to the DC conductivity. For MWNT composites below 0.8 wt.% and all studied CNF composites, the value in Figure B.1 is the frequency-dependent conductivity value, which is the AC conductivity at 0.1 Hz. For optimal EMI SE, the material's DC conductivity must be at or above the EMI SE threshold.

The data show that none of the CNF composites were close to the EMI shielding conductivity, and only the highest loading of MWNTs, 7 wt.%, reached this value. This

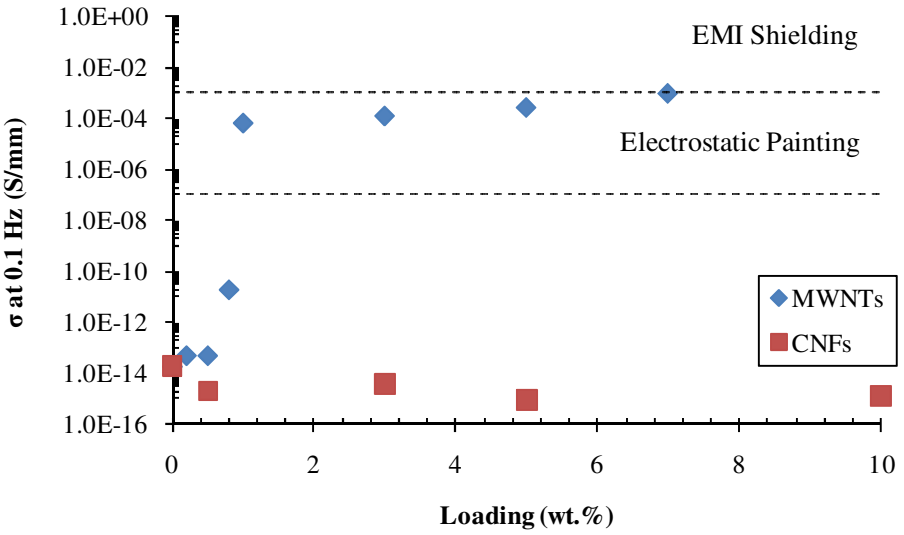

Figure B.1: MWNT and CNF composite conductivities at 0.1 Hz. Dashed lines indicate conductivity thresholds required for different applications [112, 246]. It should be noted that conductivity values for MWNT composites below 0.8 wt.% and all CNF composites are the AC conductivity values while all others are DC conductivity. AC values are included for comparison purposes.

suggests that the MWNT composites may be potential candidates for EMI shielding applications, but the loadings would need to be 7 wt.% or higher. Figure B.1 also notes thresholds for electrostatic painting and electrostatic dissipation. These are additional applications for composite materials that exhibit some electrically conducting properties; the MWNT composites above the percolation threshold (0.8 wt.%) all possess sufficient conductivity to be used in electrostatic painting. Lower loadings can be used in applications where electrostatic discharge is a problem and a material with dissipative effects is needed. While this is not a solution to the EMI issue, these are examples of other potential applications for the nanocomposites.

APPENDIX C

BUSINESS PLAN FINANCIAL ANALYSIS ASSUMPTIONS

Table C.1: Customers and penetration rates.

	Year 1	Year 2	Year 3
Tier 1 market (total companies)	25	25	20
Tier 1 penetration (%)	0	0.05	0.075
Tier 1 number of customers	0	1.25	1.5
Tier 2 market (total companies)	500	500	500
Tier 2 penetration (%)	0.005	0.0075	0.01
Tier 2 number of customers	2.5	3.75	5

Table C.2: Part sizes and weights.

Part	Weight in Kilos
Small	0.01
Medium	50
195Large	100

Table C.3: Revenues, years 1-3.

YEAR 1						
Part Size	Material Req/Unit (kilos)	Tier 1 Customers	Parts Sold	Tier 2 Customers	Parts Sold	Kilos of Material Sold
Small	0.01	0	0	3	500	15
Medium	50	0	0	3	50	7500
Large	100	0	0	3	0	0
TOTAL (kilos)						7,515
Revenues						$ 9,271,180
YEAR 2						
Part Size	Material Req/Unit (kilos)	Tier 1 Customers	Parts Sold	Tier 2 Customers	Parts Sold	Kilos of Material Sold
Small	0.01	1	0	4	750	30
Medium	50	1	50	4	100	22500
Large	100	1	0	4	0	0
TOTAL (kilos)						22,530
Revenues						$27,795,036
YEAR 3						
Part Size	Material Req/Unit (kilos)	Tier 1 Customers	Parts Sold	Tier 2 Customers	Parts Sold	Kilos of Material Sold
Small	0.01	2	0	5	1000	50
Medium	25	2	75	5	150	22500
Large	75	2	50	5	0	7500
TOTAL (kilos)						30,050
Revenues						$37,072,385

Table C.4: EBITDA, years 1-3[6].

	YEAR		
	1	**2**	**3**
REVENUES	$ 9,271,180	$ 27,795,036	$ 37,072,385
EXPENSES			
Operating			
Materials	$ 7,856,933	$ 23,555,115	$ 31,417,275
Salaries - Production	$ 80,000	$ 120,000	$ 160,000
SG&A			
Facilities	$ 60,000	$ 60,000	$ 100,000
Salaries - Sales	$ 160,000	$ 160,000	$ 160,000
Salaries - Business Mgr	$ 50,000	$ 50,000	$ 50,000
Other	$ 12,000	$ 15,000	$ 18,000
License Fees (8% of revenue)	$ 741,694	$ 2,223,603	$ 2,965,791
Total Expenses	$ 8,960,627	$ 26,183,718	$ 34,871,066
CAPITAL EXPENDITURES			
Extruder and Hopper	$ 25,000		$ 25,000
Screwblocks	$ 1,500	$ 1,500	$ 3,000
Weigh Station	$ 10,000		$ 10,000
Powdering Machine	$ 5,000		$ 5,000
Total Capital Expenditures	$ 41,500	$ 1,500	$ 43,000
TOTAL EXPENSES & CAPEX	**$ 9,002,127**	**$ 26,185,218**	**$ 34,914,066**

[6] Working capital requirements TBD

APPENDIX D

DCF AND MONTE CARLO VALUATIONS

Table D.1: DCF with sensitivity analysis

	DISCOUNT RATE					
MARGIN	25%	30%	35%	40%	45%	50%
5%	$ (2,128,012)	$ (1,958,192)	$ (1,809,227)	$ (1,677,827)	$ (1,561,324)	$ (1,457,534)
10%	$ (405,474)	$ (381,229)	$ (359,588)	$ (340,172)	$ (322,666)	$ (306,811)
15%	$ 1,317,063	$ 1,195,735	$ 1,090,050	$ 997,483	$ 915,992	$ 843,912
20%	$ 3,039,600	$ 2,772,698	$ 2,539,688	$ 2,335,138	$ 2,154,650	$ 1,994,635
25%	$ 4,762,138	$ 4,349,661	$ 3,989,326	$ 3,672,793	$ 3,393,308	$ 3,145,358
30%	$ 6,484,675	$ 5,926,625	$ 5,438,964	$ 5,010,448	$ 4,631,967	$ 4,296,081
35%	$ 8,207,212	$ 7,503,588	$ 6,888,602	$ 6,348,103	$ 5,870,625	$ 5,446,804

Table D.2: Monte Carlo valuations

Distribution Assumption[7]	Mean Valuation	Probability of Positive Valuation	Probability of > $1M Valuation
Normal	$1,585,075	100%	84.8%
Triangular[8]	$1,581,338	100%	96.8%
Uniform[9]	$1,584,022	100%	94.5%
Uniform[10]	$1,579,650	100%	79.3%
Lognormal[11]	$1,576,243	100%	85.3%
Min Extreme[12]	$1,205,538	96.2%	64.8%

[7] Triangular, Uniform, Lognormal, and Min Extreme distributions were applied only to the most sensitive variables - margin and raw materials cost. The normal distribution was used for all remaining variables.
[8] 10%
[9] 10%
[10] 20%
[11] Right skewed
[12] Left skewed

REFERENCES

[1] Bogert MT, Renshaw RR. 4-Amino-o-phthalic acid and some of its derivatives. Journal of American Chemical Society 1908; 30(7): 1135-1144.

[2] Bryant RG, "Polyimides," *Encyclopedia of Polymer Science and Technology*, 2006.

[3] http://pslc.ws.macrog/imid.htm; December 2008.

[4] Scroog CE, "History of the invention and development of polyimides," *Polyimides: fundamentals and applications*, Ed. M. K. Ghosh, K. L. Mittal, 1996; 1-6.

[5] Takekoshi T, "Synthesis of polyimides," *Polyimides: fundamentals and applications*, Ed. M. K. Ghosh, K. L. Mittal, 1996; 7-48.

[6] Harris FW, "Synthesis of aromatic polyimides from dianhydrides and diamines," *Polyimides*, Ed. D. Wilson, H. D. Stenzenberger, P. M. Hergenrother, 1990.

[7] Coburn JC, Pottiger MT, "Thermal curing in polyimide films and coatings," *Polyimides: fundamentals and applications*, Ed. M. K. Ghosh, K. L. Mittal, 1996; 207-247.

[8] Serafini TT, Delvigs P, Lightsey GR. Thermally stable polyimides from solutions of monomeric reactants. Journal of Applied Polymer Science 1972; 16(4): 905.

[9] Bryant RG, Jensen BJ, Hergenrother PM. Synthesis and properties of phenylethynyl-terminated arylene ethers. Abstracts of Papers of the American Chemical Society 1992; 203(3): 482-492.

[10] Bryant RG, Jensen BJ, Hergenrother PM. Chemistry and properties of a phenylethynyl-terminated polyimide. Journal of Applied Polymer Science 1996; 59(8): 1249-1254.

[11] Pater RH, Curto PA. Advanced materials for space applications. Acta Astronautica 2007; 61(11-12): 1121-1129.

[12] Hergenrother PM, Rommel ML. Proceedings from the International SAMPE Symposium and Exhibition 1996; 41: 1061-1072.

[13] Connell JW, Smith Jr JG, Hergenrother PM. High Performance Polymers 2003; 15(4): 375-394.

[14] Chuang KC, Criss JM, Mintz EA, Scheiman DA, Nguyen BN, McCorkle LS. Low-melt viscosity polyimide resins for resin transfer molding (RTM) II. International SAMPE Symposium 2007: Baltimore, MD.

[15] Smith Jr. JG, Connell JW, Hergenrother PM, Criss JM. Resin transfer moldable phenylethynyl containing imide oligomers. Journal of Composite Materials 2002; 36(19): 2255-2265.

[16] Criss JM, Arendt CP, Connell JW, Smith Jr. JG, Hergenrother PM. Resin transfer molding and resin infusion fabrication of high-temperature composites. SAMPE Journal 2000; 36(3):32-41.

[17] Smith Jr. JG, Connell JW, Hergenrother PM. High Temperature Transfer Molding Resins II. International SAMPE Technical Conference Series 2001; 46: 510-522.

[18] Smith Jr. JG, Connell JW, Hergenrother PM, Criss JM. Resin transfer moldable phenylethynyl containing imide oligomers. Journal of Composite Materials 2002; 36(19): 2255-2265.

[19] Criss JM, Koon RW, Hergenrother PM, Connell JW, Smith Jr. JG. High temperature VARTM of phenylethynyl/polyimide composites. International SAMPE Tech Conference Series 2001; 33: 1009.

[20] Ghose S, Watson KA, Cano RJ, Britton SM, Jensen BJ, Connell JW, Herring HM, Lineberry QJ. High temperature VARTM of phenylethynyl terminated imides. High Performance Polymers 2009; 21(5): 653-672.

[21] Jones J (ed.). Nontoxic resins advance aerospace manufacturing. NASA Spinoff 2009; http://www.sti.nasa.gov/tto/Spinoff2009/t_6.html.

[22] Thostenson ET, Ren Z, Chou TW. Advances in the science and technology of carbon nanotubes and their composites: a review. Composites Science and Technology 2001; 61(13): 1899-1912.

[23] Dresselhaus MS, Dresselhaus G, Charlier JC, Hernandez E. Electronic, thermal and mechanical properties of carbon nanotubes. Philosophical Transactions of the Royal Society A 2004; 362(1823): 2065-2098.

[24] Gao G, Cagin T, Goddard III WA. Energetics, structure, mechanical and vibrational properties of single walled carbon nanotubes (SWNT). Fifth foresight conference on molecular nanotechnology 1997. http://www.wag.caltech.edu/foresight/foresight_2.html; December 2008.

[25] Awasthi K, Srivastava A, Srivastava ON. Synthesis of carbon nanotubes. Journal of Nanoscience and Nanotechnology 2005; 5(10): 1616-1636.

[26] Iijima S. Helical microtubules of graphitic carbon. Nature 1991; 354(6348): 56-58.

[27] Wang N, Li GD, Tang ZK. Mono-sized and single-walled 4 angstrom carbon nanotubes. Chemical Physics Letters 2001; 339(1-2): 47-52.

[28] Baughman RH, Zakhidov AA, de Heer WA. Carbon nanotubes-the route toward applications. Science 2002; 297(5582): 797-792.

[29] Breuer O, Sandarara J. Big returns from small fibers: a review of polymer/carbon nanotube composites. Polymer Composites 2004; 25(6): 630-645.

[30] Moniruzzaman M, Winey KI. Polymer nanocomposites containing carbon nanotubes. Macromolecules 2006; 39(16): 5194-5205.

[31] Endo M, Koyama T, Hishiyama Y. Structural improvement of carbon-fibers prepared from benzene. Japanese Journal of Applied Physics 1976; 15(11): 2073-2076.

[32] Kelly BT. *Physics of Graphite*. London: Applied Science; 1981.

[33] Treacy MMJ, Ebbesen TW, Gibson JM. Exceptionally high Young's modulus observed for individual carbon nanotubes. Nature 1996; 381(6584): 678-680.

[34] Wong EW, Sheehan PE, Lieber CM. Nanobeam mechanics: elasticity, strength, and toughness of nanorods and nanotubes. Science 1997; 277(5334): 1971-1975.

[35] Yu MF, Lourie O, Dyer MJ, Moloni K, Kelly TF, Ruoff RS. Strength and breaking mechanism of multiwalled carbon nanotubes under tensile load. Science 2000; 282(5453): 637-340.

[36] Salvetat JP, Briggs GAD, Bonard JM, Bacsa RR, Kulik AJ, Stockli NA, Forro L. Elastic and shear moduli of single-walled carbon nanotube ropes. Physics Review Letters 1999; 82(5): 944-947.

[37] Yu MF, Files BS, Arepalli S, Ruoff RS. Tensile loading of ropes of single wall carbon nanotubes and their mechanical properties. Physical Review Letters 2000; 84(24): 5552-5555.

[38] Krishnan A, Dujardin E, Ebbesen TW, Yianilos PN, Treacy MMJ. Young's modulus of single-walled nanotubes. Physics Reviews B 1998; 58(20): 14013-14019.

[39] www.cheaptubes.com; January 2009.

[40] www.apsci.com/ppi-about.html; January 2009.

[41] Ozkan T, Maraghi M, Chasiotis I. Mechanical properties of vapor grown carbon nanofibers. Carbon 2010; 48(1): 239-244.

[42] Cadek M, Coleman JN, Barron V, Hedicke K, Blau WJ. Morphological and mechanical properties of carbon-nanotube-reinforced semicrystalline and amorphous polymer composites. Applied Physics Letters 2002; 81(27): 5123-5125.

[43] Qian D, Dickey EC, Andrews R, Rantell T. Load transfer and deformation mechanisms in carbon nanotube-polystyrene composites. Applied Physics Letters 2000; 76(20): 2868-2870.

[44] Liu TX, Phang IY, Shen L, Chow SY, Zhang WD. Morphology and mechanical properties of multiwalled carbon nanotubes reinforced nylon-6 composites. Macromolecules 2004; 37(19): 7214-7222.

[45] Meincke O, Kaempfer D, Weickmann H, Friedrich C, Vathauer M, Warth H. Mechanical properties and electrical conductivity of carbon-nanotube filled polyamide-6 and its blends with acrylonitrile/butadiene/styrene. Polymer 2004; 45(3): 739-748.

[46] Putz KW, Mitchell CA, Krishnamoorti R, Green PF. Elastic modulus of single-walled carbon nanotube/poly(methyl methacrylate) nanocomposites. Journal of Polymer Science B 2004; 42(12): 2286-2293.

[47] Ogasawara T, Ishida Y, Ishikawa T, Yokota R. Characterization of multi-walled carbon nanotube/phenylethynyl terminated polyimide composites. Composites Part A 2004; 35(1): 67-74.

[48] Haggenmueller R, Zhou W, Fischer JE, Winey KI. Productions and characterization of polymer nanocomposites with highly aligned single-walled carbon nanotubes. Journal of Nanoscience and Nanotechnology 2003; 3(1-2): 105-110.

[49] Lordi V, Yao N. Molecular mechanics of binding in carbon-nanotube-polymer composites. Journal of Materials Research 2000; 15(12): 2770-2779.

[50] Frankland SJV, Caglar A, Brenner DW, Griebel M. Molecular simulation of the influence of chemical cross-links on the shear strength of carbon nanotube-polymer interfaces. Journal of Physical Chemistry B 2002; 106(12): 3046-3048.

[51] Yumura M. Carbon nanotube industrial applications. AIST Today Internation Edition 2003; 10: http://www.aist.go.jp/aist_e/aist_today/2003_10/2003_10_p08_09.pdf.

[52] Coleman JN, Khan U, Blau WJ, Gun'ko YK. Small but strong: A review of the mechanical properties of carbon nanotube-polymer composites. Carbon 2006; 44(9): 1624-1652.

[53] Xie XL, Mai YW, Zhou XP. Dispersion and alignment of carbon nanotubes in polymer matrix: A review. Materials Science and Engineering R 2005; 49(4): 89-112.

[54] Grossiord N, Loos J, Regev O, Koning CE. Toolbox for dispersing carbon nanotubes into polymers to get conductive nanocomposites. Chemical Materials 2006; 18(5): 1089-1099

[55] Liao YH, Marietta-Tondin O, Liang Z, Zhang C, Wang B. Investigation of the dispersion process of SWNTs/SC-15 epoxy resin nanocomposites. Materials Science and Engineering A 2004; 385(1-2): 175-181.

[56] Lau K, Lu M, Lam C, Cheung H, Sheng FL, Li HL. Thermal and mechanical properties of single-walled carbon nanotube bundle-reinforced epoxy nanocomposites: the role of solvent for nanotube dispersion. Composites Science and Technology 2005; 65(5): 719-725.

[57] Du F, Fischer J, Winey K. Coagulation method for preparing single-walled carbon nanotube/poly(methyl methacrylate) composites and their modulus, electrical conductivity, and thermal stability. Journal of Polymer Science Part B 2003; 41(25): 3333-3338.

[58] Cui S, Canet R, Derre A, Couzi M, Delhaes P. Characterization of multiwall carbon nanotubes and influence of surfactant in the nanocomposite processing. Carbon 2003; 41(4): 797-809.

[59] Zhu BK, Xie SH, Xu ZK, Zu YY. Preparation and properties of the polyimide/multi-walled carbon nanotubes (MWNTs) nanocomposites. Composites Science and Technology 2006; 66(3-4): 548-554.

[60] Chen Q, Xu R, Yu D. Multiwalled carbon nanotube/polybenzoxazine nanocomposites: preparation, characterization and properties. Polymer 2006; 47(22): 7711-7719.

[61] Haggenmueller R, Du F, Fischer JE, Winey KI. Interfacial *in situ* polymerization of single wall carbon nanotube/nylon 6,6 nanocomposites. Polymer 2006; 47(7): 2381-2388.

[62] Zhu J, Kim JD, Peng H, Margrave JL, Khabashesku VN, Barrera EV. Improving the dispersion and integration of single-walled carbon nanotubes in epoxy composites through functionalization. Nanoletters 2003; 3(8): 1107-1113.

[63] Sandler J, Shaffer MSP, Prasse T, Bauhofer W, Schulte K, Windle AH. Development of a dispersion process for carbon nanotubes in an epoxy matrix and the resulting electrical properties. Polymer 1999; 40(21): 5967-5971.

[64] Haggenmueller R, Gommans HH, Rinzler AG, Fischer JE, Winey KI. Aligned single-wall carbon nanotubes in composites by melt processing methods. Chemical Physics Letters 2000; 330(3-4): 219-225.

[65] Bhattacharyya AR, Sreekumar TV, Liu T, Kumar S, Ericson LM, Hauge RH, Smalley RE. Crystallization and orientation studies in polypropylene/single wall carbon nanotube composites. Polymer 2003; 44(8): 2373-2377

[66] Moore VC, Strano MS, Haroz EH, Hauge RH, Smalley RE. Individually suspended single-walled carbon nanotubes in various surfactants. Nanoletters 2003; 3(10): 1379-1382.

[67] Lee BI, Rives JP. Dispersion of alumina powders in nonaqueous media. Colloids and Surfaces 1991; 56: 25-43.

[68] Gong X, Liu J, Baskaran S, Voise RD, Young JS. Surfactant-assisted processing of carbon nanotube/polymer composites. Chemical Materials 2000; 12(4): 1049-1052.

[69] Dalmas F, Chazeau L, Gauthier C, Masanelli-Varlot K, Dendievel R, Cavaillé JY, Forró L. Multiwalled carbon nanotube/polymer nanocomposites: processing and properties. Journal of Polymer Science B 2005; 43(10): 1186-1197.

[70] Seyhan AT, Gojny FH, Tanoğlu M, Schulte K. Critical aspects related to processing of carbon nanotube/unsaturated thermoset polyester nanocomposites. European Polymer Journal 2007; 43(2): 374-379.

[71] So HH, Cho JW, Sahoo NG. Effect of carbon nanotubes on mechanical and electrical properties of polyimide/carbon nanotubes nanocomposites. European Polymer Journal 2007; 43(9): 3750-3756.

[72] Barrau S, Demont P, Perex E, Peigny A, Laurent C, Lacabanne C. Effect of palmitic acid on the electrical conductivity of carbon nanotubes-epoxy resin composites. Macromolecules 2003; 36(26): 9678-9680.

[73] McCarthy B, Coleman JN, Czerw R, Dalton AB, Panhuis MIH, Maiti A, Drury A, Bernier P, Nagy JB, Lahr B, Byrne HJ, Carroll DL, Blau WJ. A microscopic and spectroscopic study of interactions between carbon nanotubes and a conjugated polymer. Journal of Physical Chemistry B 2002; 106 (9): 2210-2216.

[74] Schadler LS, Giannaris SC, Ajayan PM. Load transfer in carbon nanotube epoxy composites. Applied Physics Letters 1998; 73(26): 3842-3844.

[75] Martin CA, Sandler JKW, Shaffer MSP, Schwartz MK, Bauhofer W, Schulte K, Windle AH. Formation of percolating networks in multi-wall carbon-nanotube-epoxy composites. Composites Science and Technology 2004; 64(15): 2309-2316.

[76] Chen GX, Li Y, Shimizu H. Ultrahigh-shear processing for the preparation of polymer/carbon nanotube composites. Carbon 2007; 45(12): 2334-2340.

[77] Andrews R, Jacques D, Minot M, Rantell T. Fabrication of carbon multiwall nanotube/polymer composites by shear mixing. Macromolecular Materials Engineering 2002; 287(6): 395-403.

[78] Pötchke P, Bhattacharyya A, Janke A. Carbon nanotube-filled polycarbonate composite produced by melt mixing and their use in blends with polyethylene. Carbon 2004; 42(5-6): 965-969.

[79] Moniruzzaman M, Du F, Romero N, Winey KI. Increased flexural modulus and strength in SWNT/epoxy composites by a new fabrication method. Polymer 2006; 47(1): 293-298.

[80] Barber AH, Andrews R, Schadler LS, Wagner HD. On the tensile strength distribution of multiwalled carbon nanotubes. Applied Physics Letters 2005; 87(20): 203106.

[81] Demczyk BG, Wang YM, Cumings J, Hetman M, Han W, Zettl A, Ritchie RO. Direct mechanical measurement of the tensile strength and elastic modulus of multiwalled carbon nanotubes. Materials Science and Engineering A 2002; 334(1-2): 173-178.

[82] Chiu HY, Deshpande VV, Postma HWC, Lau CN, Miko C, Forro L, Bockrath M. Ballistic phonon thermal transport in multiwalled carbon nanotubes. Physical Review Letters 2005; 95(22): 226101.

[83] Hone J, Liaguno MC, Nemes NM, Johnson AT, Fischer JE, Walters DA, Casavant MJ, Schmidt J, Smalley RE. Electrical and thermal transport properties of magnetically aligned single wall carbon nanotube films. Applied Physics Letters 2000; 77(5): 666-668.

[84] Hone J, Llaguno MC, Biercuk MJ, Johnson AT, Batlogg B, Benes Z, Fischer JE, Thermal properties of carbon nanotubes and nanotube-based materials. Applied Physics A 2002; 74(3): 339-343.

[85] Ebbesen TW, Lezec HJ, Hiura H, Bennett JW, Ghaemi HF, Thio T. Electrical conductivity of individual carbon nanotubes. Nature 1996; 382(6586): 54-56.

[86] Thess A, Lee R, Nikolaev P, Dai HJ, Petit P, Robert J, Xu CH, Lee YH, Kim SG, Rinzler AG, Colbert DT, Scuseria GE, Tomanek D, Fischer JE, Smalley RE. Crystalline ropes of metallic carbon nanotubes. Science 1996; 273(5274): 483-487.

[87] Smith JG, Connell JW, Hergenrother PM. Imide oligomers containing pendent and terminal phenylethynyl groups. Polymer 1997; 38(18): 4657-4665.

[88] Hergenrother PM. The use, design, synthesis, and properties of high performance/high temperature polymers: an overview. High Performance Polymers 2003; 15(1): 3-45.

[89] Ghose S, Watson KA, Sun KJ, Criss JM, Siochi EJ, Connell JW. High temperature resin/carbon nanotube composite fabrication. Composites Science and Technology 2006; 66(13): 1995-2002.

[90] Hergenrother PM, Bryant RG, Jensen BJ, Havens SJ. Phenylethynyl-terminated imide oligomers and polymers therefrom. Journal of Polymer Science A 1994; 32(16): 3061-3067.

[91] Ghose S, Watson KA, Delozier DM, Working DC, Siochi EJ, Connell JW. Incorporation of multi-walled carbon nanotubes into high temperature resin using dry mixing techniques. Composites Part A 2006; 37(3): 465-475.

[92] Ghose S, Watson KA, Working DC, Siochi EJ, Connell JW, Criss JM. Fabrication and characterization of high temperature resin/carbon nanofiber composites. High Performance Polymers, 2006; 18(4): 527-544.

[93] Choi YK, Sugimoto K, Song SM, Gotoh Y, Ohkoshi Y, Endo M. Mechanical and physical properties of epoxy composites reinforced by vapor grown carbon nanofibers. Carbon 2005; 43(10): 2199-2208.

[94] Kasaliwal G, Godel A, Potschke P. Influence of processing conditions in small-scale melt mixing and compression molding on the resistivity and morphology of polycarbonate-MWNT composites. Journal of Applied Polymer Science 2009; 112(6): 3494-3509.

[95] Krause B, Pötschke P, Häußler. Influence of small scale melt mixing conditions on electrical resistivity of carbon nanotube-polyamide composites. Composites Science and Technology 2009; 69(10): 1505-1515.

[96] Shofner ML, Rodriguez-Macias FJ, Vaidyanathan R, Barrera EV. Single wall nanotube and vapor grown carbon fiber reinforced polymers processed by extrusion freeform fabrication. Composites Part A 2003; 34(11): 1207-1217.

[97] De Zhang W, Shen L, Phang IY, Liu TX. Carbon nanotubes reinforced nylon-6 composite prepared by simple melt-compounding. Macromolecules 2004; 37(2): 256-259.

[98] Lozano K, Files B, Rodriguez-Macias FJ, Barrera EV. Purification and functionalization of vapor grown carbon nanotubes and single wall nanotubes. Powder Materials: Current Research and Industrial Practices (TMS Fall Meeting Proceedings) 1999; 333-340.

[99] Criss Jr JM, Powell WD, Connell JW, Stallworth-Bordain Y, Brown TR, Mintz EA, Schlea MR, Shofner ML. Nano-particle enhanced polymer materials for space flight applications. SAMPE Technical Conference 2009: Baltimore, MD.

[100] Suggs K, Mintz E, and Wang XQ. Manuscript in preparation.

[101] Ogunro OO, Wang XQ. Quantum electronic stability in selective enrichment of carbon nanotubes. Nanoletters 2009; 9(3): 1034-1038

[102] Nduwimana A, Wang XQ. Energy gaps in supramolecular functionalized graphene nanoribbons. ACS Nano 2009; 3(7): 1995-199.

[103] Connell JW, Smith Jr. JG, Hergenrother PM. High Temperature Transfer Molding Resins: Status of PETI-298 and PETI-330. SAMPE Technical Conference 2003: Dayton, OH.

[104] Mitchell CA, Krishnamoorti R. Dispersion of single-walled carbon nanotubes in poly(epsilon-caprolactone). Macromolecules 2007; 40(5): 1538-1545.

[105] Pötschke P, Fornes TD, Paul DR. Rheological behavior of multiwalled carbon nanotube/polycarbonate composites. Polymer 2002; 43(11): 3247-3255.

[106] Utracki LA. Flow and flow orientation of composites containing anisometric particles. Polymer Composites 1986; 7(5): 274-282.

[107] Wong EW, Sheehan PE, Lieber CM. Nanobeam mechanics: Elasticity, strength, and toughness of nanorods and nanotubes. Science 1997; 277(5334): 1971-1975.

[108] Lisunova MO, Mamunya YP, Lebovka NI, Melezhyk AV. Percolation behaviour of ultrahigh molecular weight polyethylene/multi-walled carbon nanotubes composites. European Polymer Journal 2007; 43(3): 949-958.

[109] Sandler JKW, Kirk JE, Kinlock IA, Shaffer MSP, Windle AH. Ultra-low electrical percolation threshold in carbon-nanotube-epoxy composites. Polymer 2003; 44(19): 5893-5899.

[110] Bryning MB, Islam MF, Kikkawa JM, Yodh AG. Very low conductivity threshold in bulk isotropic single-walled carbon nanotube-epoxy composites. Advanced Materials 2005; 17(9): 1186-1191.

[111] Hu GJ, Zhao CG, Zhang SM, Yang MS, Wang ZG. Low percolation threshold of electrical conductivity and rheology in poly(ethylene terephthalate) through the networks of multi-walled carbon nanotubes. Polymer 2006; 47(1): 480-488.

[112] Ramasubramaniam R, Chen J, Liu H. Homogeneous carbon nanotube/polymer composites for electrical applications. Applied Physics Letters 2003; 83(14): 2928-2930.

[113] Garboczi EJ, Snyder KA, Douglas JF. Geometrical percolation threshold of overlapping ellipsoids. Physical Review E 1995; 52(1): 819-828.

[114] Gerhardt RA. Impedance spectroscopy and mobility spectra. Encyclopedia of Condensed Matter Physics. Eds Bassani G, Liedl G, Wyder P. Academic Press, 2005.

[115] Battisti A, Skordos AA, Partridge IK. Dielectric monitoring of carbon nanotube network formation in curing thermosetting nanocomposites. Journal of Physics D 2009; 42(15).

[116] McClory C, Chin SJ, McNally T. Polymer/carbon nanotube composites. Australian Journal of Chemistry 2009; 62(8): 762-785.

[117] Deng H, Skipa T, Zhang R, Lellinger D, Bilotti E, Alig I, Peijs T. Effect of melting and crystallization on the conductive network in conductive polymer composites. Polymer 2009; 50(15): 3747-3754.

[118] Rosca ID, Hoa SV. Highly conductive multiwall carbon nanotube and epoxy composites produced by three-roll milling. Carbon 2009; 47(8): 1958-1968.

[119] Kovacs JZ, Velagala BS, Schulte K, Bauhofer W. Two percolation threshold in carbon nanotube epoxy composites. Composites Science and Technology 2007; 67(5): 922-928.

[120] Teng CC, Ma CCM, Huang YW, Yuen SM, Weng CC, Chen CH, Su SF. Effect of MWCNT content on rheological and dynamic mechanical properties of multiwalled carbon nanotube/polypropylene composites. Composites: Part A 2008; 39(12): 1869-1875.

[121] Manchado MAL, Valentini L, Biagiotti J, Kenney JM. Thermal and mechanical properties of single-walled carbon nanotubes-polypropylene composites prepared by melt processing. Carbon 2005; 43(7): 1499-1505.

[122] Ou R, Gupta S, Parker CA, Gerhardt RA. Fabrication and electrical conductivity of poly(methyl methacrylate) (PMMA)/carbon black (CB) composites: comparison between an ordered carbon black nanowire-like segregated structure and a randomly dispersed carbon black nanostructure. Journal of Physical Chemistry B 2006; 110 (45): 22365-22373.

[123] Peng CQ, Thio YS, Gerhardt RA. Conductive paper fabricated by layer-by-layer assembly of polyelectrolytes and ITO nanoparticles. Nanotechnology 2008; 19(50): 505603.

[124] Du F, Scogna RC, Zhou W, Brand S, Fischer JE, Winey KI. Nanotube networks in polymer nanocomposites: rheology and electrical conductivity. Macromolecules 2004; 34(24): 9048-9055.

[125] Stauffer D and Aharony A. *Introduction to Percolation Theory.* Second edition. Taylor and Francis Inc., Bristol: 1992.

[126] Kirkpatrick S. Percolation and conduction. Reviews of Modern Physics 1973: 45(4) 574-588.

[127] Kayatin MJ, Davis VA. Viscoelasticity and shear stability of single-walled carbon nanotube/unsaturated polyester resin dispersions. Macromolecules 2009; 42(17): 6624-6632.

[128] Kim J, Hong SM, Kwak S, Seo Y. Physical properties of nanocomposites prepared by in situ polymerization of high-density polyethylene on multiwalled carbon nanotubes. Physical Chemistry Chemical Physics 2009; 11(46): 10851-10859.

[129] Bauhofer W, Kovacs JZ. A review and analysis of electrical percolation in carbon nanotubes polymer composites. Composites Science and Technology 2009; 69(10): 1486-1498.

[130] Dalmas F, Cavaille J-Y, Gauthier C, Chazeau L, Dendievel R. Viscoelastic behavior and electrical properties of flexible nanofiber filled polymer nanocomposites-Influence of process conditions. Composites Science and Technology 2007; 67(5): 829-839.

[131] Allaoui A, Bai S, Cheng HM, Bai JB. Mechanical and electrical properties of MWNT/epoxy composite. Composites Science and Technology 2002; 62(15): 1993-1998.

[132] Jiang XW, Bin YZ, Matsuo M. Electrical and mechanical properties of polyimide-carbon nanotubes composites fabricated by in situ polymerization. Polymer 2005; 46(18): 7418-24.

[133] Kaneto K, Tsuruta M, Sakai G, Cho WY, Ando Y. Electrical conductivities of multi-wall carbon nanotubes. Synthetic Metals 1999; 103(1-3): 2543-2546.

[134] Kim YJ, An KJ, Suh KS, Choi HD, Kwon JH, Chung YC, Kim WN, Lee AK, Choi JI, Yoon HG. Hybridization of oxidized MWNT and silver powder polyurethane matrix for electromagnetic interference shielding application. IEEE Transactions on Electromagnetic Compatibility 2005; 47(4): 872-879.

[135] Ounaies Z, Park C, Wise KE, Siochi EJ, Harrison JS. Electrical properties of single wall carbon nanotubes reinforced polyimide composites. Composites Science and Technology 2003; 63(11): 1637-1646.

[136] Kilbride BE, Coleman JN, Fraysse J, Fourney P, Cadek M, Drury A, Hutzler S, Roth S, Blau WJ. Experimental observation of scaling laws for alternating current and direct current conductivity in polymer-carbon nanotube composite thin films. Journal of Applied Physics 2002; 92(7): 4024-4030.

[137] Sahimi M, Arbabi S. Mechanics of disordered solids. II. Percolation on elastic networks with bond-bending forces. Physical Review B 1993; 47(2): 703-712.

[138] Musumeci AW, Silva GG, Liu JW, Martens WN, Waclawik ER. Structure and conductivity of multi-walled carbon nanotube/poly(3-hexylthiophene) composite films. Polymer 2007; 48(6): 1667-1678.

[139] McCullen SD, Stevens DR, Roberts WA, Ojha SS, Clarke LI, Gorga RE. Morphological, electrical, and mechanical characterization of electrospun nanofiber mats containing multiwalled carbon nanotubes. Macromolecules 2007; 40(4): 997-1003.

[140] Barrau S, Demont P, Peigney A, Laurent C, Lacabanne C. DC and AC conductivity of carbon nanotubes-polyepoxy composites. Macromolecules 2003; 36(14): 5187-5194.

[141] Wenger OS. How donor-bridge-acceptor energetic influence electron tunneling dynamics and their distance dependences. Accounts of Chemical Research 2010; 44(1): 25-35.

[142] Tian S, Wang X. Fabrication and performances of epoxy/multi-walled carbon nanotubes/piezoelectric ceramic composites as rigid piezo-dampening materials. Journal of Materials Science 2008; 43(14): 4979-4987.

[143] Yu S, Wong WM, Hu X, Juay YK. The characteristics of carbon nanotube-reinforced poly(phenylene sulfide) nanocomposites. Journal of Applied Polymer Science 2009; 113(6): 3477-3483.

[144] Potschke P, Abdel-Goad M, Alig I, Dudkin S, Lellinger D. Rheological and dielectric characterization of melt mixed polycarbonate-multiwalled carbon nanotube composites. Polymer 2004; 45(26): 8863-8870.

[145] Giunta RK, Kander RG. Analysis of the interphase of a polyimide bonded to chromic acid anodized TI-6AL-4V. Proceedings from the 23rd Annual Meeting of the Adhesion Society, Albuquerque, January 2000; SAND2000-0065C.

[146] Guth E. Theory of filler reinforcement. Journal of Applied Physics 1945; 16(1): 20-25.

[147] Celzard A, McRae E, Deleuze C, Dufort M, Furdin G, Marêché JF. Critical concentration in percolating systems containing a high-aspect-ratio filler. Physical Review B 1996; 53(10): 6209-6214.

[148] Balberg I, Anderson CH, Alexander S, Wagner N. Excluded volume and its relation to the onset of percolation. Physical Review B 1984; 30(7): 3933-3943.

[149] Nogales A, Broza G, Roslaniec Z, Schulte K, Šics I, Hsiao BS, Sanz A, Garcia-Gutiérrez MC, Rueda DR, Domingo C, Ezquerra TA. Low percolation threshold in nanocomposites based on oxidized single wall carbon nanotubes and poly(butylenes terephthalate). Macromolecules 2004; 37(20): 7669-7672.

[150] Aguilar JO, Bautista-Quijano JR, Avilés F. Influence of carbon nanotube clustering on the electrical conductivity of polymer composite films. eXPRESS Polymer Letters 2010; 4(5): 292-299.

[151] Gojny FH, Wichmann MHG, Fiedler B, Schulte K. Influence of different carbon nanotubes on the mechanical properties of epoxy matrix composites – a comparative study. Composites Science and Technology 2005; 65(15-16): 2300-2313.

[152] Kinloch IA, Roberts SA, Windle AH. A rheological study of concentrated aqueous nanotubes dispersions. Polymer 2002; 43(26): 7483-7491.

[153] Bai JB, Allaoui A. Effect of the length and the aggregate size of MWNTs on the improvement efficiency of the mechanical and electrical properties of nanocomposites – experiments investigation. Composites Part A 2003; 34(8): 689-694.

[154] Shi DL, Feng XQ, Huang YY, Hwang KC, Gao H. The effect of nanotube waviness and agglomeration on the elastic property of carbon nanotube-reinforced composites. Journal of Engineering Materials and Technology 2004; 126(3): 250-257.

[155] Song YS, Youn JR. Influence of dispersion states of carbon nanotubes on physical properties of epoxy nanocomposites. Carbon 2005; 43(7): 1378-1385.

[156] Poncharal P, Wang ZL, Ugarte D, de Heer WA. Electrostatic deflections and electromechanical resonances of carbon nanotubes. Science 1999; 283(5407): 1513-1516.

[157] Zuo HJ, Chen JS, Yang HX, Hu AJ, Fan L, Yang SY. Synthesis and characterization of melt-processable polyimides derived from 1,4-Bis(4-amino-2-trifluoromethylphenoxy)benzene. Journal of Applied Polymer Science 2007; 107(2): 755.

[158] Lawrence JG, Berhan LM, Nadarajah A. Elastic properties and morphology of individual carbon nanofibers. ACS Nano 2008; 2(6): 1230-1236.

[159] Mo TC, Wang HW, Chen SY, Yeh YC. Synthesis and characterization of polyimide/multi-walled carbon nanotube nanocomposites. Polymer Composites 2008; 29(4): 451-457.

[160] Wang Z, Liang Z, Wang B, Zhang C, Kramer L. Processing and property investigation of single-walled carbon nanotube (SWNT) buckypaper/epoxy resin matrix nanocomposites. Composites: Part A 2004; 35(10): 1225-1232.

[161] Chen GX, Shimizu H. Multiwalled carbon nanotubes grafted with polyhedral oligomeric silsesquioxene and its dispersion in poly(L-lactide) matrix. Polymer 49(4); 2008: 943-951.

[162] Bokobza L. Multiwall carbon nanotube elastomeric composites: a review. Polymer 2007; 48(17): 4907-4920.

[163] Jeong W, Kessler MR. Toughness enhancement in ROMP functionalized carbon nanotube/polydicyclopentadiene composites. Chemistry of Materials 2008; 20(22): 7060-7068.

[164] Masuda J, Torkelson JM. Dispersion and major property enhancements in polymer/multiwall carbon nanotube nanocomposites via solid-state shear pulverization followed by melt mixing. Macromolecules 2008; 41(16): 5974-5977.

[165] Kim JA, Seong DG, Kang TJ, Youn JR. Effects of surface modification on rheological and mechanical properties of CNT/epoxy composites. Carbon 2006; 44(10): 1898-1905.

[166] Kanagaraj S, Varanda FR, Zhil'tsova TV, Oliveria MSA, Simões JAO. Mechanical properties of high density polyethylene/carbon nanotube composites. Composites Science and Technology 2007; 67(15-16): 3071-3077.

[167] Gojny FH, Wichmann MHG, Köpke U, Fiedler B, Schulte K. Carbon nanotube-reinforced epoxy-composites: enhanced stiffness and fracture toughness at low nanotube content. Composites Science and Technology 2004; 64(15): 2363-2371.

[168] Halpin JC, Tsai SW. Environmental factors in composite material design. US Air Force Materials Laboratory Report 1969; AFML-TR 67-423.

[169] Halpin JC, Kardos JL. The Halpin-Tsai equations: a review. Polymer Engineering Science 1976; 16(5): 344-352.

[170] Agarwal BD, Broutman LG. Analysis and Performance of Fiber Composites. Wiley: New York, 1980.

[171] Mallick PK. Fiber-Reinforced Composites. Marcel Dekker: New York, 1993.

[172] Turi E. Thermal Characterization of Polymeric Materials; Academic Press: New York, 1981.

[173] Piloyan GO, Ryabchikov ID, Novikova OS. Determination of activation energies of chemical reactions by differential thermal analysis. Nature 1966; 212(5067): 1229.

[174] Swarin SJ, Wims AM. A method for determining reaction kinetics by differential scanning calorimetry. Journal of Thermal Analytical Calorimetry 1976; 51(4): 155-77.

[175] Sourour S, Kamal MR. Differential scanning calorimetry of epoxy cure: isothermal cure kinetics. Thermochimica Acta 1976; 14(1-2): 41-59.

[176] Kenny JM. Determination of autocatalytic model parameters describing thermoset cure. Journal of Applied Polymer Science 1994; 51(4): 761-764.

[177] Ozawa T. A new method of analyzing thermogravimetric data. Bulletin of Chemical Society of Japan 1965; 38(11): 1881-1886.

[178] Flynn JH, Wall LA. General treatment of thermogravimetry of polymers. Journal of Research of the National Bureau of Standards, Section A- Physics and Chemistry 1966; A70(6): 487-523.

[179] Vyazovkin S, Sbirrazzuoli N. Isoconversional kinetic analysis of thermally simulated processed in polymers. Macromolecular Rapid Communications 2006; 27(18): 1515-1532.

[180] Gonis J, Simon GP, Cook WD. Cure properties of epoxies with varying chain length as studied by DSC. Journal of Applied Polymer Science 1999; 72(11): 1479-1488.

[181] Ramírez C, Rico M, Torres A, Barral L, López J, Montero B. Epoxy/POSS organic-inorganic hybrids: ATR-FTIR and DSC studies. European Polymer Journal 2008; 44(10): 3035-3045.

[182] Kuan CF, Chen WJ, Li YL, Chen CH, Kuan HC, Chiang CL. Flame retardance and thermal stability of carbon nanotube epoxy composite prepared from sol-gel method. Journal of Physics and Chemistry of Solids 2010; 71(4): 539-543.

[183] Fava RA. Differential scanning calorimetry of epoxy resins. Polymer 1968; 9(3): 137-151.

[184] Guo X. Study of curing kinetics of an epoxy-amine adhesive system using a calorimetric analysis approach. Polymer-Plastics Technology and Engineering 2008; 47(11): 1109-1116.

[185] Ren H, Sun J, Zhao Q, Zhiqi C, Ling Q, Zhou Q. Cure kinetics of an epoxy resin containing naphthyl/dicyclopentadiene moieties and bis-phenoxy (3-hydroxy) phosphine oxide system and properties of cured polymer. Journal of Applied Polymer Science 2009; 112(2): 761-768.

[186] Yang LF, Yao KD, Koh W. Kinetics analysis of the curing reaction of fast cure epoxy prepregs. Journal of Applied Polymer Science 1999; 73(8): 1501-1508.

[187] Vyazovkin S, Sbirrazzuoli N. Mechanism and kinetics of epoxy-amine cure studied by differential scanning calorimetry. Macromolecules 1996; 29(6): 1867-1873.

[188] Puglia D, Valentini L, Armentano I, Kenny JM. Effects of single-walled carbon nanotube incorporation on the reaction of epoxy resin and its detection by Raman spectroscopy. Diamond and Related Materials 2003; 12(3-7): 827-832.

[189] White SR, Mather PT, Smith MJ. Characterization of the cure-state of DGEBA-DDS epoxy using ultrasonic, dynamic mechanical, and thermal probes. Polymer Engineering and Science 2002; 42(1): 51-67.

[190] Kim J, Moon TJ, Howell JR. Cure kinetic model, heat of reaction, and glass transition temperature of AS4/3501-6 graphite-epoxy prepregs. Journal of Composite Materials 2002; 36(21): 2479-2498.

[191] Liu LQ, Wagner HD. A comparison of the mechanical strength and stiffness of MWNT-PMMA and MWNT-epoxy nanocomposites. Composite Interfaces 2007; 14(4): 285-297.

[192] Barghamadi M. Curing studies of epoxy resin by 4,4'-diaminoazobenzene as curing agent reinforced with nanosilica and nanoclay particles along with impact resistance and thermal evaluation. Polymer Composites 2010; 31(8): 1465-1473.

[193] Hinkley JA. DSC study of the cure of phenynlethynyl-terminated imide oligomer. Journal of Advanced Materials 1996; 27(3): 55-59.

[194] Fang X, Rogers DF, Scola DA, Stevens MP. A study of the thermal cure of phenylethynyl-terminated imide model compound and a phenylethynyl-terminated imide oligomer (PETI-5). Journal of Polymer Science A 2000; 38(14): 2526-2535.

[195] Boswell RF, Claus SJ, Arnold F. Thermal characterization of PETI-RFI for aircraft applications. Navy publication, http://www.dtic.mil/cgi-bin/GetTRDoc?AD=ADA368626&Location=U2&doc=GetTRDoc.pdf.

[196] Li Y, Morgan RJ. Thermal cure of phenylethynyl-terminated AFR-PEPA-4 imide oligomer and a model compound. Journal of Applied Polymer Science 2006; 101(6): 4446-4453.

[197] Yang Y, Fan L, Ji M, Yang S. Phenylethynylnaphthalic endcapped imide oligomers with reduced cure temperatures. European Polymer Journal 2010; 46(11): 2145-2155.

[198] Yang Y, Fan L, Qu X, Ji M, Yang S. Fluorinated phenylethynyl-terminated imide oligomers with reduced melt viscosity and enhanced melt stability. Polymer 2011; 52(1): 138-148.

[199] Kissinger HE. Reaction kinetics in differential thermal analysis. Analytical Chemistry 1957; 29(11): 1702-1706.

[200] Xiong Y, Boey FYC, Rath SK. Kinetic study of the curing behavior of bismaleimide modified with diallylbisphenol A. Journal of Applied Polymer Science 2003; 90(8): 2229-2240.

[201] Liu L, Ye ZP. Effects of modified multi-walled carbon nanotubes on the curing behavior and thermal stability of boron phenolic resin. Polymer Degradation and Stability 2006; 94(11): 1972-1978.

[202] Sourour S, Kamal MR. Differential scanning calorimetry of epoxy cure: isothermal cure kinetics. Thermochimica Acta 1976; 14(1-2): 41-59.

[203] Fang XM, Xie XQ, Simone CD, Stevens MP, Scola DA. A solid-state C-13 NMR study of the cure of C-13-labeled phenylethynyl end-capped polyimides. Macromolecules 2000; 33(5): 1671-1681.

[204] Connell JW, Siochi EJ, Ghose S, Delozier DM, Watson KA, Working DC. Composite material having a thermally-reactive-endcapped imide oligomer and carbon nanofillers. WO/2008/054864, International application # PCT/US2007/067386. 2008.

[205] Fischer A, Jozokos T, Leacock J, Rich A. Conductive thermosets by extrusion. WO/2006/026691. International application # PCT/2005/031041. 2006.

[206] Tortoriello R. "Standard and Poor's Industry Survey - Aerospace and Defense," 12 February 2009.

[207] Smith J, Dedecker C, Doerer R. “Spring 2008 Industry Study Final Report: Aircraft Industry,” *The Industrial College of the Armed Forces*, 2008.

[208] Acevedo R. Interview, Andres Velarde, 25 February 2009.

[209] Reinhart J. Interview, Michelle Louie, 20 February 2009.

[210] Space Foundation, The Space Report 2008: Executive Summary. www.thespacereport.org/08executivesummary.pdf; April 2008

[211] PR Newswire, Aerospace Industry to Consume $57 Billion Worth of Composite Materials Between 2007-2026. www.aviationtoday.com/pressreleases/14829.html; 9 August 2007.

[212] Declining Defense, Wall Street Journal, online.wsj.com/article/SB123595811964905929.html; 2 March 2009.

[213] Michaels K. Market Trends: Aerospace Composites Market Will Quadruple by 2026, High Performance Composites, 1 January 2007.

[214] Legault MR. Aircraft simulation gets composites aware, High Performance Composites, 23 February 2009.

[215] Fox M, Shalal-Esa A. Update 1-Obama budget has more money for space exploration, *Reuters,* 26 February 2009.

[216] Carpenter D. Boeing again delays 787, http://www.huffingtonpost.com/2008/04/09/boeing-delays-787-debut-f_n_95785.html; 4 September 2008.

[217] Aerostrategy LLC, The Growing Use of Composites is Ending the 80-Year Reign of Metallic Aircraft. September 2006.

[218] Lerner I. Good growth projected for aerospace composites. www.icis.com/Articles/2008/12/15/9178930/good-growth-projected-for-aerospace-composites.html; 12 December 2008.

[219] O'Reilly Richard. Standard and Poor's Industry Survey - Chemicals, 8 January 2009.

[220] Kappes I. Interview. Andres Velarde, 25 February 2009.

[221] Carbone J. Defense is forcing new EMS tactics; Buying for defense systems is different than buying for other industries as purchase volumes are low, quality requirements are high and lifecycles are long. Purchasing 2008; 137(8).

[222] KPMG, Corporate Finance Advisory: Aerospace & Defense, Summer 2008.

[223] Tran-Le J, Thompson S, Genemans R, Davis E, Chu D, Vehmeier D. China's Impact on Metals Prices in Defense Aerospace. www.acq.osd.mil/ip; 18 October 2008.

[224] The Aluminum Association, Industry Overview. www.aluminum.org/Content/NavigationMenu/TheIndustry/Overview/default.htm; 2 November 2008.

[225] Romulus R, Averell J. *Steel and Specialty Metal Trend Analysis*, 11 July 2008.

[226] Cytec, Cytec Engineered Materials. www.cytec.com/engineered-materials/index.htm; 18 October 2008.

[227] Avimid, Avimid N Polyimide Composite, www.cytec.com/engineered-materials/products/avimidn_composite.htm; 3 February 2009.

[228] DuPont, 2008 DuPont Annual Review. www2.dupont.com/Media_Center/en_US/daily_news/april/article20090410.html; 3 February 2009.

[229] DuPont, DuPont™ Vespel® Parts Step Up to Increased Heat and Wear Needs in Aerospace. www2.dupont.com/Plastics/en_US/News_Events/article20081209.html; 29 January 2009.

[230] Black S. Are High Temperature Thermoset Resins Ready to Go Commercial? www.compositesworld.com/articles/are-high-temperature-thermoset-resins-ready-to-go-commercial.aspx; 1 November 2004.

[231] Speckmann H, Henrich R. Structural health monitoring- overview of technologies under development. www.ndt.net/article/wcndt2004/pdf/aerospace/563_henrich.pdf; 28 October 2008.

[232] Chung DDL. Structural health monitoring by electrical resistance measurement. Smart Materials and Structures 2001; 10(4): 624-636.

[233] Scheuler R, Joshi SP, Schulte K. Damage detection in CFRP by electrical conductivity mapping. Composites Science and Technology 2001; 61(6): 921-930.

[234] Todoroki A, Tanaka Y. Delamination identification of cross-ply graphite/epoxy composite beams using electric resistance change method. Composites Science and Technology 2002; 62(5): 629-639.

[235] Zhang W, Suhr J, Koratkar N. Carbon nanotubes/polycarbonate composites as multifunctional strain sensors. Journal of Nanoscience and Nanotechnology 2006; 6(4): 960-964.

[236] Li C, Chou TW. Modeling of damage sensing in fiber composites using carbon nanotubes networks. Composites Science and Technology 2008; 68(15-16): 3373-3379.

[237] Li C, Thostenson ET, Chou TW. Sensors and actuators based on carbon nanotubes and their composites: a review. Composites Science and Technology 2008; 68(6): 1227-1249.

[238] Thostenson ET, Chou TW. Carbon nanotube networks: sensing of distributed strain and damage for life prediction and self healing. Advanced Materials 2006; 18(21): 2837-2841.

[239] Du FM, Fischer JE, Winey KI. Effect of nanotube alignment on percolation conductivity in carbon nanotube/polymer composites. Physical Review B 2005; 72(12).

[240] Kang I, Schulz MJ, Kim JH, Shanov V, Shi D. A carbon nanotube strain sensor for structural health monitoring. Smart Materials and Structures 2006; 15(3): 737-748.

[241] Park M, Kim H, Youngblood JP. Strain-dependent electrical resistance of multi-walled carbon nanotube/polymer composite films. Nanotechnology 2008; 19(5): 1-7.

[242] Zhang R, Baxendale M, Peijs T. Universal resistivity-strain dependence of carbon nanotube/polymer composites. Physical Review B 2007; 76(19): 1-5.

[243] Hu N, Karube Y, Yan C, Masuda Z, Fukunaga H. Tunneling effect in a polymer/carbon nanotube nanocomposites strain sensor. Acta Materiala 2005; 56(13): 2929-2936.

[244] Liu CX, Choi JW. Strain-dependent resistance of PDMS and carbon nanotubes composite microstructures. IEEE Transactions on Nanotechnology 2010; 9(5): 590595.

[245] Bily MA, Kwon YW, Pollak RD. Study of composite interface fracture and crack growth monitoring using carbon nanotubes. Applied Composite Materials 2010; 17(4): 347-362.

[246] Miller B. Plastics World 1996; 54:73-77.